ACS MATERIALS LETTERS

www.acsmaterialsletters.org

REVIEW

Multilayer MXene Heterostructures and Nanohybrids for Multifunctional Applications: A Review

Sharif Tasnim Mahmud, Md Mehdi Hasan, Sudipta Bain, Sheikh Tamjidur Rahman, Mukitur Rhaman, Md Milon Hossain,* and Mustafa Ordu

Cite This: *ACS Materials Lett.* 2022, 4, 1174–1206

Read Online

ACCESS | Metrics & More | Article Recommendations

ABSTRACT: **MXenes (transition metal carbides and nitrides) have experienced exponential growth over the last two decades, thanks to their excellent physical, chemical, and mechanical properties. Intriguing properties like high conductivity, wear, and corrosion resistance while maintaining flexibility are the strong motivation behind the exploration of MXenes. Moreover, the large surface area and unique layered structure enhance the functionality of multilayer-MXene heterostructures and hybrids. This paper reviews the synthesis chemistry, structure properties of multilayer MXenes, and their multifunctional applications. MXene synthesis under different conditions, their hybrids and composites, intercalation, and structural geometries are discussed. The electrical, mechanical, optical, and magnetic properties of MXenes are briefly presented. Recent progress and development in MXene-based heterostructures and nanohybrids for supercapacitors, batteries, environmental and water treatment, antibacterial and tissue engineering, and electromagnetic absorption and shielding are systematically discussed. Finally, research challenges and a perspective in this specified area are addressed for potential developments.**

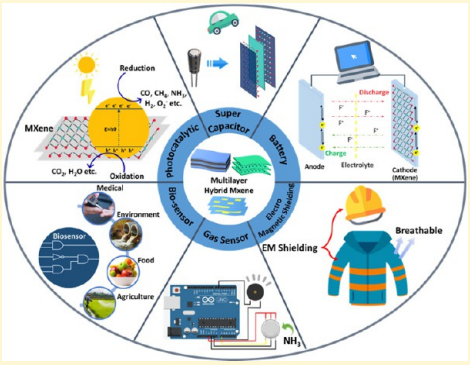

The growth of nanotechnology drives the rapid development of high-performance technologies in the 21st century. Extraordinary computational and experimental progress in materials technology has paved the way to understanding matters better and allowed the modification of materials properties at molecular and atomic levels.[1,2] The low dimensional nanomaterials are accelerating the fabrication and commercialization of nanodevices with low power consumption and superior performance.[3] The nanomaterials range from zero-dimensional (0D) to three-dimensional (3D) structures, i.e., 0D quantum dots,[4] 1D nanowires,[5] 2D nanosheets,[6] and 3D nanospheres. Since the successful exfoliation of 2D graphene in 2004,[7] the 2D nanomaterials family has experienced tremendous progress, and different multifunctional applications of 2D nanomaterials are expanding. Notable 2D nanomaterials under investigation transition metal dichalcogenides (TMDs),[8] hexagonal boron nitride (hBN),[9] phosphorene,[10] silicene,[11] 2D halide perovskite nanomaterials,[12] molybdenum disulfide (MoS_2),[13] 2D metal−organic framework (MOF) nanosheets,[14] and the transition metal carbides and/or nitrides (MXenes).[15] 2D nanomaterials have already shown promise for diverse applications utilizing unique structural features and excellent physicochemical, optical, and magnetic properties. However, the properties surprisingly differ due to the variation in crystal structure and compositions, i.e., dielectric, semiconductor, or semimetal.[16] Ultrathin atomic thickness endows 2D nanomaterials with excellent mechanical flexibility and optical transparency. Combining large lateral size, ultrahigh surface areas, and superior thermal conductivity, 2D nanomaterials becomes ideal for myriad applications.[17−19] Surface properties provide ample active sites to enhance the interaction with other nanomaterials and polymers to form hybrid structures.[20]

MXenes have experienced growing research interest since their discovery at Drexel University in 2011 by the exfoliation of Ti_3AlC_2 at room temperature. Because the transition metal carbides and nitrides include a material family of more than 60 members, the report explored a theoretically unlimited number of MXenes.[21−26] The presence of abundant surface termination

Received: February 21, 2022
Accepted: April 27, 2022
Published: May 17, 2022

MXenes (transition metal carbides and nitrides) have experienced exponential growth over the last two decades, thanks to their excellent physical, chemical, and mechanical properties. Intriguing properties like high conductivity, wear, and corrosion resistance while maintaining flexibility are the strong motivation behind the exploration of MXenes.

groups, i.e., oxygen (O), hydroxyl (−OH), and halogens (Fl, Cl), endows MXenes with superior physical and chemical properties along with ease of processability.[27,28] MXenes consist of multilayer sandwich structures that usually contain an odd number of layers, where carbon or nitrogen (X) layers are sandwiched between metals (M).[15] MXenes are represented in $M_{n+1}X_nT_x$ form, which includes transition metals (M elements), e.g., Sc, Y, Ti, Zr, Hf, V, Nb, Ta, Cr, Mo, W, Mn, carbon, and nitrogen (X elements) along with the functional surface termination groups (T_x elements).[29,30] The unique structure-derived properties such as hydrophilicity, reactivity, and high negative ζ-potential induce stable colloidal solution combined with electrical, electrochemical, optoelectronic, and magnetic properties are driving the theoretical and experimental study of MXenes.[31−33] The surface properties allow the formation of the MXene-based multilayer hybrid structure by combining MXenes with compatible nanomaterials using self-assembly,[34] polymerization,[35] and covalent functionalization.[36] The development of Mxenes-based energy application,[30] sensors,[37] catalysts,[38] environmental remediations and water treatment,[39,40] photonics and optoelectronics,[41] electromagnetic interference,[42] joule heating,[2] and membranes[43] have been reviewed and reported in recent years. However, the works on MXene-based heterostructures and hybrid structures for multifunctional applications except for supercapacitors[44] have not been reported yet, despite showing exciting properties and applications in most of the above-mentioned areas. A careful review of the multilayer MXene (ML-MXene)-based heterostructures and nanohybrid is essential to understand the trends in this research area and the areas that require attention in the future to develop structures with superior stability and functionality.

This review provides a comprehensive insight into the structure−property−application relationship of MXene-based hybrid structures and the introductory discussion on MXenes to clarify the basic concepts behind the development. The first section of the work provides a brief discussion on the synthesis of MXene and its hybrid structures. The subsequent sections highlight the structural attributes of MXenes, the geometrical morphology of the MXene hybrids, and the effects on the properties. Later, the properties of the MXenes, i.e., electrical, mechanical, optical, and magnetic, are introduced. Subsequently, the applications of MXene hybrid/composites in energy storage, i.e., capacitors and batteries, sensing, catalysis for the environment, biomedical, and electromagnetic shielding, have been presented. The review presents a critical discussion on each section to identify the research gaps. Finally, the paper provides pressing challenges and possible solutions for future directions of multilayer-MXene hybrid research.

Subsequently, the applications of MXene hybrid/composites in energy storage, i.e., capacitors and batteries, sensing, catalysis for the environment, biomedical, and electromagnetic shielding, have been presented.

SYNTHESIS OF MXENE

MXenes are the class of transition metal carbide, nitride, and carbonitrides, synthesized by the selective etching of the "A" element in the MAX phase.[45] MAX particles are transformed into a loosely packaged accordion-like structure from the solid, dense state, resembling exfoliated graphite, and referred to as loosely formed, multilayer, or ML-MXenes flakes.[45,46] Figure 1 shows a periodic table with highlighted elements that commonly occur in the formation of MXenes. The chemical composition of MXene is generally represented by $M_{(n+1)}X_nT_x$, where "M" is an early transition metal, "A" represents the materials from the group 13 or 14 of the periodic table, and "X" indicates the carbon or nitrogen, so basically, these materials are nitrides and carbides. The molar ratio number, "*n*", usually means 1, 2, 3, or 5.[47] The surface chemical groups on MXene sheets are represented as "T". When "A" is etched from the MAX phase, "T" preserves the charge neutrality in MXene, which depends on the nature of the etchants. The compositions of "T" are currently F, O, and OH because of an F-contained etchant. It is predicted that around 70 MXene varieties can be prepared from the MAX phase or non-MAX phase.[48−50] The following section discusses the most significant MXene multilayer and hybrid multilayer formation methods.

Multilayer MXene. Two major routes explored for the synthesis of MXene are the top-down and the bottom-up approaches.[51] The top-down approach in MXene production refers to the process of reducing the size of bulk material/powder or removing part of the bulk structure to leave micro to nanometer particles.[48,49] On the one hand, selective etching and exfoliation are categorized as top-down processes. On the other hand, physical vapor deposition (PVD) and chemical vapor deposition (CVD) are categorized as the bottom-up processes.[51,52] The top-down approach is usually preferred for the preparation of ML-MXenes because the first successful selective etching of aluminum from Ti_3AlC_2 for the production of multilayer Ti_3C_2 was achieved with a top-down method. MXene synthesis begins with the etching of the MAX phase to replace element "A" (e.g., aluminum) atomic layer with surface termination groups such as −OH, −O, and −F to form the $M_{(n+1)}X_nT_x$.[53] Hydrogen and van der Waals bonds resulting from the etching process hold the layers of the MXene together.[54] Wet chemical etching with hydrofluoric acid (HF) synthesizes multilayered MXene flakes of different compositions such as Ti_2CT_x, $Ti_3C_nT_x$, Nb_2CT_x, and V_2CT_x.[46,55] Different structures of MXenes such as scrolls, nanotubes, and multilayer Ti_3C_2 were obtained following sonication in addition to nanosheets.[49,56] A synthesis map of $Ti_3C_2T_x$ using HF and in situ HF at room temperature and delamination methods are presented in Figures 1 and 2.[48,49,57]

Although HF is the primary etchant in the MXene fabrication processes, alternative etchants have been explored due to the highly volatile and hazardous characteristics of HF.[58] Molten salts,[46,59] alkaline solutions,[60,61] and hydrothermal treat-

https://doi.org/10.1021/acsmaterialslett.2c00175
ACS Materials Lett. 2022, 4, 1174−1206

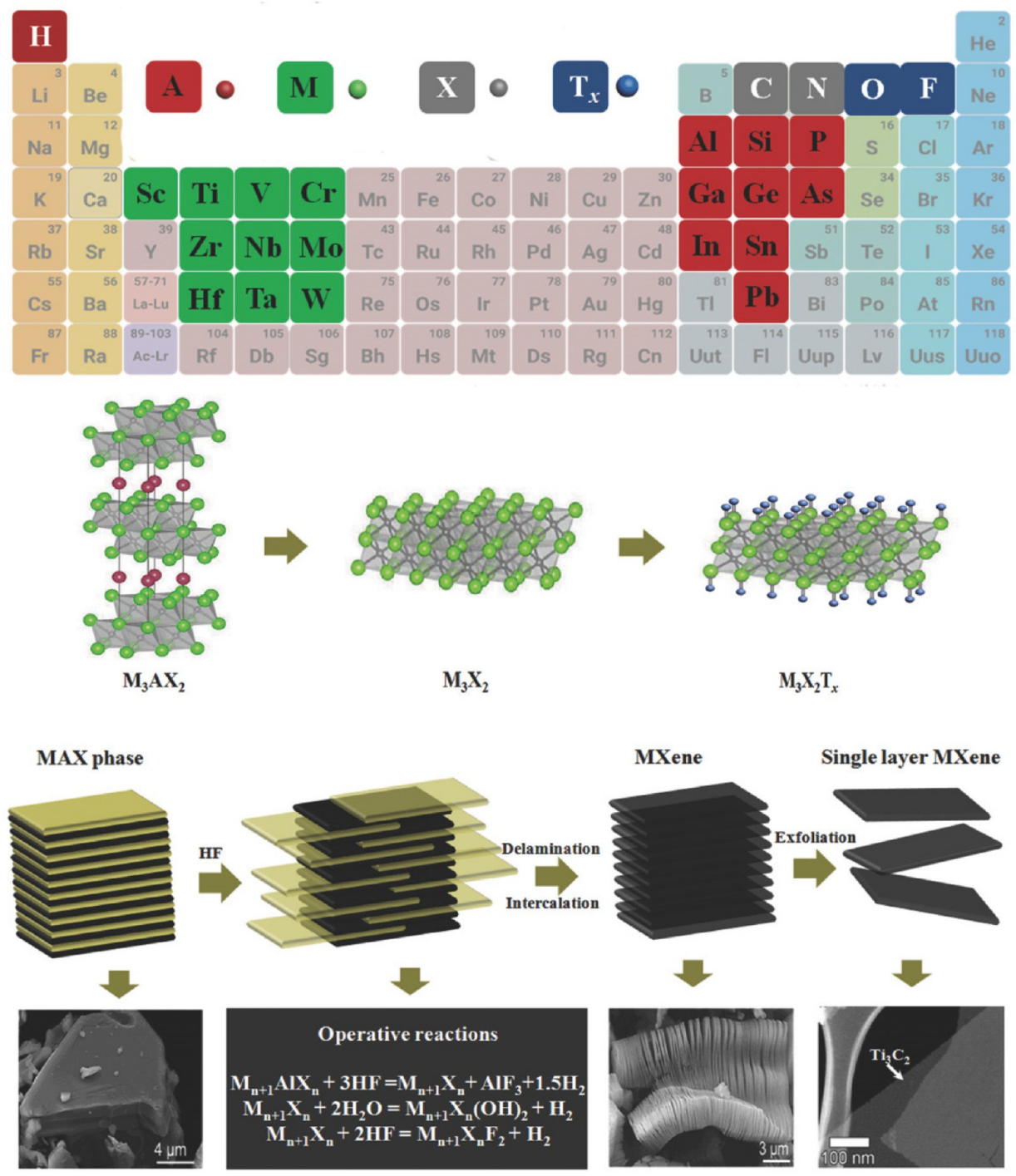

Figure 1. Periodic table with highlighted elements used in MAX processes and Schematic of MXene synthesis process using HF etchant. (Reproduced with permission from ref 56. Copyright 2018, WILEY-VCH Verlag GmbH & Co. KGaA.)

ment[60,62,63] widened the synthesis routes and the resultant properties. Bifluorides of potassium, sodium, and ammonium are the reported alternative etchants for selective etching of Al from Ti_3AlC_2.[58,64,65] However, HF-assisted synthesis of MXene causes intercalation of cations with fluoride or bifluoride salts and exhibits greater interlayer spacing. The interlayer spacing increases by the combination of HF and fluoride salts compared to the etching only with HF.[58,64]

A lower HF concentration (5−10 wt %) containing acid mixtures is used for in situ HF synthesis. To synthesize Mo_2TiC_2 and $Mo_2Ti_2C_3$ from the Mo_2TiAlC_2 and $Mo_2Ti_2AlC_3$ MAX phases, etchants based on HF/HCl are used.[66,67] For the LiF/HCl etching route, the molar concentration of the two reactants defines the required amount/concentration of HF, LiCl production, and remnant HCl. In situ HF etchants utilizing LiF/HCl yielded processable Ti_3C_2 MXene when an intercalant (Li^+) was introduced into the etchant solution. The concentration of H^+ exchanged with Li^+ is achieved by varying the concentration of exchanged cations which determines the intercalation mechanism of the LiF/HCl. However, the scalability of these methods is challenging due to the presence of unetched MXene during exfoliation.[55,68] Alkaline etchants

https://doi.org/10.1021/acsmaterialslett.2c00175
ACS Materials Lett. 2022, 4, 1174−1206

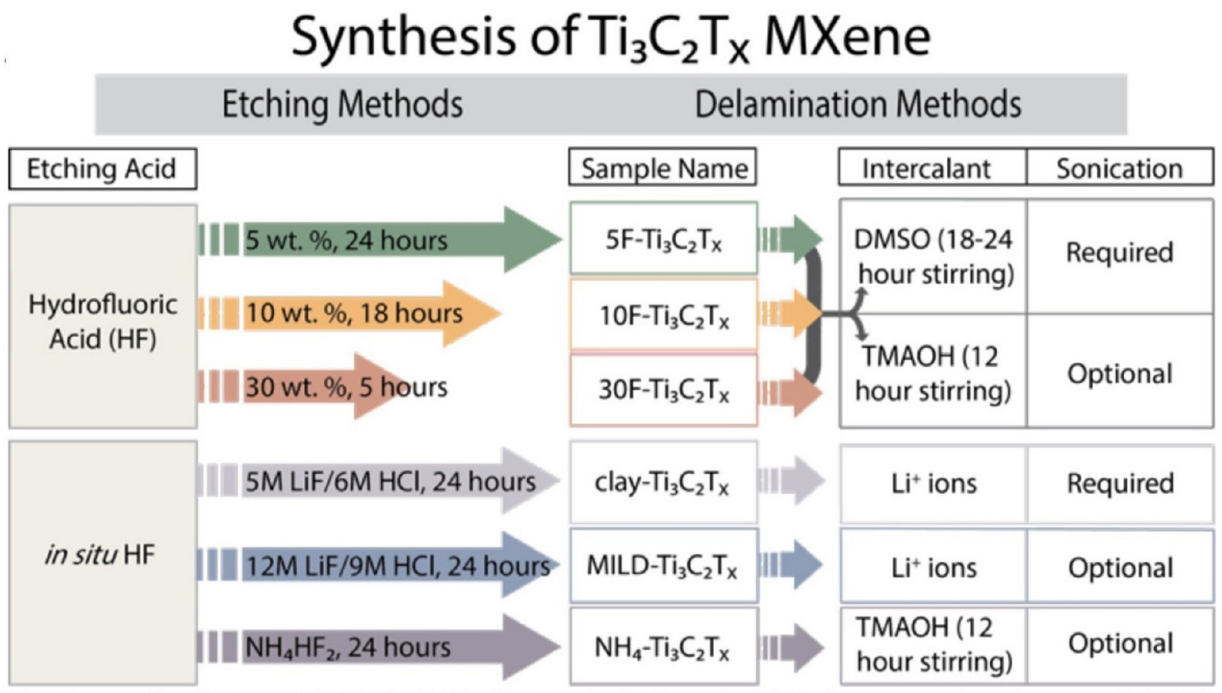

Figure 2. Etching with HF (top) and in situ HF (below). In the HF route, three different concentrations with different durations are used to synthesize $Ti_3C_2T_x$. (Reproduced with permission from ref 55. Copyright 2017, American Chemical Society.)

have the capability of etching Ti_3AlC_2 or other layered precursors utilizing suitable binding properties with Al. The removal of Al in alkaline conditions often involves hydrothermal treatment at higher temperatures or pressures.[46,59,69] Conventional HF aqueous acidic solutions are ineffective in etching nitride-based MAX phases. Therefore, the nitride MXene, especially Ti_4N_3, involves selective etching of Al from Ti_4AlN_3 by using molten salts such as potassium fluoride (KF), sodium fluoride (NaF), and lithium fluoride (LiF).[46,66] A list of different types of MXenes synthesized from various precursors and etchants is presented in Table 1.

Multilayer MXene Heterostructures and Nanohybrids. MXenes are thermodynamically metastable with great surface energy and a high percentage of exposed metal atoms present on the surface. These properties are negatively influenced by oxygen regardless of oxygen phases, even under ambient conditions.[90,91] MXene in the ambient atmosphere imparts new functionalities combined with different nanoparticles to produce hybrid MXenes.[92,93] Among different 2D materials, MXenes have exceptional surface tunability and adjustable physical and chemical properties, making them a promising material for hybridization. In particular, exfoliated 2D MXene hybrids with nanoparticles and polymers are utilizable as the base for constructing new functional hybrid materials.[56] The high surface-to-volume ratio, surface control, and outstanding electrochemical properties of MXene are beneficial for the applications of MXene hybrids.[69]

Combining the compatible components in a heterostructure material at the molecular level often leads to superior physical, mechanical, chemical, and electrochemical properties suitable for high-performance applications. These properties can be further improved by tuning the elemental compositions, morphologies, shapes, and molecular-level interactions/interfaces.[94,95] The broader spectrum of organic molecules and the existence of more than 20 compositions of MXenes with distinct properties exhibit the enormous potential of MXene heterostructures and hybrids. MXene hybrids and heterostructures with tunable shapes, properties, and morphologies can be synthesized by rationally choosing the MXene and components within a hybrid. ML-MXene hybrid synthesis can be categorized into organic molecules and polymer self-assembly,[96−98] oxidant-free monomer polymerization into polymers,[99−101] and covalent functionalization.[102−104] The complex molecular interaction such as $\pi-\pi$ stacking interlinkage, hydrogen bonds, and van der Waals interconnection between the organic functional group and the 2D solid-state materials dictates the self-assembled hybrid structure.[105,106] Polymerization of chemical oxidants requires the deposition of the conducting polymer in the existence of a host material, and the fabrication of conducting polymer hybrids requires monomer addition to the acidic solution of an oxidant.[66,68,107] In situ polymerization improves the dispersion of MXene in polymers, interfacial adhesion between MXene and the polymer matrix, and improvement in mechanical, electrical, and thermal properties. To initiate the polymerization process, an oxidant such as ammonium persulfate (APS) is used in the oxidative chemical deposition of polyaniline (PANI) on a substrate and the surface of various materials.[107] Several other methods including electrophoretic deposition (EPD),[108] ultrasonication treatment,[109] facile self-assembly process,[110] stirrings followed by vacuum filtration,[111] primitive calcination,[112] incubation,[87] and mechanical high-speed agitation[113] have also been reported. The mechanical agitation method involves a simple physical mixture and affects the dispersion and the interface. Table 2 summarizes the synthesis conditions and potential applications of the ML-MXene heterostructures and hybrids.

The stability of the MXene in a hybrid structure is critical for various applications and the long-term stability is determined by preventing oxidation. The degradation mechanisms differ depending on the type of MXene; for example, in the presence of water, Ti_3C_2 MXene degrades to a cloudy-white solution of

https://doi.org/10.1021/acsmaterialslett.2c00175
ACS Materials Lett. 2022, 4, 1174−1206

Table 1. Synthesis of ML-MXene with Different Etchants and Conditions

ML-MXene	precursors	etchants (time, temperature)	purpose/application	ref
Ti_3C_2	Ti_3AlC_2	5 wt % HF (24 h, RT)	optimization of synthesis parameters	55
		10 wt % HF (24 h, RT)		
		30 wt % HF (4 h, RT)		
Ti_2C	Ti_2AlC	13.5 M LiF in 6 M (15 h, 40 °C)	hybrid Li-ion battery (LIB)	70
Ti_3C_2	Ti_3AlC_2	34.5 M LiF in 10 M HCl (24 h, 35 °C)		
Ti_2C	Ti_2AlC	1.6 M FeF_3 in 6 M HCl (25 h, 50 °C)	performance of new etchants on MAX phases	71
Ti_3C_2	Ti_3AlC_2	2.3 M FeF_3 in 6 M HCl (24 h, 30 °C)		
Ti_2C	Ti_2AlC	21.5 M KF in 12 M HCl (24 h, 30 °C)	storage of natural gas	72
		21.5 M NaF in 12 M HCl (24 h,30 °C)		
		21.5 M NH_4F in 12 M HCl (24 h, 30 °C)		
Ti_3C_2	Ti_3AlC_2	31 M KF in 12 M HCl (24 h, 30 °C)		
		31 M NaF in 12 M HCl (24 h, 30 °C)		
		31 M NH_4F in 12 M HCl (24 h, RT)		
Ti_3C_2	Ti_3AlC_2	40 wt % HF (24 h, RT)	fabrication of Sn_4^+ ion decorated nanocomposites for Lithium ion battery (LIB)	73
Ti_3C_2	Ti_3AlC_2	50 wt % HF (2 h, 50 °C)	effect of HF solution on Ti_3AlC_2 powders	53
		50 wt % HF (10 h, RT)		
Ti_3C_2	Ti_3AlC_2	50 wt % HF (22 h, RT)	interaction of layered MXene	74
Ti_3C_2	Ti_3AlC_2	50 wt % HF (18 h, RT)	MXene for high volumetric capacitance	75
Ti_3C_2	Ti_3AlC_2	5 M LiCl in 6 M HF (24 h, 25 °C)	effects of the presence of LiCl during the chemical etching	76
Ti_3C_2	Ti_3AlC_2	1 M NH_4HF_2 (12 h, 60 °C)	etching with bifluoride ($NaHF_2$, KHF_2, NH_4HF_2) in single-stage process	64
		1 M $NaHF_2$ (12 h, 60 °C)		
		1 M KHF_2 (12 h, 60 °C)		
Ti_3C_2	Ti_3AlC_2	27.5 M NaOH (12 h, 270 °C)	fluorine-free method, e.g., alkali-etching strategy at high temperature	61
Ti_3C_2	Ti_3AlC_2	NH_4F, hydrothermal (24 h, 150 °C)	preparation by hydrothermal method and analysis of electrochemical properties	63
Nb_2C	Nb_2AlC	50 wt % HF (90 h, RT)	anode material for LIB	77
V_2C	V_2AlC	50 wt % HF (90 h, RT)		
V_2C	V_2AlC	3.35 M NaF in 12 M HCl (48 h, 90 °C)	preparation with NaF at high temperature as anode for LIB	78
Zr_3C_2	$Zr_3Al_3C_5$	1 M $NaHF_2$ (12 h, RT)	comparison between structural stability of $Zr_3C_2T_z$ and $Ti_3C_2T_z$ MXenes	79
		1 M KHF_2 (12 h, RT)		
Mo_2TiC_2	Mo_2TiAlC_2	50 wt % HF (48 h, 55 °C)	synthesis and analysis of $Mo_2TiC_2T_x$, $Mo_2Ti_2C_3T_x$, and $Cr_2TiC_2T_x$	80
$Mo_2Ti_2C_2$	$Mo_2Ti_2AlC_2$	50 wt % HF (96 h, 55 °C)		
Cr_2TiC_2	Cr_2TiAlC_2	5 M LiF in 6 M HCl (42 h, 55 °C)		
Nb_4C_3	Nb_4AlC_3	50 wt % HF (96 h, RT)	synthesis of phase-pure Nb_4C_3 with formula M_4X_3	81
$(Nb,Ti)_4C_3$	$(Nb,Ti)_4AlC_3$	50 wt % HF (90 h, 50 °C)	$Nb_4C_3T_x$ multilayer MXene for energy storage applications	82
		10 M LiF in 12 M HCl (180 h, 50 °C)		
Ti_3C_2	Ti_3SiC_2	30 wt % HF + (oxidant), e.g., (HNO_3, $KMnO_4$, $(NH_4)2S_2O_8$, or $FeCl_3$) (47 h, 40 °C)	oxidant-assisted selective etching of Si from Ti_3SiC_2	83
$Ti_3C_2T_z$	Ti_3AlC_2	10 wt % HF (24 h, 25 °C) + LiCl, LiBr, LiI	intercalation and deintercalation mechanism	84
		48 wt % HF + HCl, HBr, HI, H_3PO_4, or H_2SO_4		
Ti_3C_2	Ti_3AlC_2	40 wt % HF (48 h, 60 °C) + Ti_3C_2 calcinated high temp., 200−1200 °C	vacuum calcination for better electrochemical and thermal properties for LIB	85
$Ti_3C_2T_x$	Ti_3AlC_2	5, 10, and 30 wt % HF (24, 18, 4 h, RT)	thermal gravimetry and mass spectrometry up to 1500 °C under a He atmosphere	86
		5 wt % HF + H_2SO_4 (96 wt %, HCl (37 wt %)		
Nb_2CT_x	Nb_2AlC	50 wt % HF (48−120 h, 50 °C)		
Mo_2CT_x	Mo_2Ga_2C	50 wt % HF (48−120 h, 50 °C)		
$Ti_3C_2T_x$	Ti_3AlC_2	40% wt. HF + 30 min sonication and stirred (168 h, RT)	biomedical application with their biocompatibility, hydrophilic property	87
$Ti_3C_2T_x$	Ti_3AlC_2	6 M HCl + LiF (40 h, 45 °C)	humidity sensor	88
$Ti_3C_2T_x$	Ti_3AlC_2	9 M HCl + LiF (ice bath) (24 h, 35 °C)	exfoliation via water freezing method	89

titanium dioxide (TiO_2) anatase. Hybridization has the potential to improve the long-term stability of MXene.

The conducting polymer/monomers on the MXene surface are polymerized by oxidants such as ammonium persulfate and other oxidants. MXenes decompose into TMO-carbon hybrids with a high oxide load on the carbon sheets. The majority of MXenes oxidation research focuses on Ti-based compounds.[114] Wang et al.[115] reported hydrothermal oxidation of $Ti_3C_2T_x$ and applied the oxidized composite for photocatalysis. The electron microscopy image showed that heterogeneous TiO_2 nanoparticles nucleated to form a heterojoint structure on the surface of Ti_3C_2.[115,116] The sonication of dimethylformamide (DMF)-

https://doi.org/10.1021/acsmaterialslett.2c00175
ACS Materials Lett. 2022, 4, 1174−1206

Table 2. Synthesis Conditions for Different ML-MXene Heterostructure and Hybrid with Their Potential Application

ML-MXene	precursors	etchants (time, temperature)	hybrid synthesis method	purpose/application	ref
$Ti_3C_2T_x$-sodium alginate (SA)	Ti_3AlC_2	LiF in 6 M HCl (24 h, 35 °C)	self-assembly	electromagnetic interference (EMI) shielding	66
2D niobium carbide (Nb_2C)-PVP(polyvinylpyrrolidone)	Nb_2AlC	60 mL of a 50% HF (48 h, RT)	mixing	phototherapy of cancer	113
$Ti_3C_2T_x$/poly-EDOT (3,4-ethylenedioxythiophene) hybrids	Ti_3AlC_2	LiF (2 g) in HCl (9 M, 20 mL), 24 h, 35 °C	mixing	EDOT induced polymerization mechanism of charge-transfer	120
Ti_3C_2-DOX (doxorubicin hydrochloride)	Ti_3AlC_2	10 mL of 9 M HCl containing 1 g of LiF (72 h, RT)	mixing	biocompatible, tumor-specific effective cancer cell killing and tumor tissue destruction	121
$Mo_{1.33}C$ MXene- PEDOT:PSS (poly(3,4-ethylenedioxythiophene) polystyrenesulfonate)	$(Mo_{2/3}Sc_{1/3})_2AlC$	20 mL of 48% HF (24 h, RT)	mixing	ultrathin flexible solid-state supercapacitor	122
Ti_3C_2-PPy (polypyrrole)	Ti_3AlC_2	10 mL of 48% HF (8 h, 60 °C)	self-assembly	improve both PPy-based electrode capacity and cycle stability	123
$Ti_3C_2T_x$-SO_3H	Ti_3AlC_2	20 mL of 49% HF (72 h, 25 °C)	mixing	efficient proton transfer pathways for enhanced conduction	124
Ti_3C_2-LLDPE	Ti_3AlC_2	49% HF (24 h, 60 °C)	mixing	MXenes enhance the crystallization and kinetics of thermal degradation of LLDPE	125
$Ti_3C_2T_x$/PVA (poly vinyl alcohol) composites	Ti_3AlC_2	10 mL of 50 wt % HF solution (18 h, RT)	mixing	Raman spectroscopy	126
Ti_3C_2/UHMWPE (ultrahigh molecular weight polyethylene)	Ti_3AlC_2	100 mL of 49% HF solution for (24 h, RT)	mixing	morphology, structure, and properties of the Ti_3C_2/UHMWPE nanocomposites	127
$Ti_3C_2T_x$-PDAC (poly diallyldimethylammonium chloride)	Ti_3AlC_2	30 mL of 6 M HCl (45 h, 40 °C)	layer-by-layer (lbl) assembly	conductive coatings for wearable electronics and biometric sensors	98
$Ti_3C_2T_x$/PPy hybrids	Ti_3AlC_2	15 mL of 40 wt % HF solution (24 h, RT)	oxidative polymerization	high-performance electromagnetic wave absorption	128
polyaniline (PANI)-Ti_3C_2	Ti_3AlC_2	20 mL of 1 M HCl (6 h, 2 °C)	mixing	supercapacitor electrode material with high specific capacitance and excellent cycling stability	129
PANI@TiO_2/$Ti_3C_2T_x$	Ti_3AlC_2	3 M HCl (24 h, 180 °C)	self-assembly	hierarchical structure composite for next-generation electrochemical capacitors electrode	130
$Ti_3C_2T_x$/glycine hybrids	Ti_3AlC_2	LiF (2 g) stirred in 20 mL of 9 M HCl (24 h, 35 °C)	mixing	interaction mechanism of MXene, $Ti_3C_2T_x$, and amino acid-glycine on charge storage	103
pyrrole (C_4H_4NH) and $Ti_3C_2T_x$ hybrids	Ti_3AlC_2	20 mL of 9 M HCl (was added to 7.5 M (2 g) of LiF (2 h, 35 °C)	mixing	pyrrole intercalation, orientation, and metal-free polymerization on $Ti_3C_2T_x$ MXene	100
CNF (cellulose nanofiber) and $Ti_3C_2T_x$ hybrids	Ti_3AlC_2	2 g of LiF, 40 mL of 9 M HCl (24 h, 35 °C)	mixing	high-performance EMI films	131
MXene/MPFs nanosheets	Ti_3AlC_2	LiF (1.5 g), 30 mL of 9 M HCl (72 h, 60 °C)	mixing	flexible supercapacitor	132
Silver nanowire (AgNW) and MXene nanosheets	Ti_3AlC_2	LiF (3.2 g), 40 mL of 9 M HCl (24 h, 35 °C)	mixing	lightweight EMI shielding materials	133
MCF(MXene/C hybrid foam) and MCF/epoxy	Ti_3AlC_2	3.6 g LiF, 40 mL of 9 M HCl (24 h, 35 °C)	mixing	EMI shielding	134
PDMAEMA (poly dimethylamino ethyl methacrylate)-Ti_2CT_x hybrid	Ti_3AlC_2	10 mL of concentrated HF (40%) (24 h, 80 °C)	mixing	temperature sensing	135
Cu-$Ti_3C_2T_x$	Ti_3AlC_2	40% 50 mL HF (24 h, 60 °C)	mixing	all-solid-state super- capacitor	136
$Ti_3C_2T_x$-rGO (graphene oxide) hybrids	Ti_3AlC_2	1.0 g of LiF in 20 mL of 12 mol/L HCl (24 h, 35 °C)	self-assembly	high temperature and fire-resistant thermoplastic polyurethane elastomer (TPU)	137
$Ti_3C_2T_x$ and Ni nanochain hybrid	Ti_3AlC_2	2 g of LiF, 40 mL of 9 M HCl (24 h, 35 °C)	mixing	EM wave absorption and shielding	138
SnS_2/Sn_3S_4-Ti_3C_2 hybrid	Ti_3AlC_2	40 mL of 45% HF (72 h, 25 °C)	self-assembly	facile solvothermal and calcination process	139
MoS_2@$Ti_3C_2T_x$ MXene hybrid	Ti_3AlC_2	48% 50 mL of HF (24 h, RT)	mixing	electrochemical apt sensor (MEA) for sensitive and rapid quantification of thyroxine (T4)	116

intercalated MXene and other materials (e.g., graphene oxide [GO]) in deionized (DI) water followed by centrifugation results in the MXene-hybrid dispersion.[117,118] Yan et al.[119] reported the hybrid electrode films via electrostatic self-assembly of the MXene/rGO (reduced graphene oxide). The diallyl dimethylammonium chloride (G-PDDA) suspension was injected into the MXene solution under stirring and later exposed to a sonic probe.[119]

Structure and Intercalation of Multilayer MXene. Besides the surface termination group, intercalation significantly affects the properties of the MXene. Water, organic molecules, and metal ions are commonly intercalated into MXene and play a remarkable role in tailoring the functionality of MXene. On the one hand, organic molecules improve the electrochemical capacitance, while water intercalation surges the interlayer spacing, and surface absorption and also influences the gas transport behavior.[51,140−146] Simulation shows the effect of different termination groups on altering the bandgap and the Fermi level of MXene.[147] On the other hand, exposure of the "M" metal to the air decreases the dimension of the structure.[49] Modification of the surface porosity and microstructure using the heteroatoms leads to higher performance.[148] A higher surface area is advantageous for the fabrication of energy storage and advanced electrode materials.[149]

To achieve a single atomic layer in 2D, material delamination is done. Different procedures can be followed to delaminate the

https://doi.org/10.1021/acsmaterialslett.2c00175
ACS Materials Lett. 2022, 4, 1174−1206

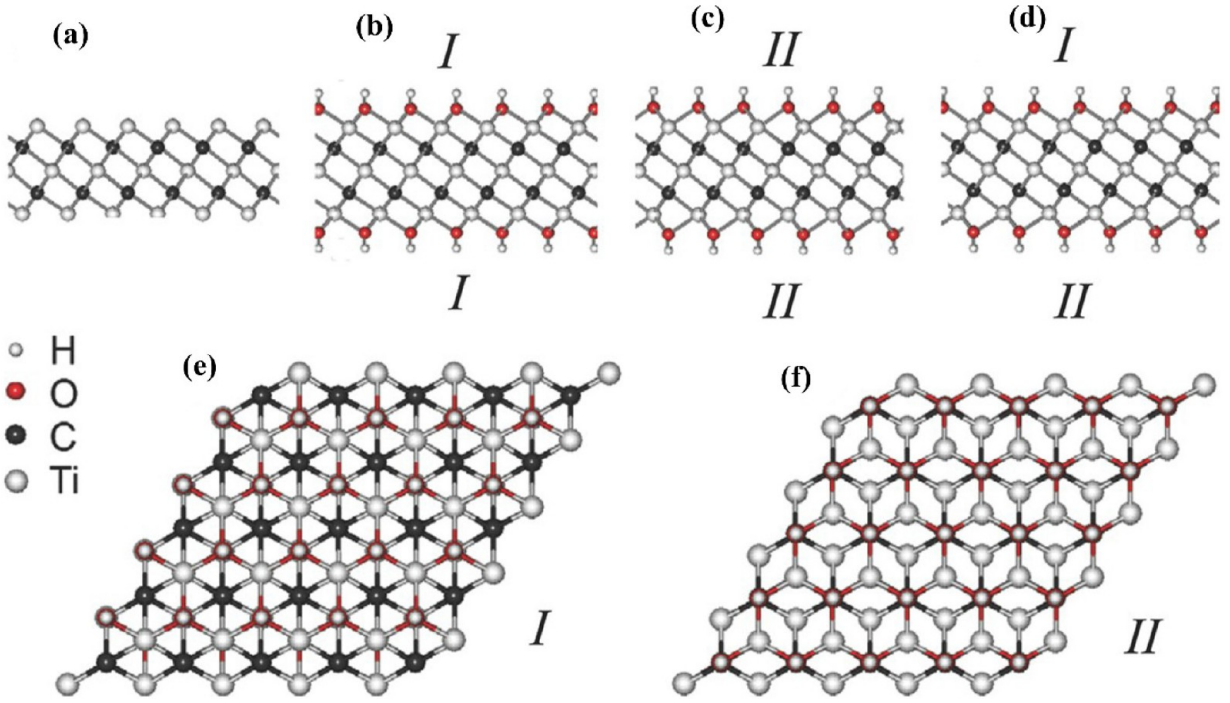

Figure 3. Surface atom arrangements of functionalized MXenes in various configurations: (a) pure Ti_3C_2, (b) I-$Ti_3C_2(OH)_2$, (c) II-$Ti_2C(OH)_2$, and (d) III-$Ti_3C_2(OH)_2$ (combination of b and c). Top views of (e) I-$Ti_3C_2(OH)_2$ and (f) II-$Ti_3C_2(OH)_2$. (Reproduced with permission from ref 29. Copyright 2013, WILEY-VCH Verlag GmbH & Co. KGaA.)

multilayer structure, i.e., mechanical cleavage, chemical intercalation and exfoliation, and liquid exfoliation.[150,151] The delaminated $Ti_3C_2T_x$ shows uneven edges, tiny dark particles on the surface, and the size decreases incrementally. The particle may be partially oxidized, and the vacancies progressively become holes on the surface that lead to strength loss.[152,153] The defects in MXene batteries react irreversibly with the cations and lower the initial Coulombic efficiency. In turn, this affects the conductivity of MXene.[154,155] In contrast, atomic defects like vacancies and antisites in 2D materials can alter the electronic behavior, leading to changes in the electronic structure as well as optical and magnetic properties. Defects in ML-MXenes become more challenging to examine due to the increased number of atoms over the material.[156]

Intercalation and surface group modification enhance the performance and capacitance of the MXene sheets as an electrode material. Cation intercalation improves the gravimetric capacitance in $Ti_3C_2T_x$, whereas controllable surface modification exploits the energy storage capacity. Termination in the presence of low terminal group concentration results in a higher redox reaction on the surface of $Ti_3C_2T_x$ and increases the capacitance.[157,158]

CHARACTERIZATION OF STRUCTURAL GEOMETRY OF MULTILAYER MXENE

The first structure of ML-MXenes was proposed as a stacked Ti_3C_2 layer at the OH end based on density functional theory (DFT) simulations.[74,159] Using the X-ray diffraction (XRD) pattern, researchers determined that the empirical C parameter value of the geometrically optimized structure of the fully hydroxylated MXene corresponds to the experimental finding. Therefore, the presence of hydroxyl and fluorine in combination cannot be ruled out. The accordion-like expanded structure normally observed in scanning electron microscopy (SEM) should not be taken as the only indication of effective etching of Al from MAX phases, and thus selective etching should be verified by both XRD and energy dispersive X-ray analysis (EDX) analyses.[29,84] Morphology of MXene MAX phase powder represents MXene multilayer powder produced with a lower HF concentration. In this particular case, selective removal of Al can be confirmed by the absence of the MAX phase (e.g., Ti_3AlC_2) peak in the X-ray diffraction pattern.[55]

Mixed surface termination groups, such as −F, −OH, and −O, affect the stability of MXene, which is exacerbated by the possibility of the presence of water molecules in the interlayer space between the layers. DFT investigations have revealed the existence of two orientations that are energetically advantageous for T in $Ti_3C_2T_2$. $Ti_3C_2T_2$ undergoes two different configurations (Figure 3). A hybrid arrangement (configuration III, Figure 3d) of configuration I and configuration II, as opposed to each other, is frequently explored in situations when one or both of the configurations are incompatible.[159,160] To determine the structural stability of distinct $Ti_3C_2F_2$ and $Ti_3C_3(OH)_2$ configurations, relative DFT simulations are used to compare the results as total energy diminishes in the order of I > III > II. Therefore, both the −F and −OH groups are more likely to use configuration I than the other groups. The steric repulsion between T groups and C atoms causes the lowest structural instability in configuration II, which is the most stable configuration. During geometry optimization, another possible configuration in which T terminations are bonded just above the Ti(1) atoms of Ti_3C_2 is unstable and regularly switches from configuration I to configuration III. The stacking of the layers, as well as the intermediate materials between them, has a considerable impact on the framework's energy efficiency.[29,159]

The molecular level combination of compatible materials into a hybrid enhances physical, mechanical, chemical, and electrochemical properties.[161] Additionally, molecular-level interac-

https://doi.org/10.1021/acsmaterialslett.2c00175
ACS Materials Lett. 2022, 4, 1174−1206

tions/interfaces, morphologies, and shapes can be changed by tuning the chemical compositions. The intercalation of polymers/organic molecules/metal oxide/2D materials (e.g., graphene) between multilayer MXene is end-group dependent as demonstrated by XRD patterns of different hybrids.[62] Furthermore, self-assembly of the hybrid MXenes is possible due to the electrostatic interaction between the positively charged side chain functional groups of the polymer/organic compound and the negatively charged layered MXene sheets.[55,62]

Electrical Properties. MXenes have good electronic properties, thanks to the availability of narrow band gaps and demonstrate excellent conductivity resulting in fast charge transfer.[90,162,163] Generally, MXene has a conductivity ranging from 1 to a few thousand S cm^{-1}.[164] For instance, the electrical conductivity of $Ti_3C_2T_x$ can exceed 2000 S cm^{-1}.[165] The multilayered $Ti_3C_2T_x$ increases the contact between electrode and electrolyte and increases the electron transfer rate due to Ti−C bare layers that enhance the interfacial interaction between the electrolyte and electrode and result in better electrochemical energy storage.[139] In lithium-ion batteries (LIBs), the multilayered $Nb_4C_3T_x$ showed a better capacity and cycling performance resulting from large interlayer spacing after etching.[166] Large interlayer spacing and specific surface area can be obtained by exfoliating multilayered MXene to a few layers or a single-layer structure.[29]

Moreover, MXenes showed metallic properties with a high density of state when the surface was not terminated. The outer surface of the transition metal plays an essential role in the electronic behavior of MXenes than the inner surface.[167] Replacing the two exterior transition metals of $Ti_3C_2T_x$ with $Mo(Mo_2Ti)C_2T_x$, electronic properties changed from metallic to a semiconductor.[168] Resistance of the $Mo_xV_{4-x}C_3$ increased with the decrease in the Mo content; however, the resistivity showed a significant change with the rise in temperature.[169] Electrochemical impedance spectroscopy of pristine Ti_3C_2, alkalized Ti_3C_2, and sulfur decorated Ti_3C_2 MXenes showed that the consumption of the sulfur group had a better electronic contact upon sodiation/desodiation. The merged resistance of sulfur decorated MXene was simulated and the lowest value of 202.4 Ω was reported.[170]

Mechanical Properties. MXenes have high mechanical strength, excellent flexibility, dimensional stability, and flame retardancy.[134,164,171,172] As in the electrical properties, surface termination processes also alter the mechanical properties of MXenes.[167] The matrix interface bonding is improved by the functional groups, which results in improved properties of bonding and electrical conductivity in polymer composites.[172] The integration of MXene to polymer matrix or epoxy-based composites improves the mechanical properties.[164,173] For MCF (MXene coated cotton fabric), the addition of $Ti_3C_2T_x$ increased the cell density and improved the mechanical properties like Young's modulus and hardness of fiber due to the cross-linking. This also enhanced the EMI shielding performance of MCF.[134] It is reported that some mechanical properties like toughness, flexural strength, and hardness are increased by 300%, 150%, and 300% respectively in the 2 wt % composite of $Ti_3C_2T_x/Al_2O_3$.[174] For a 5 vol % composite of $Ti_3C_2T_x$/Cu, the tensile strength increases by 40%.[172] PVC has a tensile strength of 20.8 MPa, but in PVC/MXene composites it is found that it increases by 21.73%, 51.53%, 156.73%, 173.55%, and 174.08% with the addition of 2, 4, 8, 10, 15 wt % of MXene, respectively. The same thing happens for Young's Modulus, which increases by 1.64, 18.3, 173.62, 177.47, and 177.19%.[175] The TPU (thermoplastic polyurethane)/MXene shows improvement in tensile strength and elongation at break with a 0.5 wt % composition of MXene. The elongation at break increases by 15.4% and tensile strength by 41.2%.[176] Another study shows that an MXene/CNF composite indicates a nacre-like structure, which shows a variation in the mechanical properties with a change in the content of d-$Ti_3C_2T_x$. However, for an optimal value of 50 wt %, 135.4 ± 6.9 MPa, 16.7 ± 0.7%, 14.8 ± 0.4 MJ/m3, and 3.8 ± 0.3 GPa are found as tensile strength, fracture strain, toughness, and Young's Modulus, respectively. The composite of 40 × 15 mm dimensions can withstand a weight of ∼500 g without breaking.[177] The MXene composite with PSZ (polysilazane) and ABN (aggregated boron nitride) shows another improvement in tensile strength. Without the presence of MXene in the composite MXene-PSZ, the tensile strength is 4.22 MPa while with MXene that number increases to 6.20 MPa, an increase of 147%. MXene-PSZ-ABN/PVA shows a 283% increase to 11.96 MPa.[178] However, filler material content higher than the threshold value may degrade the mechanical properties and cause processing issues.

Optical Properties. MXenes show a plasmonic resonance suitable for laser science.[179] The capability of demonstrating second harmonic generation, Kerr effect, optical ratification, and saturable absorption are essential for compact, high-power, and ultrafast femtosecond pulsed lasers.[180] The formation of a hybrid surface oxide layer with $Ti_4N_3T_x$ MXene showed visible light absorption at energies greater than 2.0 eV.[181] The $Ti_3C_2T_x$ demonstrated 77% of transmittance with visible light at 550 nm and increased to 90% when intercalated with NH_4HF_2. In contrast, the transmittance value for the thin film of the Ti_3AlC_2 MAX phase is 30%. The absorbance showed a linear relationship with the thickness of the intercalated film of $Ti_3C_2T_x$. The imaginary part of the dielectric function tensor or function of the photon wavelength is used to evaluate absorption, reflection, and transmittance. The plasmonic energy is estimated to be 10, 11.63, 10.81 and 11.38 eV for Ti_2C, Ti_2N, Ti_3C_2 and Ti_3N_2, respectively, using the reflectivity and energy loss curve.[182] 2D $Ti_3C_2T_x$ shows a superior electromagnetic wave absorption capacity, making it ideal for light to heat conversion devices. The localized surface plasmon resonance effect renders ultrathin $Ti_3C_2T_x$ nanosheets with higher adsorption and conversion efficiency of near-infrared laser irradiation.[149]

Magnetic Properties. Spin-polarized density functional calculations showed the nonmagnetic behavior of MXene at the ground state. This phenomenon originated from the strong covalent bond between the metal, the "X" element, and the attached group. The previous transition metals in MXenes have a lower number of valence electrons that resulted in limited unpaired electron spins and are the key reason for the nonmagnetic properties of such MXene.[183] External strain alters the covalency of the bonds, which showed a release in the "d-orbital" electron. As a result, magnetism can appear even in the absence of the magnetic system.[182]

The magnetic behavior of MXenes depends on the d-orbital of the transition metal atom. There are bonding σ and an antibonding σ^* states in the M−X, and M−T bonds. Under oxidation, the antibonding conditions remain unfilled. So, the only electron in the nonbonding d-orbitals remains responsible for the magnetic behavior.[184] The pristine monolayer Ti_2X (C, N) (like Ti_2C, Ti_2N) showed a magnetic behavior due to the third electrons present on the surface of the Ti atom.[185−187] Cr_2C is the first in the MXene family to have half-metallic

https://doi.org/10.1021/acsmaterialslett.2c00175
ACS Materials Lett. 2022, 4, 1174−1206

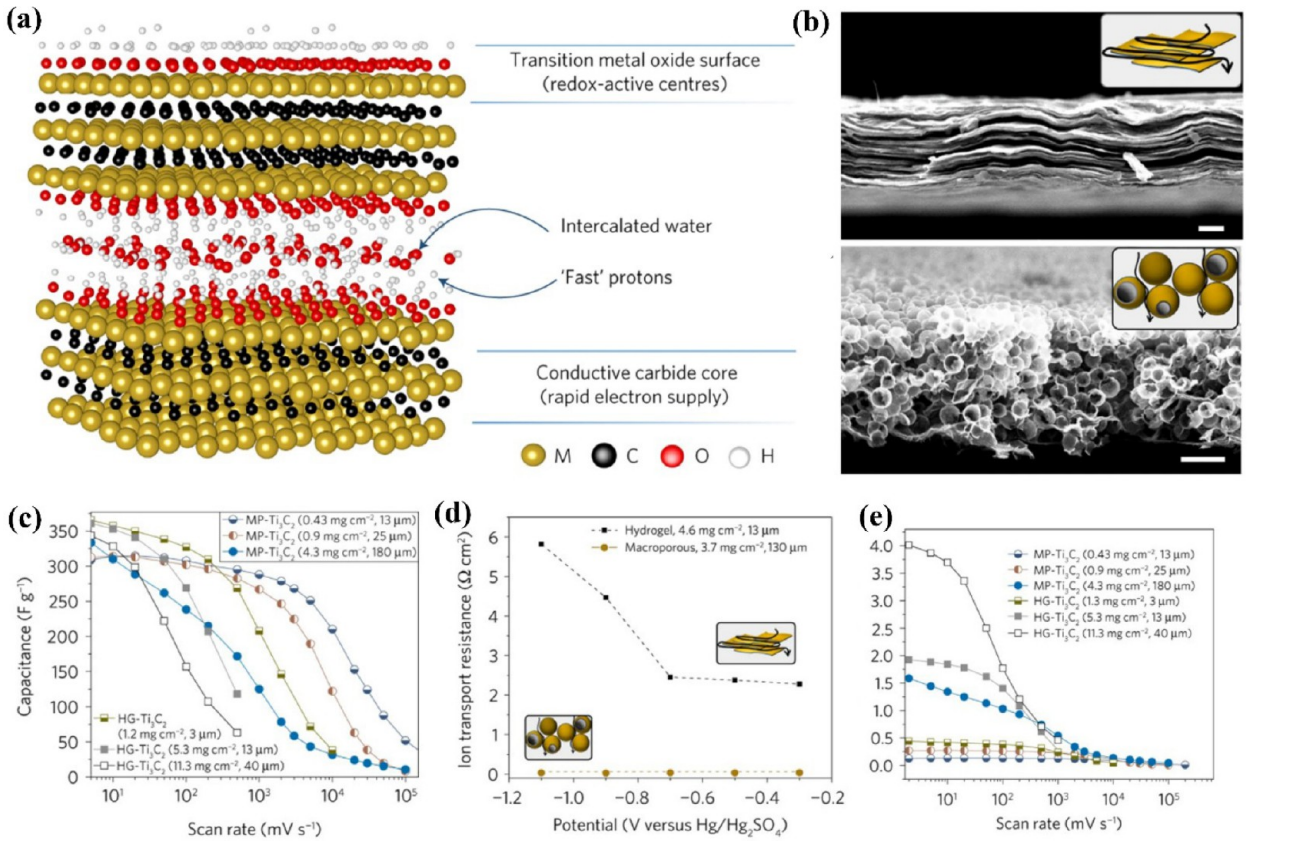

Figure 4. (a) Illustration of MXene structure. (b) SEM image of a cross-section of $Ti_3C_2T_x$ ML-MXene and microporous templated $Ti_3C_2T_x$ electrode (scale 5 μm). (c, d, and e) Rate performance of different MXene films and mass loadings represented in gravimetric and areal capacitance between the hydrogel and microporous MXene. (Reproduced with permission from ref 203. Copyright 2017, Springer Nature.)

behavior for its metallic spin-up channel and an insulating spin-down channel in the structure.[185] Other research indicated that functional groups inhibit the ferromagnetic properties of MXene.[188] Wang et al. stated that if the tensile strain is increased regularly, the magnetic moment increases, and the transition in ferromagnetism from nonmagnetism is observed.[189] Yue et al. found that the magnetic moments of Fe_2C are a total of (3.95 μ_B). This moment comes from the Fe site, which is 1.96 μ_B, and the adjacent C atoms are polarized antiferromagnetically with a moment of −0.10 μ_B.[190] For the Mn centered double transition MXene, it was found that the moment value is up to 4 μ_B per unit cell and the Curie temperature is 1133 K for single-metal MXene.[191,192] As mentioned earlier, surface termination also dictates the magnetic behavior. Lv et al. have predicted that unterminated Cr_2C is a ferromagnetic half-metal, and both properties are lost upon termination.[193] This same behavior was observed for Cr_7FeC_4. Before termination, Cr_7FeC_4 is metallic and after termination with O, the resultant $Cr_7FeC_4X_8$ becomes half metal. On the other hand, doping with Fe, the bandgap of $Cr_8C_4F_8$ decreased but remained as a bipolar antiferromagnetic semiconductor.[194] In other cases, it was found that a transition metal having more valence electrons can increase the magnetic moment. Other research also found that Fe_2C shows more robust ferromagnetic ordering than Ti_2C, where Fe has more valence electrons than Ti.[190] Bae et al. performed PBE+U, SCAN, and HSE06, and they found V_2CO_2, V_2CF_2, and Mo_2CF_2 to be magnetic.[195] Research on Zr_2N showed a max of 1626 μeV per cell magnetic anisotropy energy if the strain value is 2%. The value is 203 μeV for Zr atoms, which is greater than Co(65 μeV) in bulk. This indicates that the Zr_2N has a greater magnetic behavior.[196]

Supercapacitor. Electrochemical energy storage devices, such as the supercapacitor (SC), have gained attraction with the global energy demand for hybrid vehicles and flexible electronics. SCs store energy on the electrode surface through electrosorption of charge carrier ions.[197,198] 2D materials have an atomic thickness, ample active surface sites, and excellent mechanical properties ideal for the electrode material of SCs.[157,197] MXenes have shown superior super capacitance, thanks to the outstanding conductivity, large specific surface area, and available redox sites.[157] MXene multilayer and hybrid multilayer capacitance have been explored using the electroactive redox pseudocapacitance characteristics, embedding ability, and conductivity characteristics to improve energy storage capacity.[199] Because of the fast redox (pseudocapacitive) surface storage process, devices are capable of storing more energy than electrical double-layer capacitors (EDLCs). Furthermore, the high capacitance of ML-MXene electrode materials leads to an increase in the energy density and cyclic ability of SCs. Because of its high electrical and thermal conductivity, $Ti_3C_2T_x$ is predicted to be a suitable choice for solid-state SCs according to theoretical projections.[152,199,200] The thin-film electrodes used in conventional SCs are typically sandwich structures, and the in-plane architecture will open the door to further downsizing.[201] The in-plane configuration of the electrode array offers significant advantages over traditional sandwich structures and fiber-based structures. Accessibility to the edges of the electrodes to the electrolyte results in ultrahigh power density superior to that of batteries and traditional

https://doi.org/10.1021/acsmaterialslett.2c00175
ACS Materials Lett. 2022, 4, 1174−1206

Table 3. Progress in Multilayer MXene and Their Heterostructures-Based SC with Related Parameters

ML-MXene and ML-hybrid MXene	electrode type	electrolyte	rate	capacity retention	cycle number	volumetric capacitance	ref
$Ti_3C_2T_x$	macroporous electrode	3 M H_2SO_4	10 V s^{-1}	210 F g^{-1}	10000	1500 F cm^{-3}	203
V_2C	sheet-like free-standing electrode	1 M Na_2SO_4	2 mV s^{-1}	164 F g^{-1}	10000	–	205
V_2CT_x	film electrode	seawater	2 A g^{-1}	181.1 F g^{-1}	5000	317.8 F cm^{-3}	204
$Ti_3C_2T_x$-G	hybrid films-like electrode	3 M H_2SO_4	2 mV s^{-1}	–	20000	1040 F cm^{-3}	119
$Ti_3C_2T_x$-MPFs	hybrid films-like electrode	3 M H_2SO_4	1 mA cm^{-3}	–	30000	694.2 F cm^{-3}	132
TiO_2/C-$Ti_3C_2T_x$-MXene/NiO	free-standing electrode	1 M KOH	1 A g^{-1}	92.0 mA h cm^{-3}	5000/58.6%	–	93
Ti_3C_2/CNTs	hybrid films-like electrode	6 M KOH	1 A g^{-1}	134 F g^{-1}	10000	–	108
$Ti_3C_2T_x$-MgO (expanded MXene)	sheet-like free-standing electrode	1 M KOH	1 A g^{-1}	180 F g^{-1}	8000/87%	203 F g^{-1}	208
Co_3O_4-MXene/rGO	hybrid films-like electrode	6 M KOH	1 A g^{-1}	345 F g^{-1}	10000/90%	–	209
d-$Ti_3C_2T_x$	binder-free film electrodes	1 M KOH	1.5 A g^{-1}	140 F g^{-1}	10000	–	210
Nb_2CT_x/CNT	hybrid films-like electrode	1 M H_2SO_4	5 A g^{-1}	–	5000/80.3%	–	211
$Ti_3C_2T_x$/BC composites	porous electrodes	1 M H_2SO_4	30 mA cm^{-2}	416 F g^{-1}	10000/96.5%	2084 mF cm^{-2}	212
Ti_4C_3	free-standing electrode	0.1 M H_2SO_4	1 V s^{-1}	–	2000/89%	520 F cm^{-3}	213
Ti_3C_2	three-electrode system	1 M H_2SO_4	1 A g^{-1}	517 Fg^{1-}	10000/99%	550 F g^{-1}	157
Ti_2CT_x	porous electrodes	30 wt % KOH	1 A g^{-1}	51 F g^{-1}	6000/86%	–	92
$Ti_3C_2T_x$	three-electrode system	3 M H_2SO_4	0.5 A g^{-1}	351 F g^{-1}	10000/90.5%	1142 F cm^{-3}	152
PPy/Ti_3C_2	polymer-based free-standing flexible electrodes	0.5 M H_2SO_4	10 mA cm^{-2}	126 F g^{-1}	20000/70%	406 F cm^{-3}	123
p-C_3N_4/ Ti_2CT_x	hybrid films-like electrode	6 M KOH	1 A g^{-1}	327 F g^{-1}	5000/96.2%	–	214
Ti_2CT_x-GO	hybrid films-like electrode	1 M H_2SO_4	1.5 A g^{-1}	–	3000/90%	586.4 F cm^{-3}	117
TCBOC/$Ti_3C_2T_x$	three-electrode system	1 M H_2SO_4	1 A g^{-1}	–	5000/85%	396.5 F cm^{-3}	215
NiO/C- $Ti_3C_2T_x$	porous electrodes	1 M KOH	1 A g^{-1}	51 F g^{-1}	5000/72.1%	60 F cm^{-3}	93

SCs.[201,202] Lukatskaya et al.[203] reported that the proper design of electrodes could bring MXene capacitance closer to its theoretical limit. For example, macroporous electrode structures allow outstanding capacitance retention even at charge−discharge rates above 1 V s^{-1}, i.e., 210 F g^{-1} at 10 V s^{-1}, better than hydrogel-based electrodes (Figure 4).[203]

Apart from electrode design, different etching processes also affect the specific capacity by forming different functional groups on the MXene surface. Superior electrochemical performance of V_2CT_x (etching Al layers from the V_2AlC MAX phase using NaF +HCl at 90 °C for 72 h) has made this preferable as an SC electrode to other MXenes and used as an SC electrode in adequate seawater electrolytes. V_2CT_x MXene is thinner than $Ti_3C_2T_x$, resulting in higher ion diffusion speeds.[204] For example, an etching process with a combination of lithium fluoride (LF) and HCl acid was used to successfully synthesize high-purity V_2C.[205] The uniform multilayer structure of V_2C showed a higher capacity after 10 000 cycles, good cycle stability, and a 90% specific capacity retention rate. However, V_2C's capacitance gradually decreased with increasing scan rates because of incomplete penetration of the electrolyte within a short time. The combination of the 2D conductive carbide layer and hydrophilic hydroxyl-terminated surface facilitated excess capacitance of 300 F cm^{-3}, higher than that of porous carbon. This higher capacitance of MXene is further enhanced by the intercalation of various cations like Na^+, K^+, NH_4^+, Mg^{2+}, and Al^{3+}.[75]

However, pure multilayer MXene is easy to collapse and pile up, affecting the performance and stability of electrode material for SCs. Intercalation, doping, or composite of MXene improve the electrochemical performance of SCs.[93,206] Two methods have been discussed to avoid the restacking of $Ti_3C_2T_x$-MXene layers: a straightforward hard templating technique and a pore-forming approach. Furthermore, to overcome the limitations of the SC, different modifications and hybridizations have been performed along with the design as listed in Table 3.

A multilayer MXene-based hybrid electrode for SC was prepared by the electrophoretic deposition (EPD) method. The EPD method produces a strong binder-free Ti_3C_2/CNTs composite film, preventing the restacking of MXene nanosheets and improving electrochemical performance.[108] For SCs, negatively charged MXene nanosheets and charged reduced graphene oxide (rGO) nanosheets were used for electrostatic self-assembly to fabricate a highly conductive film SC.[119] The hybrid structure as self-restacking of MXene multilayers increased interlayer spacing and facilitated the rapid diffusion and transport of electrolyte ions. The fabricated SC demonstrated superior performance with an ultrahigh volumetric energy density of 32.6 Wh L^{-1}. The symmetric SC also exhibited a maximum volumetric power density of up to 74.4 kW L^{-1}.[119,207] As flexible free-standing electrodes, hydrogen-bonded MXene, $Ti_3C_2T_x$, and 2D metal-porphyrin frameworks (MPFs) hybrid films were proposed to overcome the low conductivity and low structural stability of 2D MPFs. The synergistic effect of MXene ($Ti_3C_2T_x$) and MPF resulted in larger interlayer spacing, "MPF to MXene to MPF" interconnected conductive network, and complete utilization of active sites. This facilitated the rapid migration of ions and electrons and reduced the electrolyte migration path of ions (Figure 5a−c).[132]

Metal oxide-based $Ti_3C_2T_x$ MXene showed higher conductivity and a larger specific surface area, which are of great importance and considered the main factors in improving SC efficiency. By a simple and efficient hydrothermal process, NiO nanosheets were effectively formed on the surface of $Ti_3C_2T_x$ MXene in a highly hierarchical porous honeycomb-like structure

https://doi.org/10.1021/acsmaterialslett.2c00175
ACS Materials Lett. 2022, 4, 1174−1206

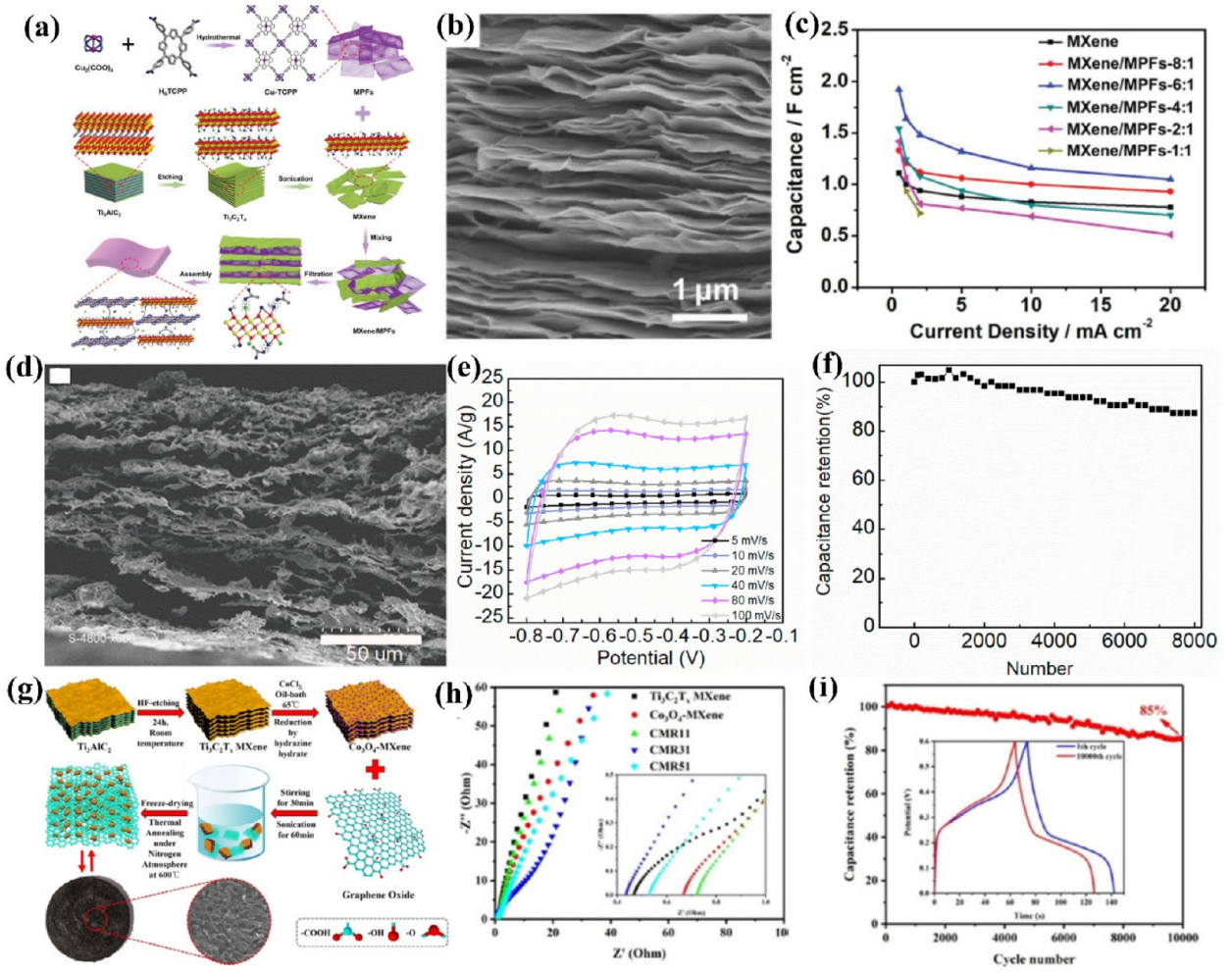

Figure 5. (a) Synthesis of interlayer hydrogen-bonded MXene/MPFs films is illustrated in this diagram. (b) SEM images (cross-section) of MXene/MPFs film. (c) MXene and MXene/MPFs areal capacitances in various ratios. (Reproduced with permission from ref 132. Copyright 2019, WILEY-VCH Verlag GmbH & Co. KGaA.) (d) SEM image shows crumped layer-like morphology MgO-expanded MXene. (e) CV curves for different scan rates. (f) Cyclic capacity for 8000 charge−discharge cycles at current rate 5 A g^{-1}. (Reproduced with permission from ref 208. Copyright 2020, Elsevier Ltd.) (g) Step-by-step preparation of the Co_3O_4-MXene/rGO hybrid porous material is depicted in this diagram. (h) Nyquist plots of $Ti_3C_2T_x$ MXene and Co_3O_4-MXene and Co_3O_4-MXene: rGO (CMR) with different percentage ratio electrodes on the EIS. High-frequency range is shown in the inset. (i) CMR31 electrode's cycling stability was tested over 10 000 cycles at 3 A g^{-1}. The CV curves recorded at the 1st and 10 000th cycles are shown in the inset. (Reproduced with permission from ref 209. Copyright 2019, Wiley-VCH Verlag GmbH & Co. KGaA.)

by Xia et al.[93] The Ni-dMXNC (TiO_2/C-$Ti_3C_2T_x$-MXene/NiO) electrode showed a great specific capacity of 60.7 mA h g^{-1} at a high current rate of 1 A g^{-1}, corresponding to 92.0 mAh cm^{-3} volumetric specific capacity and a reasonable rate of retention capacity.[93] The open morphology of the expandable MXene multilayer, which was created utilizing metal oxide (MgO) nanoparticles as rigid templates, was based on crumpled layers (Figure 5d−f). As the volume of active expanded electrode materials was considered, the volumetric energy density reached 10 W h L^{-1}. The device capacitance gradually increased to more than 110% at 25 F g^{-1} during the first 5000 charge−discharge cycles.[208]

A significant amount of MXene research has been reported developing alternative or inexpensive electrode materials with strong capacitances. Co_3O_4 is considered one of the best alternative materials due to its low cost, high theoretical capacitance, and environmental sustainability. A hybrid multilayer porous MXene aerogel was prepared by Liu et al.[209] as Co_3O_4-MXene/rGO as an SC electrode. The higher specific capacitance of 345 F g^{-1} was achieved at 1 A g^{-1}, which is notably higher than that of the electrodes $Ti_3C_2T_x$ MXene, rGO, and MXene/rGO (Figure 5g−i).[209] Figure 5 also shows how metal oxide, MPF, Co_3O_4, and graphene-based hybrid composite significantly improve the capacitance. MXenes are predominantly studied in aqueous electrolytes and are outperformed by the capacitance of most carbon-based and pseudocapacitive materials. However, X-ray diffraction/adsorption, electrochemical quartz crystal microbalance in gravimetric and dissipative modes, and nuclear magnetic resonance were used to examine the charge storage behavior of multilayer MXene electrodes in aqueous electrolytes. They are often combined with molecular dynamics (MD) and DFT modeling to validate the obtained results. However, further research is required for a better understanding of the charge storage mechanism for SCs. Table 3 lists the capacitance and related parameters for multilayer MXene and their heterostructures.

Batteries. It is particularly favorable to use 2D MXenes and their heterostructures in rechargeable batteries because of their

https://doi.org/10.1021/acsmaterialslett.2c00175
ACS Materials Lett. 2022, 4, 1174−1206

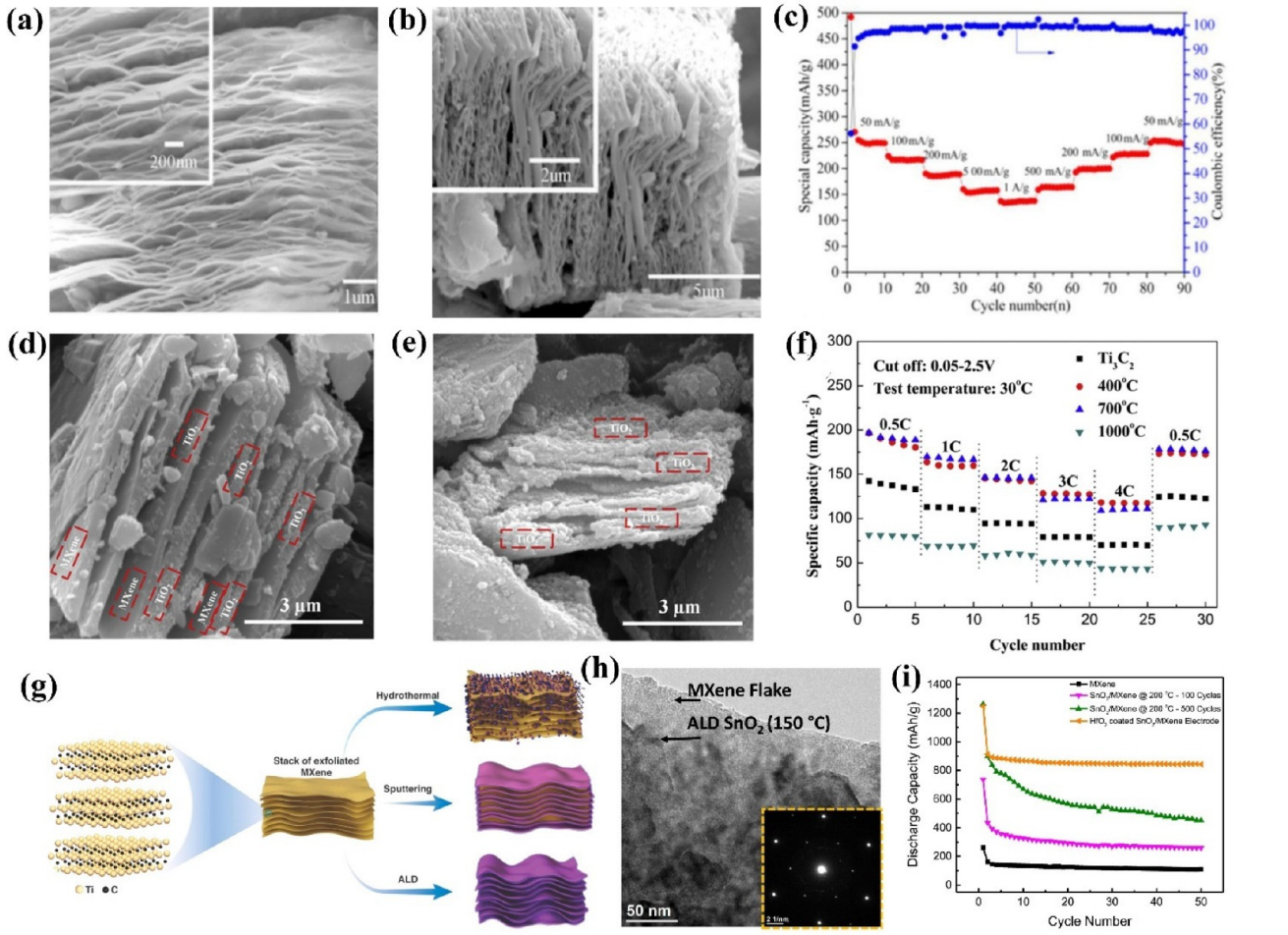

Figure 6. (a and b) SEM images of exfoliated V_2AlC. (c) Specific capacity of V_2C. (Reproduced with permission from ref 78. Copyright 2017, The Electrochemical Society.) (d and e) Ti_3C_2 surface morphologies before and after vacuum calcination when heated in air at different temperatures. (f) Rate capacity at various current rates. (Reproduced with permission from ref 85. Copyright 2018, Elsevier Ltd.) (g) Different methods for depositing SnO_2 on Ti_3C_2 MXene sheets. Exfoliated MXene sheets are shown on the left, and MXene hybrid electrodes after SnO_2 deposition is on the right. An exfoliated MXene sheet stack is presented in the center. (h) TEM image of MXene sheets coated with a 50 nm-thick layer of SnO_2. (i) Discharge capacity over 50 cycles at 500 mA g^{-1} HfO_2 coated SnO_2/MXene electrodes. (Reproduced with permission from ref 227. Copyright 2017, Elsevier Ltd.)

high electrical conductivity and high hydrophilicity, which are both beneficial for improved efficiency. The high capacity for various cations in the interlayer of MXene contributes to the overall efficiency of the battery system. Reversible energy storage in rechargeable batteries is essentially dependent on the insertion and extraction of alkali metal ions, such as Li^+, K^+, Na^+, and Mg^{2+}, in and out of the battery.[216,217] The most frequently used LIB uses graphite anodes as the commercial energy storage. However, the limited capacity restricts the graphite anodes and may fail to meet the ever-growing need for energy storage in the future. However, metallic or narrow bandgap semiconductor characteristics of ML-MXene and their derivatives are highly advantageous for LIB applications.[144,218,219] Naguib et al.[49] evaluated the viability of Ti_3C_2 MXene for LIBs as anode materials and later widely investigated both experimentally and computationally as LIB anodes and cathodes.[220,221] The adsorption and migration of Li ions on the exposed F- and OH-terminated Ti_3C_2 MXene surface were validated. Furthermore, Ti_3C_2 MXene is a potential candidate for LIB anodes where low operating voltage and diffusion barriers are required.[217] The electrochemical behaviors, Li^+ uptake potential of Ti_3C_2, and intercalation with dimethyl sulfoxide (DMSO) showed the charge and discharge capacities of 264.5 and 123.6 mA h g^{-1}, respectively, with a Coulombic efficiency of 47%.[220] The superior initial irreversible capacity of Ti_3C_2 contributes to the formation of the electrode surface SEI (solid electrolyte interphase) film and the irreversible reduction of electrochemically active surface groups. DMSO intercalation expands the *d*-spacing of MXene, and increases the storage capacity of Li ions.[220] A high degree of conversion was achieved (>90 wt %) for V_2C MXene prepared using the quasi-2D structure V_2AlC powders with NaF and HCl, etching at 90 °C. This can be attributed to prolonged cycling, especially at high charge/discharge rates, which expose increased electrochemically active sites (Figure 6a–c).[78] Li diffusion is expected to occur in ML-MXenes through the [1000] and [0100] crystalline directions. Using DFT simulations, the Li storage potential of functionalized MXenes like Sc_2C,[222] Ti_2C,[223] Ti_3C_2,[220] V_2C,[78] Cr_2C,[224] and Nb_2C[225] were examined.[226] Among those MXenes, the reversible capacity is the largest for V_2CO_2, and the highest diffusion barrier for MXene, indicating that it may be ideal for lightweight and high-capacity batteries.[168]

While laminated MXenes have high electronic conductivity, MXene electrodes as a hybrid composite with carbon

https://doi.org/10.1021/acsmaterialslett.2c00175
ACS Materials Lett. 2022, 4, 1174–1206

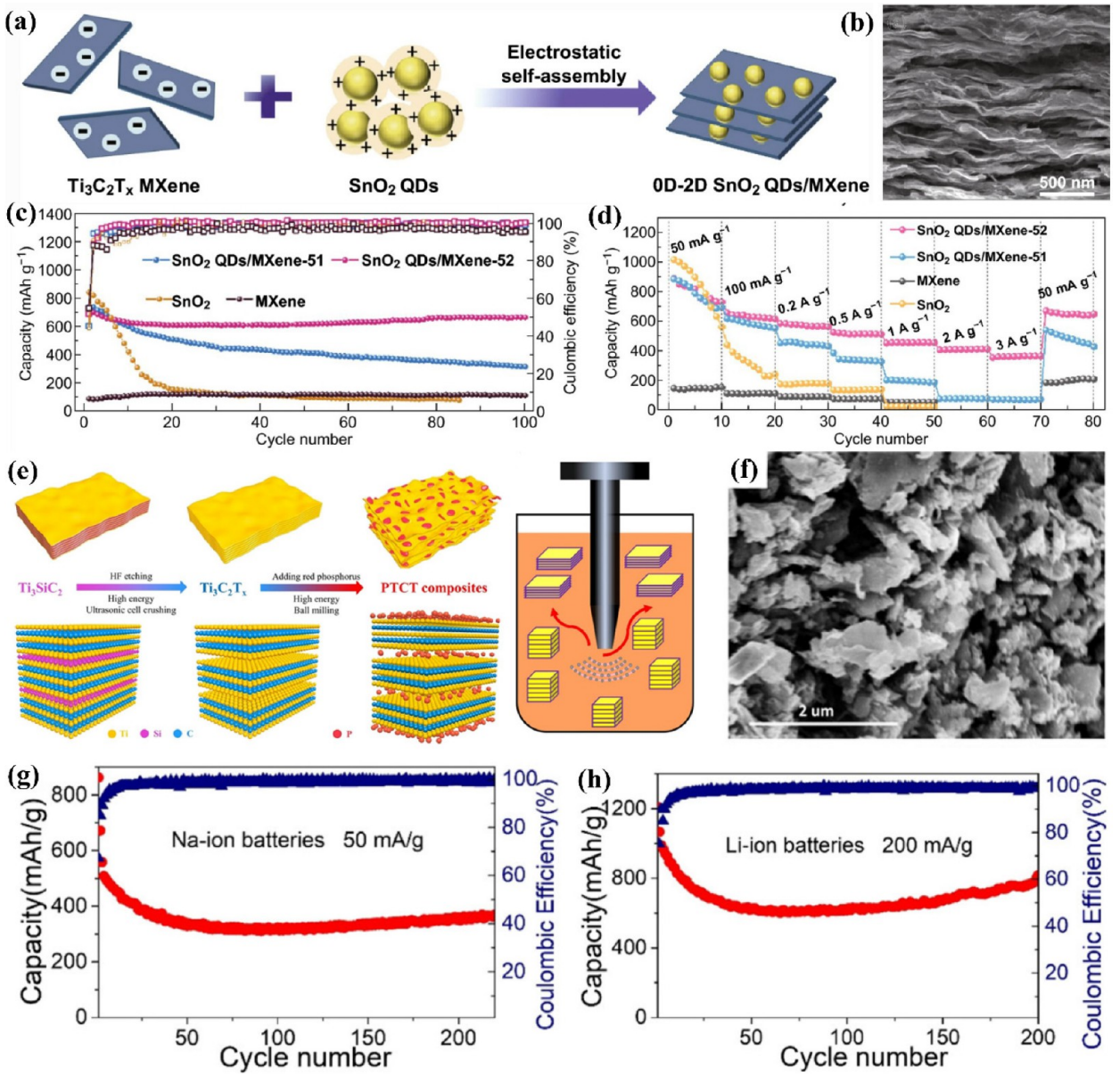

Figure 7. (a) Schematic illustration and (b) morphology for the prepared 0D-2D QDs SnO_2/MXene hybrids. (c) Cycle stability and (d) rate performance of LIB electrodes of all specimens. (Reproduced with permission from ref 162. Copyright 2019, The Authors.) (e) Fabrication of PTCT composite materials. (f) SEM image of PECT-MXene hybrid composite. (g) PTCT composite hybrid cycling performance of sodium-ion battery at current rate 50 mA g^{-1}. (h) 200 mA g^{-1} cycle performance with greater red P concentration for LIBs. (Reprinted (adapted) with permission from ref 230. Copyright 2019, American Chemical Society.)

additives,[69,118,228] metal oxide,[227,229] or polymer derivatives[230] demonstrated enhanced conductivity. Researchers have proposed many methods for producing highly conductive MXenes for high-performance applications, including oxidation, doping with metal oxides, and doping with heteroatoms. In the case of LIB anodes, the oxidation of $Ti_3C_2T_x$ in an oxygen-poor environment can result in the formation of TiO_2 (anatase) disordered composite material with excellent electrochemical performance that can be used as a negative electrode material.[115,231] As an example, a hierarchical composite of 2D niobium carbide MXene (Nb_2CT_x) in CO_2 synthesized via one-step controllable partial oxidation enhanced electrochemical performance. The oxidized Nb_2CT_x charge storage extends 198 and 152 C g^{-1} at 5 and 20 mV s^{-1}, respectively.[69] A systematic study on thermal stability in different atmospheres showed that vacuum calcination improves the electrochemical properties of MXene Ti_3C_2 multilayer for Li-ion batteries.[85] Ti_3C_2 powders, after vacuum calcination, showed much higher capacitance than initial Ti_3C_2 as LIBs anode. After heating at 400 and 700 °C for 100 cycles at a current rate of 1 C, the primary capacitance of 126.4 and 147.4 mA h g^{-1} rose by 45 and 69%, respectively. It exhibited outstanding rate capability due to changes in surface chemistry of TiO_2 (Figure 6d–f).[85]

The utilization of metal oxide in conjunction with ML-MXene hybridization can considerably boost the cycle capacity of the LIB, as previously stated. As an excellent chemical modifier, metal oxides such as tin dioxide (SnO_2) improve the cycling stability of MXene by acting as a catalyst. As a result of its high theoretical potential, SnO_2 is regarded a suitable choice as the anode material in LIBs.[232] It substantially increases the

https://doi.org/10.1021/acsmaterialslett.2c00175
ACS Materials Lett. 2022, 4, 1174–1206

Table 4. ML-MXene-Based Structures as Electrode Material for Batteries

structures	battery type	electrode	initial capacity (mAh g^{-1})	current density	capacity retention (mAh g^{-1})	number of cycles	coulombic efficiency	ref
$Ti_3C_2T_x$ and nonaqueous Na^+ electrolyte	Na-ion	anode	270	20 mA g^{-1}	70	100	95%	240
2D Ti_3C_2	Li-ion	anode	264.5	1 C	118.7	75	47%	220
V_2C MXene	Li-ion	anode	467	1 C	291	20	98.6%	78
$Ti_3C_2T_x$	Li-ion	anode	426	1 C	180	50	87%	221
f-Ti_3C_2	Li-ion	anode	410	1 C	200	50	–	226
V_2CO_2	Li-ion	anode	335	1 C	276	50	–	218
2D (Ti_2CT_x) nanosheets	Li-ion	anode	1015	100 mA g^{-1}	389	50	–	246
Nb_2C	Li-ion	anode	780	0.5 C	420	100	near 100%	247
Ti_2CT_x	Na-ion	anode	360	1 C	175	100	65%	248
V_2O_x@V_2CT_x	Zn-ion	cathode	304	2 mA g^{-1}	84	200	81.6%	244
SnO_2-Ti_3C_2	Li-ion	anode	1030.1	100 mA g^{-1}	360	200	34.4%	229
$Ti_3C_2X_2$	Na-ion	anode	379	1 A g^{-1}	80	120	56%	236
PDDA-BP/Ti_3C_2 nanosheet	Na-ion	anode	1112	0.1 A g^{-1}	658	2000	68.7%	249
red phosphorus $Ti_3C_2T_x$ (PTCT)	Li-ion	anode	906	50 mA g^{-1}	505	90	97.9%	230
SnS-$Ti_3C_2T_x$	Na-ion	anode	412.8	100 mA g^{-1}	255.9	50	70.4%	237
$CoNiO_2$	Na-ion	anode	463	100 mA g^{-1}	188.4	140	98.7%	238
sulfur-Ti_3C_2	Na-ion	anode	413	2 A g^{-1}	135	1000	near 100%	170
$Ti_3C_2T_x$@Sb-0.5	Na-ion	anode	353	2 mA g^{-1}	200	500	98%	239
$Ti_3C_2T_x$	Na-ion	anode	110	30 mA g^{-1}	73	70	100%	241
$Ti_3C_2T_x$@C	Mg-ion	cathode	198.7	10 mA g^{-1}	123.3	400	85%	242
V_2C	Li-ion	anode	492	0.2 C	290	50	99.4%	250
MoS_2/MXene	K-ion	anode	453.5	50 mA g^{-1}	145.5	50	66.5%.	245
V_2CT_x	Al-ion	cathode	335	10 mA g^{-1}	112	20	90%	243
SnO_2@MXene	Li-ion	anode	736	50 mA g^{-1}	258	50	92%	227
MoS_2@$Ti_3C_2T_x$	Li-ion	anode	1140	0.05 C	501	500	91.4%	251
SnS_2/Sn_3S_4@Ti_3C_2 MXene	Li-ion	anode	708	100 mA g^{-1}	426.3	100	37.3%	139

electrochemical efficiency of the composite SnO_2-MXene.[227,229] For SnO_2-Ti_3C_2 nanocomposites synthesized by the hydrothermal deposition of SnO_2 nanoparticles on Ti_3C_2, MXene retained almost 50% of the initial capacitance even after 200 cycles, i.e., showed capacitance of 1030 mAh g^{-1} at 100 mA g^{-1} and 360 mAh g^{-1} at 200 cycles.[229] A low-temperature atomic layer deposition (ALD) of metal oxides on MXene provides advantages such as prevention of oxidation and structure over the hydrothermal process.[227] To increase the stability even further, ALD is followed by the deposition of a conformal thin passivation layer of inactive HfO_2 in conjunction with SnO_2-MXene. At 500 mA g^{-1}, the HfO_2 coated SnO_2-MXene electrodes demonstrated a specific capacity of 843 mA h g^{-1} after 50 cycles of operation (Figure 6g–i).[227]

To further improve the capacity retention and cyclic ability of SnO_2-based MXene hybrid, SnO_2 quantum dots (QDs) were self-assembled on $Ti_3C_2T_x$ MXene sheets electrostatically to produce SnO_2/MXene hybrids and have a distinctive 0D-2D structure. Dimensionless SnO_2 QDs (about 4.7 nm) are distributed uniformly over 2D $Ti_3C_2T_x$ ML-MXene sheets with a controlled loading percentage. The hybrid of SnO_2 and QDs/MXene exhibited excellent high-density lithium storage of 887.4 mAh g^{-1} at 50 mA g^{-1}. Besides, the lithium storage capacity after 100 cycles was 659.8 mAh g^{-1} at 100 mA g^{-1} with 90% capacitance retention. The special 0D-2D geometry provides large electrochemically active sites with high specific capacitance to augment the electrochemical efficiency of electrode materials (Figure 7a–d).[162]

One of the most prevalent elements on the planet is silicon dioxide (SiO_2), which is a cost-effective and environmentally friendly option as an energy source. Although SiO_2 remains inactive against Li, it can be engineered to react directly via a simple process.[233] Mu et al.[234] successfully prepared a microspherical SiO_2/MXene hybrid material composed of a layered MXene. The Stober and spray drying methods were combined for the first time, and the SiO_2 nanoparticles were securely anchored by bonding. Bonding between the SiO_2 nanoparticles and the MXene matrix enhanced structural stability throughout long-term cycling. In addition, the laminated MXene matrix has greater elasticity to reduce the volume change of SiO_2 nanoparticles and facilitate the transmission of electrons and (Li^+) lithium ions. Consequently, with a high reversible power of 838 mA h g^{-1} at 100 mA g^{-1}, the SiO_2/MXene anode offers superior electrochemical efficiency with excellent cycle stability with a capacity retention of 97% over 100 cycles.[234]

Fe_2O_3 nanoparticles are suitable anode materials for batteries because of their high cyclic rate performance. A series of Fe_3O_4@Ti_3C_2 hybrids were synthesized by the ultrasonic mixture of Ti_3C_2 MXene and Fe_3O_4 nanoparticles.[109] Ti_3C_2 ML-MXene can hold a certain amount of Fe_3O_4 nanoparticles as a carrier and the Fe_3O_4@Ti_3C_2 hybrids showed superior electrochemical efficiency than pure Fe_3O_4 or Ti_3C_2. The Fe_3O_4@Ti_3C_2 hybrid prepared as anode material with a weight ratio of 2:5 indicates a significant reversible power of 747.4 mAh g^{-1} at a current rate of 1 C after 1000 cycles. The Fe_3O_4@Ti_3C_2 electrode showed a much lower charge transfer resistance and a better cyclic ability for LIBs.[109] Furthermore, a lightweight, freestanding and binder-free silicon/MXene composite paper has been directly used as an anode for LIBs.[111] This unique architecture showed adaptability to large volume expansion, enhanced the conductivity of composite materials, prevented MXene sheets from restacking, provided additional active sites, and promoted effective ion migration. The device exhibited

https://doi.org/10.1021/acsmaterialslett.2c00175
ACS Materials Lett. 2022, 4, 1174–1206

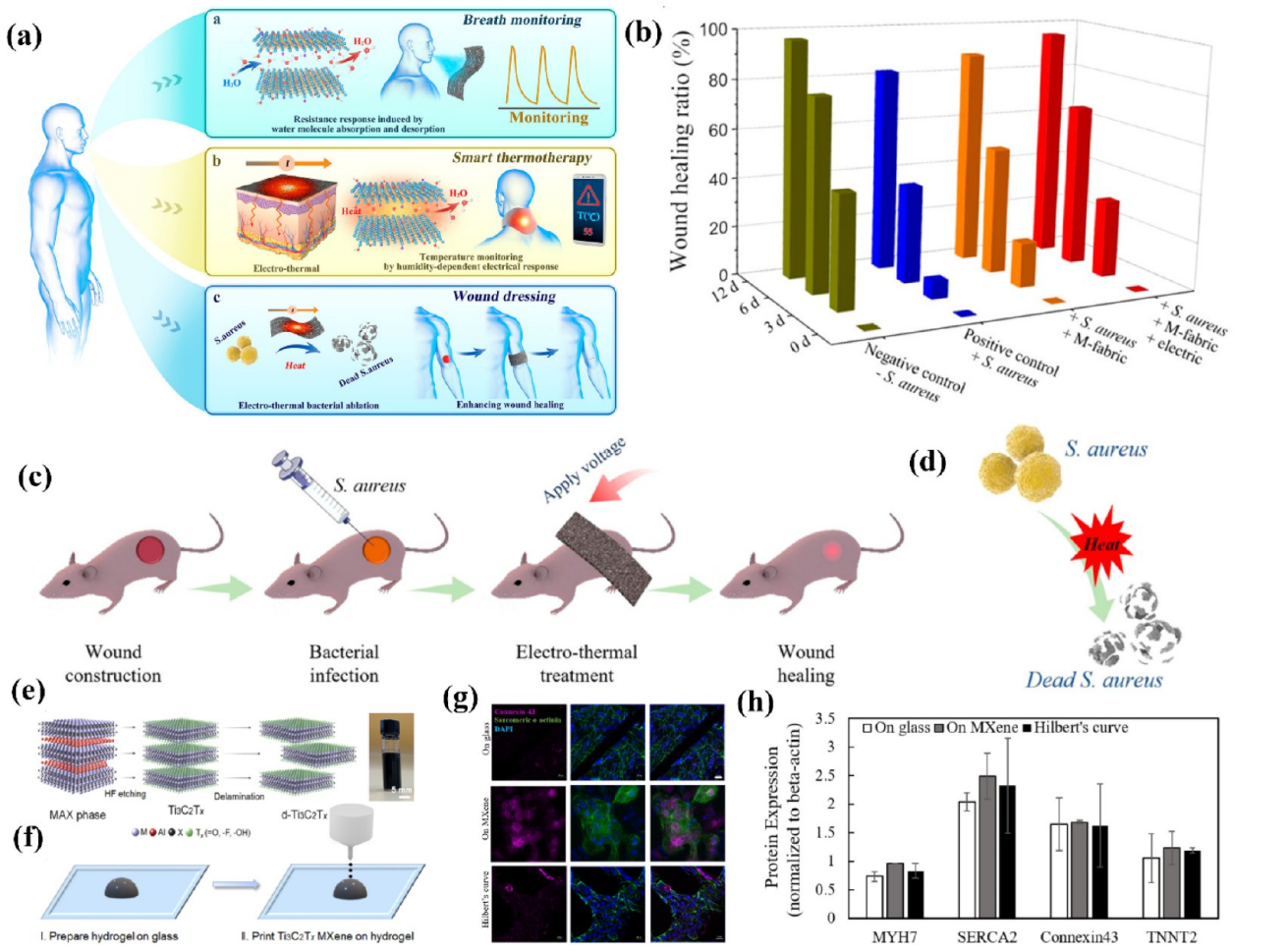

Figure 8. (a) Schematic diagram showing potential applications of MXenes in mobile healthcare and medical therapy fields. (b) Wound healing/tissue regeneration percentage in various recovery timeframes with different methods of treatment. (c) Representation for the development of a bacteria-infected model together with Joule therapy with the use of MXene. (d) Bacterial killing by resulting heat is depicted schematically. (Reproduced with permission from ref 266. Copyright 2020, American Chemical Society.) (e) Schematic diagram of selective HF etching of layers of Ti_3AlC_2 MAX phases to prepare Ti3C_2T_x MXene. (f) Schematic representation of printing $Ti_3C_2T_x$ MXene-hydrogel composite. (g) On day 7, immunostaining and qRT-PCR examination of iCMs were performed. (h) Western blotting quantitative analysis. (Reproduced with permission from ref 267. Copyright 2020, Elsevier Ltd.)

excellent performance after 100 cycles at a high capacity of 2118 mAh g^{-1} with a 200 mA g^{-1} current density.[111]

A successful method for investigating more efficient anode materials for LIBs is combining transitional metal oxides with MXene. The high specific surface area of the nanosized SnS_2/Sn_3S_4 hybrid also improves the interaction between electrolytes and electrodes. The hybrid confines in the multilayer stacks serve as a spacer to reduce the restacking layer propensity and enhance the limited capacitance of Ti_3C_2. After 100 cycles, the SnS_2/Sn_3S_4-MXene hybrid shows strong cycling stability of 462.3 mA h g^{-1} at 100 mA g^{-1} and a superior rate efficiency of 216.5 mA h g^{-1} at 5000 mA g^{-1}.[139] Apart from LIB, lithium−sulfur (Li−S) and lithium−oxygen (Li−O_2) batteries have also drawn great attention due to their energy intensity. 3D metal carbide MXene/rGO hybrid layered nanosheets were examined as the cathode host material for Li−S batteries.[118] This composite cathode achieved a good initial capacity of 1144.2 mAh g^{-1} and a high capacity retention level of 878.4 mA h g^{-1} after 300 cycles. The unique MXene and rGO nanosheets 3D layer formation with functional 2D surfaces are more effective at trapping sulfur and lithium polysulfides.[118] The Ni-$Ti_3C_2T_x$ hybrid produced via a simple hydrothermal and high-temperature calcination method was recently introduced as a cathode for the Li−O_2 battery. Because of their unique catalytic activity, Ni nanoparticles with a diameter of 20 nm can accelerate the decomposition of Li_2O_2. Utilizing the advantages of the two materials, the Ni-$Ti_3C_2T_x$ hybrid battery is used as the positive electrode of the Li−O_2 battery, with a maximum specific capacity of 20 264 mA h g^{-1} at 100 mA g^{-1} and 10 699 mA h g^{-1} at 500 mAg^{-1} for the first cycle.[235]

Electricity grid storage solutions on a large scale are necessary to store and use renewable resources efficiently. Because the relative abundance of Li in the Earth's crust is only 20 ppm, it is time to reconsider the feasibility of Li for large-scale electrochemical energy storage.[236] In recent years, Na,[170,230,237−241] Mg,[242] Al,[243] Zn,[244] and P[245] have demonstrated many advantages over LIBs, such as abundant raw materials, less costly, and less standard potential. With different components, conductivity, hydrophilicity, and adjustable surface functional groups, ML-MXene is a two-dimensional layered substance that has significant potential to improve the quality of Li-, K-, Ca-, Na-, Al-, and Mg-ion batteries and different types of energy storage systems (Table 4). Excellent electrochemical efficiency of ML-MXene materials for all nonlithium energy storage

https://doi.org/10.1021/acsmaterialslett.2c00175
ACS Materials Lett. 2022, 4, 1174−1206

Table 5. Antibacterial Activity and Tissue Engineering Application ML-MXene and Composites

multilayer hybrid MXene	result	application	ref
$Ti_3C_2T_x$/cellulose composite hydrogel with doxorubicin hydrochloride drug	100% tumor cell killing efficiency achieved at 808 nm light illumination.	photothermal treatment	275
Au/MXene and Au/Fe_3O_4/MXene composites	No teratogenic effect was found for these composites. In addition, the ability to destroy tumor cells increased with an increase in laser power density at 1.5 W cm^{-2}.	photothermal treatment	276
surface modification of Ti_3C_4/MnO_x composite with soybean phospholipid	A high rate of photothermal conversion and tumor cell ablation activity was achieved.	photothermal treatment	277
Ti_3C_4 MXene and chitosan	The range limit of detection was between 18 nM and 7.8 μM for sarcosine.	biosensor	278
TiO_2/$Ti_3C_2T_x$/Cu_2O	The sensor can detect the glucose level in the blood serum with a range between 100 nM and 10 μM.	biosensor	279
Ti_3C_2/CuS	Presence of cholesterol in a range of 10−100 μM was detected.	biosensor	280
Ti_3C_2/Prussian blue (PB)	The sensitivity of MXene/PB was higher in comparison with carbon nanotubes/PB and graphene/PB where the value was 52.3, 40.5, and 29.74 μA mM^{-1}, respectively.	biosensor	281
$Ti_3C_2T_x$/graphene hybrid film	The open structure of the hybrid film allows glucose oxidase to enter the pores, which helps to control the stability of the film. Therefore, the film exhibits excellent electrochemical activity toward glucose biosensing.	biosensor to detect glucose	282
Aβ_{42} imprinted MIP/delaminated $Ti_3C_2T_x$ /MWCNTs/GCE composite	The sensitivity range was achieved between 1.0 and 100.0 fg mL^{-1} and the detection limit (LOD) was 0.3 fg mL^{-1}.	biosensor for alzheimer's disease	283
molecularly imprinted polymer (MIP)			
multiwall carbon nanotube (MWCNT)			
glassy carbon electrode (GCE)			
by using a hydrothermal technique, a Ti_3C_2 and nickel−cobalt layered double hydroxide (NiCo-LDH) composite was created, which was then coated on a GCE	The sensitivity of this sensor was achieved at 64.75 μA m M^{-1} cm^{-2} at a low response time of 3 s with a linear range of 0.002−4.096 mM and a low limit of detection of 0.53 μM.	glucose biosensor	284

systems has been demonstrated. Recently, a new strategy for preparing multilayer $Ti_3C_2T_x$ nanosheets used abundant Ti_3SiC_2 MAX phase by high-energy ultrasonic cell breaking and extraction and a low-concentration etchant to break the Ti−Si bond of the MAX phase. To form a nanodots/$Ti_3C_2T_x$ (PTCT) composite material, a unique P−O−Ti bonded red phosphorus was combined with $Ti_3C_2T_x$ ML-MXenes. When used as an electrode for a LIB or sodium-ion battery (SIB), the PTCT electrode showed excellent cycle stability in 1000 cycles. By increasing the P content, the capacitance of the LIB increases to 818.2 mA h g^{-1} after 200 cycles. For the SIB, it showed an initial capacity of 863.8 mA h g^{-1} at a current density of 50 mA g^{-1}. It retains the capacity of 370.2 mAh g^{-1} after 200 cycles, indicating good sodium storage in MXene-based materials (Figure 7e−h).[230] There are many significant advances for implementing multilayer MXene-based hybrid materials in the field of energy storage. Further studies into the practical applications of MXene-based materials for electrochemical energy storage are still desirable.

Biomedical Applications. The nanostructure and the controllable chemical structure of ML-MXene provide unique properties for biomedical applications.[252−257] This section discusses the applications of the multilayer MXene in antibacterial activity, tissue engineering, photothermal therapy, bioprinting, bioimaging, and biosensors.

Antibacterial Activity. Skin is the largest organ in the human body. When any disruption occurs in the skin, it is known as a wound; the antibacterial activity plays a crucial role during the healing process of the wound.[258,259] Recently, hybrid ML-MXene was used to fabricate wound dressing because of its unique properties. The glutaraldehyde cross-linked $Ti_3C_2T_x$/chitosan electrospun composite mat showed excellent antibacterial activity against *Escherichia coli* as a wound dressing.[260] Direct adsorption of chitosan onto the bacterial cell surface blocks the membrane transport channel and causes cell deaths. The MXene-based composite can absorb water quickly to form a hydrogel.[261] A composite structure was prepared by incorporating multilayered $Ti_3C_2T_x$ into chitosan/sodium hyaluronate through the freeze-drying process. This 2D MXene was stabilized by L-ascorbic acid, which helps to prevent surface oxidation of MXene. The freeze-dried composite structure formed a hydrogel in Biocorp and showed excellent antibacterial activity. However, the higher amount of MXene reduced the porosity of the composite system. The addition of 5 wt % MXene into the chitosan/sodium hyaluronate exhibited 99% removal of *Staphylococcus aureus* bacteria with controlled porosity of the composite structure.[262] Although hydrogels play a significant role in the healing, these might cause problems with inflammatory responses.[263] Therefore, the electrical stimulation method of wound healing was adopted to utilize the skin's electrical conductivity of 2.6 to 1 × 10^{-4} mS.[264] Regenerated bacterial cellulose with a 2 wt % $Ti_3C_2T_x$ MXene hydrogel fabricated by a freeze-drying method showed higher electrical conductivity of 7.04 × 10^{-4} S cm^{-1} and thermal stability was achieved. This composite hydrogel wound dressing was treated with a skin defect rat model with and without electrical stimulation. The regenerated bacterial cellulose/MXene wound dressing with electrical stimulation effectively decreased the infected area within 14 days.[265] Apart from the electrical stimulation, the Joule heating effect is also effective for the antibacterial activity of wound dressing. Dip-coated nonwoven cellulosic fabric in Ti_3C_2 MXene generates 100 °C heat at 6 V to kill *S. aureus* bacteria with 100% repaired wounds without damaging any cells at the wound site (Figure 8a−d).[266]

Tissue Engineering. Increasing global demand for organ transplantation is one of the most severe concerns nowadays. This huge demand for organs can be met by fabricating artificial organs through tissue engineering.[268,269] Three key factors, i.e., cell seed, scaffold, and stimulating factors, significantly affect tissue engineering.[270] Along with different stimulating factors, electrical stimulation helps cell alignment, migration, proliferation, and differentiation.[271] Therefore, electroconductive materials like polyaniline, polypyrrole, poly(3,4-ethylene dioxythiophene), polythiophene, polyacetylene, and poly(p-phenylene), poly(p-phenylenevinylene), poly p-phenylene-sulfide, silicon, and melanin are popular for tissue engineering.[272] In addition, MXenes have become an attractive material for tissue engineering due to their antibacterial, anti-

https://doi.org/10.1021/acsmaterialslett.2c00175
ACS Materials Lett. 2022, 4, 1174−1206

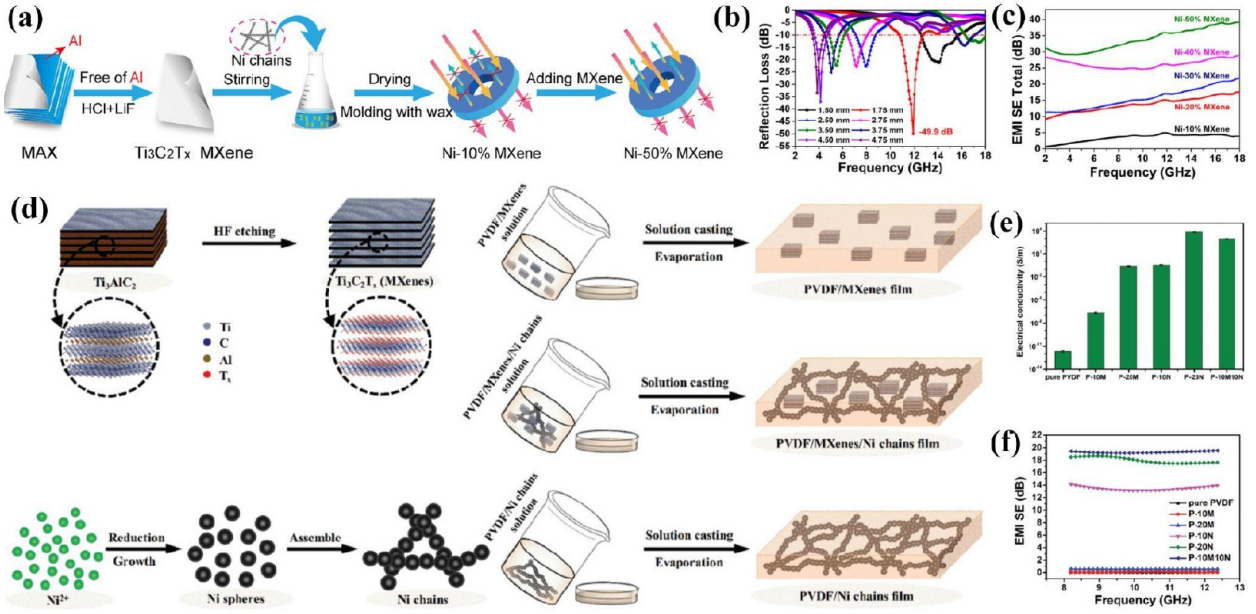

Figure 9. (a) Schematic representation of the fabricated MXene/Ni hybrids. (b) Electromagnetic absorption performance of Ni-10% MXene at various thicknesses with minimal reflection loss curves. (c) MXene/Ni hybrids shielding performance. (Reprinted with permission from ref 138. Copyright 2019, American Chemical Society.) (d) Diagram depicting the PVDF/MXene/Ni chain composite film production process. (e) Various composite films' electrical conductivities. (f) EMI shielding efficiency (SE) of 0.10 mm composite films. (Reproduced with permission from ref 293. Copyright 2019, WILEY-VCH Verlag GmbH & Co. KGaA.)

inflammatory, immunomodulatory properties, and cytocompatibility.[50] A composite hydrogel scaffold fabricated by incorporating ML-MXene and honey into chitosan showed excellent biocompatibility with no cytotoxicity to the stem cells. Honey and chitosan both have therapeutic properties, and the addition of MXene helped enhance the mechanical properties of the scaffold and swelling ability.[273] $Ti_3C_2T_x$ MXene was printed on polyethylene glycol hydrogel by aerosol jet printing with different patterns such as straight line, bowtie, and Hilbert's curve. Induced pluripotent stem cell obtained Cardiomyocyte (iCM) cells were seeded onto these patterns to improve the alignment. In addition, the number of living cells experiences a rise from 85% to 93% 7 days after seeding.[267] Figure 8e–h shows different patterns for iCM cells on a MXene-polyethylene glycol composite hydrogel. To accomplish linear alignment of iCMs, the straight line was adopted. Hilbert's curve patterns, which can track the propagation of Ca^{2+} signal, were picked for their unique characteristics in addition to their iCM alignment capabilities. The $Ti_3C_2T_x$ MXene-PEG hydrogels had a better alignment of the iCMs for all patterns.

The presence of functional groups on the MXene provides a particular environment for cell attachment, cell proliferation, and distribution. The fiber diameter of the MXene/poly-L-lactic acid (PLLA)/polyhydroxyalkanoates (PHA) electrospun composite was larger than that of the PLLA-PHA nanosheets. However, the water contact angle of the MXene composite scaffold was found to be 112.76°, which was lower than for PLLA-PHA sheets. Functional groups in MXene improved the uniform cell distribution and decreased the contact angle.[274] MXenes have also demonstrated efficient application in cancer treatment, biosensing, bioimaging, and 3D printing of organs, as listed in Table 5.

Electromagnetic Absorption and Shielding. Electronic devices have become inseparable parts of daily life in the modern era, and the world has started the transition toward the 5G telecommunication technology.[285,286] These electronic devices generate electromagnetic waves that have a significant detrimental effect on the human body. The electromagnetic interference (EMI) shielding devices restrict the waves within a particular area to lower the adverse impact on living organisms.[287]

The efficiency of EMI shielding devices depends on the electrical conductivity of the material which is at least 1 S/m. However, the shielding efficiency is not only dependent on the inherent properties of materials such as conductivity, permittivity, and permeability but also on the structure. Multilayered MXenes have been used for improving the EMI shielding efficiency and EM wave absorption by altering each layer's depth and dielectric characteristics.[288−290] The multilayer structure and the large specific area of $Ti_3C_2T_x$ help to provide additional electron transit routes that improve the EM wave absorption.[291] Although the absorption band of $Ti_3C_2T_x$ hybrid absorbers is outstanding, issues such as a high matching impedance and a restricted effective absorption bandwidth range constrained their uses.[292]

$Ti_3C_2T_x$ MXene/Ni chain hybrids with Ni-10% MXene, fabricated by a hydrothermal process, demonstrated an effective electromagnetic wave absorbing property at a thickness of 1.75 mm with the reflective loss of −49.9 dB at 2.1 GHz. At this point, high dielectric and magnetic losses were experienced. The total EMI shielding effectiveness experienced a rise with the increase of MXene from 10% to 50%, as a higher content of MXene helped to increase the electrical conductivity. A similar trend was also observed in the case of sample thickness. The highest EMI shielding effectiveness of 66.4 dB was achieved for Ni-50% MXene with a thickness of 2.8 mm and 33.8 dB for the thickness of 1.3 mm (Figure 9a–c).[138]

A polyvinylidene fluoride (PVDF)/MXene/Ni chain composite film with 20 wt % MXene, produced by a solution casting method, failed to meet the practical requirement of electrical

https://doi.org/10.1021/acsmaterialslett.2c00175
ACS Materials Lett. 2022, 4, 1174−1206

Table 6. Electromagnetic Wave Absorption Properties of Hybrid MXene

hybrid material	manufacturing method	sample thickness (mm)	reflection loss (dB)	effective absorption bandwidth (GHz)	sample thickness (mm)	frequency (GHz)	ref
Ti_2CT_x/PVA	freezing-dry	3.9	−18.7	–	–	8.2	295
$TiO_2/Ti_3C_2T_x$ /RGO	hydrothermal method	2.5	−65.3	4.3	2	–	296
MXene $Ti_3C_2T_x$ @RGO aerogel	hydrothermal method with freeze-drying	2.05	−31.2	5.4	2.05	8.2	297
$Ti_3C_2T_x$ MXene/Metal nanoparticles	cosolvothermal method	–	−52.6	3.7	3	8.4	298
rGO/Nb_2CT_x/Fe_3O_4	hydrothermal and an electrostatic self-assembly method	–	−59.17	6.8	2.5	11.8	299
Ti_3C_2/Fe_3O_4/PANI	–	–	−40.3	5.2	1.9	15.3	300
RGO/$Ti_3C_2T_x$/Fe_3O_4	ultrasonic spray	–	−51.2	6.5	2.9	14.4	301
$Ti_3C_2T_x$ MXene/gelatin nanocomposite aerogel	freeze casting method	2	−59.5	6.24	2	14.04	302
$CoFe_2O_4/Ti_3C_2$	solvothermal process	1.5	−30.9	8.5	1.5	8.3−16.8	303
FeCo-Ti_3C_2 MXene	hydrothermal method	1.6	−17.86	8.8	1.6	9.2−8.0	304
$Ti_3C_2T_x/TiO_2$/PANI	hydrothermal and in situ polymerization	2.18	−65.61	5.92	2.10	13.92	305

Table 7. EMI Shielding Properties of Hybrid MXene

hybrid material	method	filler content	conductivity	shielding effectiveness (dB)	sample thickness	frequency (G Hz)	ref
$Ti_3C_2T_x$/PVDF	solvent assisted mixing and compression molding	22.55 vol %	0.988 S m^{-1}	48.47 ± 3.5	2 mm	12.5	306
$Ti_3C_2T_x$/Epoxy	solution casting	15 wt %	105 S m^{-1}	41	2 mm	8.2−12.4	307
$Ti_3C_2T_x$ /PEDOT:PSS	vacuum-assisted filtration	7:1	340.5 S m^{-1}	42.10	11.1 μm	8.2	308
aramid nanofiber/$Ti_3C_2T_x$	vacuum-assisted filtration	80 wt %	879.0 S cm^{-1}	40.6	3.2 μm	8.2	309
d-$Ti_3C_2T_x$ /electrospun regenerated cellulosic nanofibers	vacuum-assisted filtration	–	46.3 S cm^{-1}	42.7	15 μm	2−18	310
$Ti_3C_2T_x$/cellulose nanofiber/silver	vacuum-assisted filtration	17.67 wt %	588.2 S m^{-1}	50.7	46 μm	12.4	311
$Ti_3C_2T_x$/delignified wood cellulose	–	–	6333 S m^{-1}	39.3	2 mm	12.4	312
PDMS coated M-filter ($Ti_3C_2T_x$ /cellulose filter paper)	dip coating	1.89 vol %	2756 S m^{-1}	43	0.2 mm	12.4−18 GHz	313
$Ti_3C_2T_x$/PVA	multilayer casting	19.5 wt %	716 S m^{-1}	44.4	0.027 mm	8−12	314
$Ti_3C_2T_x/Fe_3O_4$-PANI	vacuum-assisted filtration	10:5	–	62	16.7 μm	8.2−12.4	315
d-$Ti_3C_2T_x$/aramid nanofiber	vacuum-assisted filtration	10:1	–	34.71	12 μm	8.2	316
chitosan/$Ti_3C_2T_x$	vacuum-assisted filtration	75 wt %	1402 ± 70 S m^{-1}	34.7 ± 2	37 μm	8.2−12.4	317

conductivity for EMI shielding materials, i.e., 1 S m^{-1}. This is due to the low number of electron transport between the MXenes. On the other hand, the electrical conductivity was increased to 33.3 S m^{-1} for 50 wt % of MXene. Interestingly, the superior electrical conductivity was achieved of 892 S m^{-1} for PVDF with 10 wt % MXene and 10 wt % Ni chains composite. This composite exhibited the highest EMI shielding effectiveness value of 26 and 34.4 dB for a sample thickness of 0.24 and 0.36 mm, respectively (Figure 9d−f).[293] A MXene/polyurethane composite was produced by spray coating of $Ti_3C_2T_x$ MXene on single (SMPUF) and both sides (DMPUF) of an electrospun polyurethane fabric. The DMPUF experienced a rise in electrical conductivity of 11.5 S m^{-1}, which achieved the highest EMI shielding effectiveness of 21 dB above the commercial level compared to SMPUF.[294] The electromagnetic wave absorption and the EMI shielding properties of hybrid MXene are listed in Tables 6 and 7.

Environment and Water Treatment. MXenes have a potential application for environmental issues[318−321] such as water treatment, heavy metal removal by working as ion separation membranes,[322] capacitive deionization,[323] antimicrobial coatings,[324] and photocatalytic degradation.[325] Moreover, the carbonyl functionalized $Ti_3C_2T_x$ MXene (TCCH) showed superior performance in the removal of U(VI) and Eu(III).[326] Wang et al.[327] used 2D V_2CT_x for removing actinides from aqueous solutions, which was highly efficient for U(IV) sorbent (Figure 10a−c).[327] Delaminated $Ti_3C_2T_x$ nanosheets demonstrated a metal ions reduction capability, consisting of Cr (VI), Cu, and Ag.[328−331] The test of U(VI)/Eu(III) contained radioactive wastewater showed a remarkable 80% contaminant removal in just 30 min by the TCCH adsorbent, which increased to 90% with the increase in treatment time up to 3 h. Carboxyl groups play a significant role in the efficiency of MXene and the aryl diazonium salt also enhanced the firmness/solidity of the material in water. The maximum adsorption capacity was reported as 344.8 and 97.1 mg g^{-1} for U and Eu.[326]

ML-MXenes as a separation membrane could be used in the following three ways: (i) as a skeleton while fabricating, (ii) mixing of materials with MXene for the fabrication, and (iii) as a coating material.[333] Alkalized $Ti_3C_2T_x$ showed good performance for the Pb(II) removal and assumed that 1 kg of MXene is efficient for the treatment of 4500 kg of water (Table 5). MXenes showed great hydrophilic properties and strong interaction with polymers, providing a better fabrication faculty. A casting method for the fabrication of Ti_3C_2-SO_3H resulted in increased water uptake and proton conduction properties in the membrane.[322] MXene showed the capability of Cr ion removal,

https://doi.org/10.1021/acsmaterialslett.2c00175
ACS Materials Lett. 2022, 4, 1174−1206

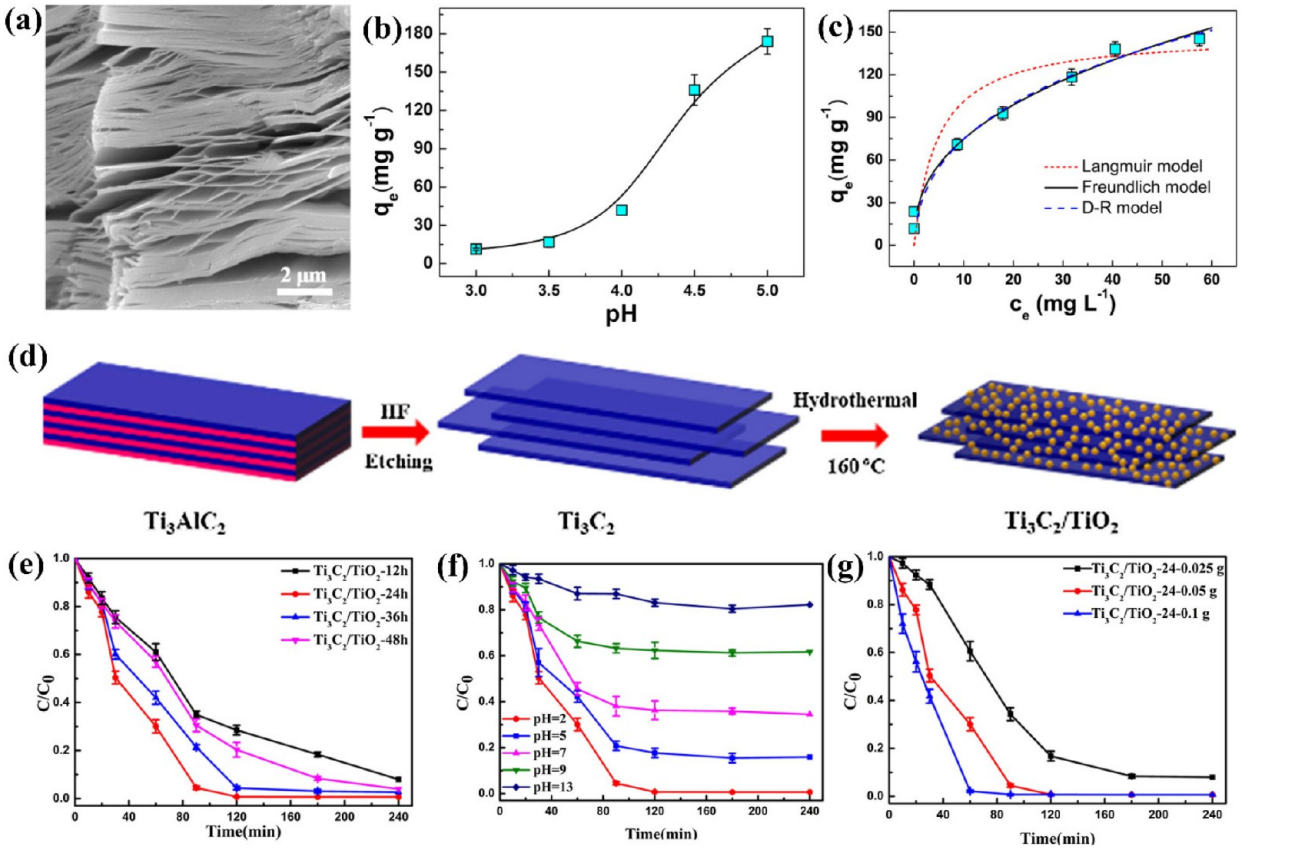

Figure 10. (a) At pH 4.5, SEM images of U(VI) absorbed. (b and c) Function of pH and earliest U(VI) concentration, U(VI) absorption from aqueous solution onto multilayered V_2CT_x. (Reproduced with permission from ref 327. Copyright 2016, American Chemical Society.) (d) Schematic diagram of the composition of Ti_3C_2/TiO_2 hybrid composite. (e) For different hydrothermal treatment times, the percentage extraction of Cr(VI) in 50 mL 50 mg L^{-1} solution (pH 2.0). (f) Cr(VI) extraction in 50 mL of a 50 mg L^{-1} solution Ti_3C_2/TiO_2 composite material concentration: 0.05 g L^{-1} (pH dependent). (g) Effectiveness of the Ti_3C_2/TiO_2-24 composite material's dosage on Cr(VI) elimination in 50 mL of a 50 mg L^{-1} solution (pH 2.0). (Reproduced with permission from ref 332 Copyright 2019, Elsevier Ltd.)

Table 8. MXenes Used for Different Toxic Metal Removal from an Aqueous Environment

MXene	adsorption capacity or reduction efficiency	condition of adsorption			toxic materials	ref
		temperature	time	pH		
Ti_3C_2	80 mg g^{-1}	298 K	14 h	–	Cr(VI)	336
$Ti_3C_2T_x$	250 mg g^{-1}	at RT	72 h	5.0	Cr(VI)	328
(analogous urchined rutile) TiO_2-C (u-RTC)	~225 mg g^{-1}	–	120 min	3.0–6.0	Cr(VI)	337
Ti_3C_2/TiO_2	99.35%	–	12 min	7> acidic	Cr(VI)	332
nZVI (Nano zerovalent iron)-alk-Ti_3C_2	194.87 mg g^{-1}	–	~1500 min	2.0	Cr(VI)	338
$Ti_3C_2T_x$	78.45 mg g^{-1}	298 K	3 min	5.0	Cu(II)	339
$Ti_3C_2T_x$-PDOPA(poly dihydroxyphenylalanine) (Amino acid modified)	18.36 mg g^{-1}	298 K	1 h	7.0	Cu(II)	340
$Ti_3C_2T_x$/PmPD(poly(m-phenylenediamine))-5/1	540.47 mg g^{-1}	–	~700 min	2.0	Cr(VI)	341
MoS_2/MXene (functionalized MXene)	1435.2 mg g^{-1}	–	2 min	2.0–11.0	Hg(II)	342
$Ti_3C_2T_x$	9.3 mg g^{-1}	298 K	2 h	7.0	Ba(II)	343
MXene/alginate	382.7 mg g^{-1}	~323 K	15 min	5.0–7.0	Pb(II)	344
$Ti_3C_2T_x$-KH570 (silane coupling agent)	147.97 mg g^{-1}	303 K	2 h	1.0–6.0	Pb(II)	345
magnetic $Ti_3C_2T_X$ nanocomposite	1128.41 mg g^{-1}	298 K	24 h	6.0	Hg(II)	346
$Ti_3C_2(OH)_xF_{1-x}$	2400 mg g^{-1}	–	~250 min	2.5–6.0	PO_4^{3-}	347
$Ti_3C_2T_x$ core–shell spheres containing sodium alginate molybdenum	932.84 mg g^{-1}	298 K	24 h	4.5	Hg(II)	348
Ti_2CT_x nanosheets biosurfactant functionalized	232.9 mg g^{-1}	303 K	24 h	5.0	Pb(II)	349
$Ti_3C_2T_x$	36.6 mg g^{-1}	293 K	2 h	6.0	Pb(II)	350

and 99.35% of Cr(VI) was successfully removed using Ti_3C_2/TiO_2 nanosheets (Figure 10d–g).[332]

The functional groups like −O and −OH enhance the ability of MXene as a water-absorbent. The high surface area of MXene

https://doi.org/10.1021/acsmaterialslett.2c00175
ACS Materials Lett. 2022, 4, 1174–1206

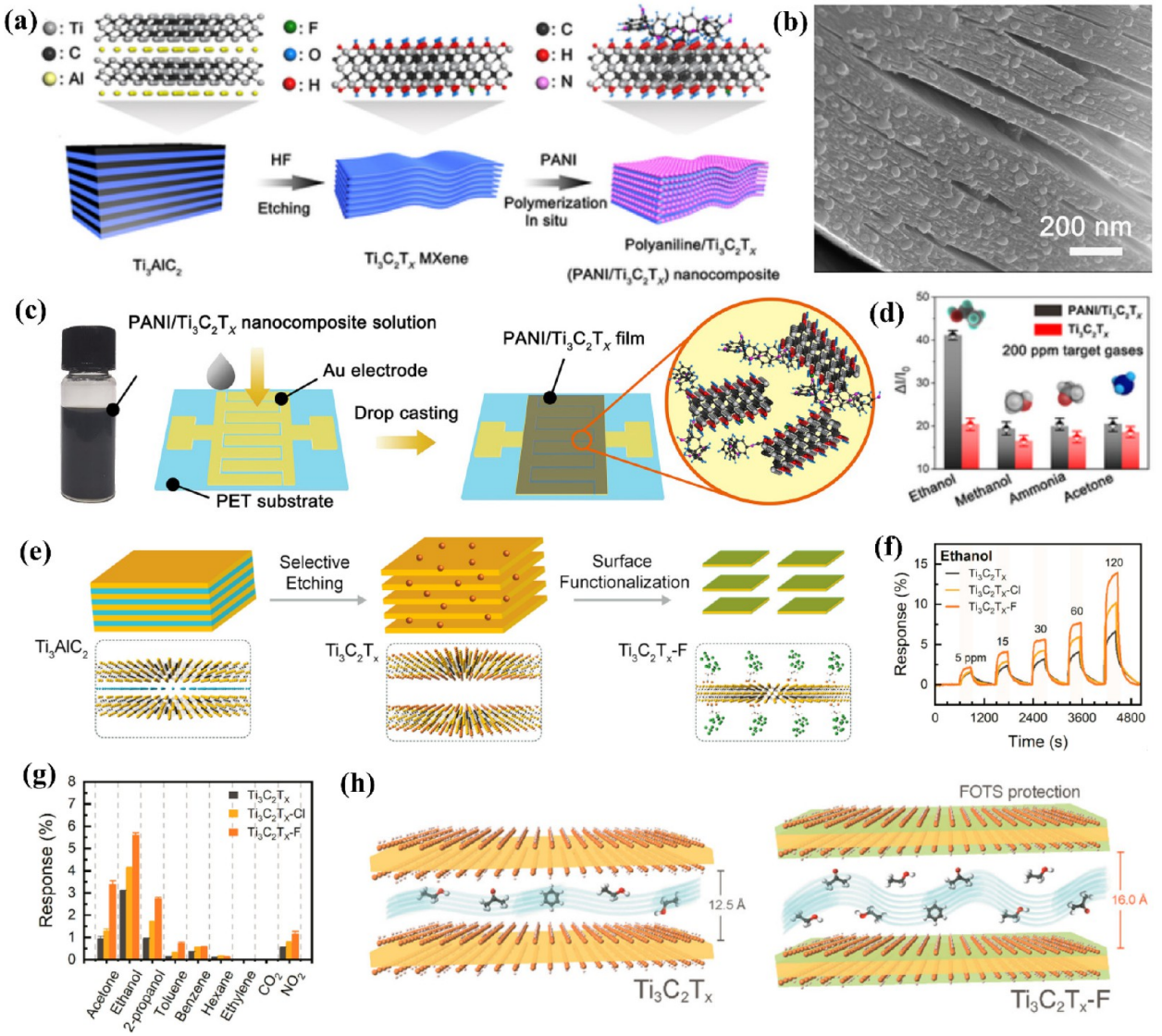

Figure 11. (a) Synthesis of PANI/$Ti_3C_2T_x$. (b) SEM image of PANI/$Ti_3C_2T_x$. (c) Illustration of the electrode before and after coating PANI/$Ti_3C_2T_x$ nanocomposites and PANI particles size distribution. (d) Flexible $Ti_3C_2T_x$ and PANI/Ti_3C_2T sensors for ethanol, methanol, ammonia, and acetone at room temperature. (Reproduced with permission from ref 360. Copyright 2019, The Authors.) (e) Surface-modified $Ti_3C_2T_x$ nanosheets. (f) Pure MXene and modified MXene sensors dynamic response curves. (g) Maximum sensor response varies on the various gas exposure. (h) $Ti_3C_2T_x$ and $Ti_3C_2T_x$-F schematics after exposure to VOCs (Reproduced with permission from ref 361. Copyright 2020, American Chemical Society.)

offers a direct ion exchange and reduction capability for various cations and organic molecules (Table 8).[334] MXenes also possess outstanding catalytic activities to numerous pollutants, e.g., Ag nanoparticle-loaded MXenes prepared by intercalating dimethyl sulfoxide showed a superior catalytic behavior to 4-nitrophenol and 2-nitroaniline.[335] Furthermore, $Ti_3C_2T_x$ nanosheets demonstrated remarkable reduction ability by removing the Cr(VI) ions by concurrently reducing Cr(VI) to Cr(III) and absorbing the reduced Cr(III) ions.[328]

Organic materials, e.g., dyes and antibiotics, are some of the most dangerous pollutants of recent decades. Proper degradation of these materials is crucial for pollution management. ML-MXenes play a vital role as a cocatalyst in photocatalytic degradation, demonstrated using semiconductor materials like TiO_2, g-C_3N_4, Ag_3PO_4, and Bi_2WO_6.[351] The 2D MXene enhances charge carrier transfer from the photocatalysts to the MXene and forms a Schottky barrier on the photocatalyst/MXene interface. The interface helps to inhibit the recombination of electron−hole.[352] Moreover, MXene's charge accumulation causes a negative shift and alignment of the Fermi level, improving the photocatalytic performance.[353] For example, 2D Niobium Carbide Nb_2CT_x possesses a Fermi Level lower than the $Ti_3C_2T_x$, which can be used as a cocatalyst.[354]

The oil film layer of thickness greater than 1 μm on the water surface affects the diffusion of oxygen in the water, restricts the photosynthesis process of algae, and affects the regular growth of underwater organisms. Oils have a carcinogenic effect on aqueous life as well.[355] Pure MXene membrane shows lower-level retention of dye; however, the addition of GO improves the wettability. A well-arranged layered structured membrane prepared by combining 2D GO and MXenes may balance the permeability of water and organic materials and the molecular repulsion of dye.[355] This membrane showed excellent durability to washing, i.e., retained dimensional stability for 3 days when

https://doi.org/10.1021/acsmaterialslett.2c00175
ACS Materials Lett. 2022, 4, 1174−1206

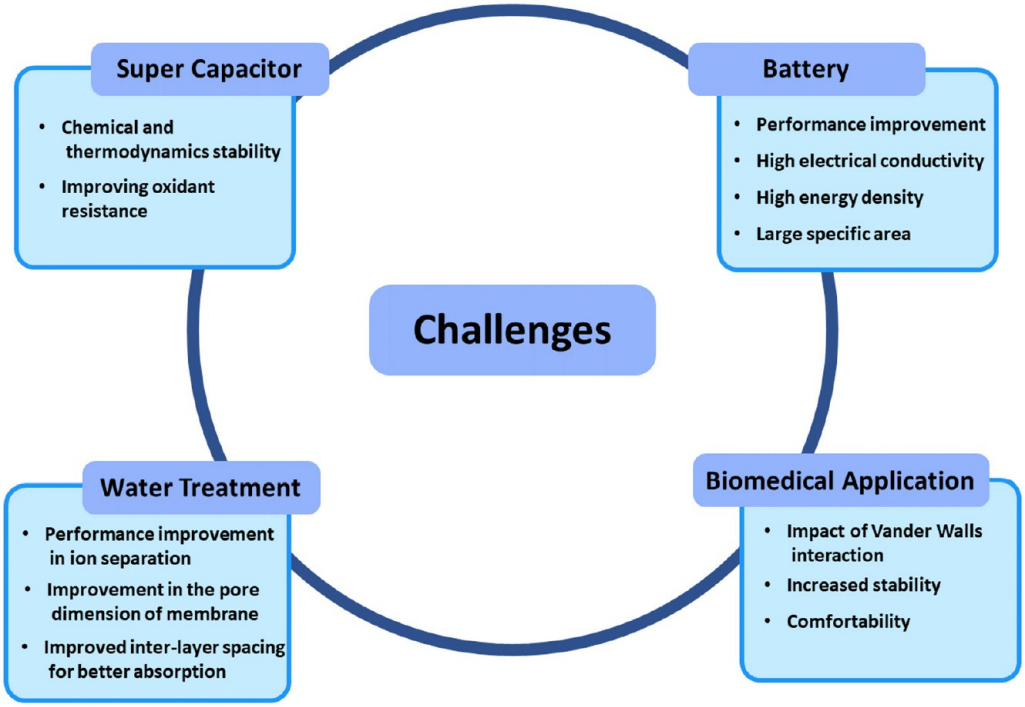

Figure 12. Schematic of insight on potential research and challenges scope in MXene-based hybrid nanocomposites.

washed in an ethanol solution. The presence of hydroxyl and fluorenyl groups on the surface of the MXenes forms a strong hydrogen bond with nylon and results in excellent stability.[355]

Anodic exposure of MXene ($Ti_3C_2T_x$) to anodic potential in an aqueous solution oxidizes the nanomaterial generating TiO_2 layer, or TiO_2 domain. Then TiO_2 gets dissolved by F ions, and the electrochemical activity of the resulting nanomaterials gets lower than that of the original $Ti_3C_2T_x$.[356,357] Therefore, $Ti_3C_2T_x$ demonstrates ultrasensitivity to H_2O_2 when used for the electrochemical reaction in the cathode potential window.[358] 2D metal carbide MXenes, which offer good metallic conductivity for minimal noise and a functional surface for a high signal, overpower the sensitivity of traditional semiconductive channel materials. $Ti_3C_2T_x$ MXene-based gas sensors demonstrates low detection limits around 50 to 100 ppb for volatile organic compound (VOC) gases at room temperature.[359] The very low noise also leads to 2 orders of magnitude greater signal-to-noise ratio than other 2D materials. The device surpasses the best-known sensors as the $Ti_3C_2T_x$ sensor shows elevated hydrogen-bonded gas selectivity. The practical LOD below 50 ppb and the conceptual LOD of VOC gas below 50 ppb are the lowest without pretreatment in any 2D material-based gas sensor working at room temperature.[359]

Nanocomposite like polyaniline/MXene (PANI/$Ti_3C_2T_x$) mixtures have been reported by the integration of DFT simulation and bulk electrical sensitivity measurement to demonstrate the high electrocatalytic sensitivity.[360] PANI nanoparticles are decorated on the surface of $Ti_3C_2T_x$ nanosheets by the low-temperature in situ polymerization. Integration of PANI induces significant sensitivity to detection, fast recovery/response, and good mechanical stability at room temperature. The compound sensing material showed high ethanol sensitivity of 200 ppm and 41.1% in ethanol utilizing the complementary properties of the composite material and the highly active $Ti_3C_2T_x$ MXene. A fast response time of 0.4/0.5 s at room temperature, making it easy for real-time VOC gas detected by next-generation sensing materials (Figure 11a–d).[360]

MXene's poor stability against oxidation and hydration in humid environments makes it unsuitable for long-term storage and application. It has been found that the surface treatment with fluoroalkyl silane (FOTS) containing $Ti_3C_2T_x$ compounds increases the mechanical and environmental stability of a superhydrophobic surface, as well as the sensing efficiency.[361] FOTS functionalization protects the sensor response when measuring the dynamic behavior of the $Ti_3C_2T_x$-F sensor to 30 ppm ethanol in the range of 5–80% relative humidity. DFT simulation results showed that ethanol adsorption energy and the local structural deformation of $Ti_3C_2T_x$-high F induced by ethanol adsorption help increase the sensitivity of the gas (Figure 11e–h).[361] As one of the most effective instruments for detecting noxious gases, gas sensors provide an essential means of monitoring gas concentrations and environmental data to ensure production safety. For these reasons, improving the sensitivity, selectivity, and stability of sensors have become prime factors of research.[362]

FUTURE PERSPECTIVE OF ML-MXENE AND ML-HYBRID MXENE

Recently, MXene, exfoliated from layered MAX stages, is experiencing exponential growth. The complexity in the synthesis process of MXenes has decreased over the years, and only etching and exfoliation are sufficient to make pure MXenes. The properties of the 2D materials depend on the synthesis process, so diversity in the material used for synthesis can escalate the applications. The developments include synthesizing simple MXenes to hybrid ML-MXenes and the exfoliation of novel MXenes, characterization of electronic and optical properties, and magnetic properties for diverse applications. MXenes can expand the application horizons by exploiting their numerous surface morphologies, surface function tunability, various magnetic orders, and significant spin–orbit coupling.

https://doi.org/10.1021/acsmaterialslett.2c00175
ACS Materials Lett. 2022, 4, 1174–1206

Furthermore, the addition of MXene can augment the conductivity of heterostructured and hybrid materials by several orders of magnitude, leading to future applications. The significant performance improvement of ML-MXene hybrid nanocomposites is attributed to the synergistic effects of high electrical conductivity, large specific area, and surface chemistry. Pristine MXene is susceptible to the environment and the environmental vulnerability of MXene could reduce by producing various heterostructures and hybrids. Investigation of the impact of van der Waals interactions on the stability and electronic properties of hybrid ML-MXenes will provide researchers with more flexibility to design new structures for various applications. The effect of multilayer and monolayer on the electronic property should also be studied thoroughly. The conventional electrodes show decay and make crystal-like structures by reacting with the Li-ions within the battery. A durable, eco-friendly, and efficient solution to the traditional battery is crucial and MXenes as an electrode material shows great potential. Comprehensive theoretical studies are required to understand the principles of the electrochemical factors that influence them and optimize the corresponding performances of 2D ML-MXenes as electrode materials in LIBs or SCs.

However, to fully utilize 2D heterostructures in energy storage applications, simple, rapid, and inexpensive synthesis procedures must be developed. Developing MXene synthesis methods that can improve accuracy in regulating the lateral size and number of layers of the delaminated MXene flakes is a bottleneck to the design and fabrication of high-performance ML-MXene-based electrodes. Molten Lewis salts have been used to make Ti- and V-based MXenes, but alternative MXenes with different "M" and surface terminations should be investigated. At this time, safer and more environmentally sustainable ways for manufacturing MXene have been proposed, and other solutions to this challenge are expected in the upcoming days.

The versatility of ML-MXene hybrid nanocomposites has demonstrated fascinating prospects and received widespread attention in water treatment. Although the new ML-hybrid MXene-based nanomaterials promise to develop high-performance membranes, there are still several challenges (Figure 12) to address for long-term stability. Also, eco-toxicological and life-cycle evaluations of ML-MXene-based nanomaterials require further exploration to widen the applicability of ML-hybrid MXene-based nanostructures. Designing and developing effective ML-MXenes and MXene-based hybrids requires identifying the catalytic mechanisms under reaction conditions using in situ characterization techniques and theoretical calculations. Analyzing the synergistic activity of reinforcing transition metals and other active components on ML-MXenes is required to fine-tune the behavior and selectivity. MXenes quickly oxidize in the air, and increasing the stability of the ML-MXenes hybrid is crucial for catalysis application. Furthermore, there is a lack of understanding of the relationship between surface termination and photocatalytic activity, particularly for electrocatalyst reactions. The composition relationship between catalytic efficiency and MXenes with unique surface terminations is critical to identifying the ever-increasing applications of ML-hybrid MXenes. However, strong chemical etching used in MXene production results in many flaws or vacancies on the surface of the generated MXene flakes. Defective sites are prone to oxidative degradation processes with water and/or oxygen, reducing MXenes' intrinsic characteristics and limiting their practical applicability. Because many MXene-derived materials and devices are typically manufactured using such solutions, the longevity of MXene solutions is critical. MXenes distributed in aqueous solutions are not only oxidized but they also oxidize at a faster pace than freestanding MXenes. Furthermore, because of the numerous potential parallel processes involved, the oxidation mechanism of MXenes in an aqueous environment is highly difficult. As a result, the mechanism of MXene breakdown in an aqueous environment is yet unknown. Despite the numerous obstacles, more concentrated efforts should be made to investigate fluoride-free and ecologically friendly etchants as a viable alternative to traditional HF. By reducing the diameter of 2D MXene materials, the relative surface area and reactivity will be increased. This showed that the surface functional groups have a significant impact on MXene's electrochemical characteristics. Modifying morphology, on the other hand, is critical for increasing active sites. The customized porosity and curved geometry of 2D MXene flakes can create high surface area and adjusted pore size and volume, which could help versatile applications.

Comprehensive investigations into the dielectric relaxation and electromagnetic response of ML-MXene-based materials are also essential. ML-MXene and different heterostructures and hybrids of MXene can be specifically constructed and developed by hybridization and assembly based on advanced theoretical guidance for various applications with lightweight, high performance, good impermeability, thermal property, and excellent mechanical properties.

AUTHOR INFORMATION

Corresponding Author

Md Milon Hossain − *Department of Mechanical and Aerospace Engineering, Cornell University, Ithaca, New York 14850, United States; Department of Textile Engineering, Chemistry and Science, North Carolina State University, Raleigh 27606, United States;* orcid.org/0000-0001-8416-0631; Phone: +1919 986 5713; Email: mh2276@cornell.edu

Authors

Sharif Tasnim Mahmud − *School of Textile Science and Engineering, Wuhan Textile University, Wuhan, Hubei 430079, China*

Md Mehdi Hasan − *UNAM - Institute of Materials Science and Nanotechnology, Bilkent University, Ankara 06800, Turkey*

Sudipta Bain − *Department of Fashion Design and Technology, Uttara University, Dhaka 1230, Bangladesh;* orcid.org/0000-0002-9387-6145

Sheikh Tamjidur Rahman − *Department of Textile Engineering, Khulna University of Engineering and Technology, Khulna 9203, Bangladesh*

Mukitur Rhaman − *Department of Textile Engineering, Khulna University of Engineering and Technology, Khulna 9203, Bangladesh*

Mustafa Ordu − *UNAM - Institute of Materials Science and Nanotechnology, Bilkent University, Ankara 06800, Turkey*

Complete contact information is available at: https://pubs.acs.org/10.1021/acsmaterialslett.2c00175

Notes

The authors declare no competing financial interest.

REFERENCES

(1) Teo, B. K.; Sun, X. H. Silicon-Based Low-Dimensional Nanomaterials and Nanodevices. *Chem. Rev.* **2007**, *107* (5), 1454−1532.

(2) Hasan, Md. M.; Hossain, Md. M.; Chowdhury, H. K. Two-Dimensional MXene-Based Flexible Nanostructures for Functional Nanodevices: A Review. *Journal of Materials Chemistry A* **2021**, *9* (6), 3231−3269.
(3) Mazzola, L. Commercializing Nanotechnology. *Nat. Biotechnol.* **2003**, *21* (10), 1137−1143.
(4) Wang, Z.; Hu, T.; Liang, R.; Wei, M. Application of Zero-Dimensional Nanomaterials in Biosensing. *Front. Chem.* **2020**, *8*. DOI: 10.3389/fchem.2020.00320.
(5) Garnett, E.; Mai, L.; Yang, P. Introduction: 1D Nanomaterials/Nanowires. *Chem. Rev.* **2019**, *119* (15), 8955−8957.
(6) Zhang, H.; Cheng, H.-M.; Ye, P. 2D Nanomaterials: Beyond Graphene and Transition Metal Dichalcogenides. *Chem. Soc. Rev.* **2018**, *47* (16), 6009−6012.
(7) Novoselov, K. S.; Geim, A. K.; Morozov, S. V.; Jiang, D.; Zhang, Y.; Dubonos, S. V.; Grigorieva, I. V.; Firsov, A. A. Electric Field Effect in Atomically Thin Carbon Films. *Science* **2004**, *306* (5696), 666−669.
(8) Chowdhury, T.; Sadler, E. C.; Kempa, T. J. Progress and Prospects in Transition-Metal Dichalcogenide Research Beyond 2D. *Chem. Rev.* **2020**, *120* (22), 12563−12591.
(9) Kim, K. K.; Lee, H. S.; Lee, Y. H. Synthesis of Hexagonal Boron Nitride Heterostructures for 2D van Der Waals Electronics. *Chem. Soc. Rev.* **2018**, *47* (16), 6342−6369.
(10) Carvalho, A.; Wang, M.; Zhu, X.; Rodin, A. S.; Su, H.; Castro Neto, A. H. Phosphorene: From Theory to Applications. *Nat. Rev. Mater.* **2016**, *1* (11), 1−16.
(11) Molle, A.; Grazianetti, C.; Tao, L.; Taneja, D.; Alam, M. H.; Akinwande, D. Silicene, Silicene Derivatives, and Their Device Applications. *Chem. Soc. Rev.* **2018**, *47* (16), 6370−6387.
(12) Shi, E.; Gao, Y.; Finkenauer, B. P.; Akriti; Coffey, A. H.; Dou, L. Two-Dimensional Halide Perovskite Nanomaterials and Heterostructures. *Chem. Soc. Rev.* **2018**, *47* (16), 6046−6072.
(13) Gupta, D.; Chauhan, V.; Kumar, R. A Comprehensive Review on Synthesis and Applications of Molybdenum Disulfide (MoS2) Material: Past and Recent Developments. *Inorg. Chem. Commun.* **2020**, *121*, 108200.
(14) Zhao, M.; Huang, Y.; Peng, Y.; Huang, Z.; Ma, Q.; Zhang, H. Two-Dimensional Metal−Organic Framework Nanosheets: Synthesis and Applications. *Chem. Soc. Rev.* **2018**, *47* (16), 6267−6295.
(15) VahidMohammadi, A.; Rosen, J.; Gogotsi, Y. The World of Two-Dimensional Carbides and Nitrides (MXenes). *Science* **2021**, *372* (6547). DOI: 10.1126/science.abf1581.
(16) Tan, C.; Cao, X.; Wu, X.-J.; He, Q.; Yang, J.; Zhang, X.; Chen, J.; Zhao, W.; Han, S.; Nam, G.-H.; Sindoro, M.; Zhang, H. Recent Advances in Ultrathin Two-Dimensional Nanomaterials. *Chem. Rev.* **2017**, *117* (9), 6225−6331.
(17) Zhang, H. Ultrathin Two-Dimensional Nanomaterials. *ACS Nano* **2015**, *9* (10), 9451−9469.
(18) Li, H.; Song, Z.; Zhang, X.; Huang, Y.; Li, S.; Mao, Y.; Ploehn, H. J.; Bao, Y.; Yu, M. Ultrathin, Molecular-Sieving Graphene Oxide Membranes for Selective Hydrogen Separation. *Science* **2013**, *342* (6154), 95−98.
(19) Zhang, X.; Shao, Z.; Zhang, X.; He, Y.; Jie, J. Surface Charge Transfer Doping of Low-Dimensional Nanostructures toward High-Performance Nanodevices. *Adv. Mater.* **2016**, *28* (47), 10409−10442.
(20) Song, F.; Hu, X. Exfoliation of Layered Double Hydroxides for Enhanced Oxygen Evolution Catalysis. *Nat. Commun.* **2014**, *5* (1), 4477.
(21) Naguib, M.; Kurtoglu, M.; Presser, V.; Lu, J.; Niu, J.; Heon, M.; Hultman, L.; Gogotsi, Y.; Barsoum, M. W. Two-Dimensional Nanocrystals Produced by Exfoliation of Ti3AlC2. *Adv. Mater.* **2011**, *23* (37), 4248−4253.
(22) Ahmed, A.; Hossain, M. M.; Adak, B.; Mukhopadhyay, S. Recent Advances in 2D MXene Integrated Smart-Textile Interfaces for Multifunctional Applications. *Chem. Mater.* **2020**, *32* (24), 10296−10320.
(23) Faruk, M. O.; Ahmed, A.; Adak, B.; Marzana, M.; Hossain, M. M.; Mukhopadhyay, S. High Performance 2D MXene Based Conducting Polymer Hybrids: Synthesis to Emerging Applications. *J. Mater. Chem. C* **2021**, *9* (32), 10193−10215.
(24) Marzana, M.; Morsada, Z.; Faruk, Md. O.; Ahmed, A.; Khan, Md. M. A.; Jalil, M. A.; Hossain, Md. M.; Rahman, M. M. Nanostructured Carbons: Towards Soft-Bioelectronics, Biosensing and Theraputic Applications. *Chem. Rec.* **2022**, *n/a* (n/a), e202100319. .
(25) Ahmed, A.; Sharma, S.; Adak, B.; Hossain, M. M.; LaChance, A. M.; Mukhopadhyay, S.; Sun, L. Two-Dimensional MXenes: New Frontier of Wearable and Flexible Electronics. *InfoMat* **2022**, *4* (4), No. e12295.
(26) Ahmed, A.; Adak, B.; Faruk, Md. O.; Mukhopadhyay, S. Nanocellulose Coupled 2D Graphene Nanostructures: Emerging Paradigm for Sustainable Functional Applications. *Ind. Eng. Chem. Res.* **2021**, *60* (30), 10882−10916.
(27) Wu, Y.; Sun, Y.; Zheng, J.; Rong, J.; Li, H.; Niu, L. Exploring MXene-Based Materials for next-Generation Rechargeable Batteries. *J. Phys. Energy* **2021**, *3* (3), 032009.
(28) Schultz, T.; Frey, N. C.; Hantanasirisakul, K.; Park, S.; May, S. J.; Shenoy, V. B.; Gogotsi, Y.; Koch, N. Surface Termination Dependent Work Function and Electronic Properties of Ti3C2Tx MXene. *Chem. Mater.* **2019**, *31* (17), 6590−6597.
(29) Naguib, M.; Mochalin, V. N.; Barsoum, M. W.; Gogotsi, Y. 25th Anniversary Article: MXenes: A New Family of Two-Dimensional Materials. *Adv. Mater.* **2014**, *26* (7), 992−1005.
(30) Anasori, B.; Lukatskaya, M. R.; Gogotsi, Y. 2D Metal Carbides and Nitrides (MXenes) for Energy Storage. *Nat. Rev. Mater.* **2017**, *2* (2), 1−17.
(31) Akuzum, B.; Maleski, K.; Anasori, B.; Lelyukh, P.; Alvarez, N. J.; Kumbur, E. C.; Gogotsi, Y. Rheological Characteristics of 2D Titanium Carbide (MXene) Dispersions: A Guide for Processing MXenes. *ACS Nano* **2018**, *12* (3), 2685−2694.
(32) Lim, S.; Park, H.; Yang, J.; Kwak, C.; Lee, J. Stable Colloidal Dispersion of Octylated Ti3C2-MXenes in a Nonpolar Solvent. *Colloids Surf., A* **2019**, *579*, 123648.
(33) Jiang, X.; Kuklin, A. V.; Baev, A.; Ge, Y.; Ågren, H.; Zhang, H.; Prasad, P. N. Two-Dimensional MXenes: From Morphological to Optical, Electric, and Magnetic Properties and Applications. *Phys. Rep.* **2020**, *848*, 1−58.
(34) Zhang, L.; Bi, J.; Zhao, Z.; Wang, Y.; Mu, D.; Wu, B. Sulfur@Self-Assembly 3D MXene Hybrid Cathode Material for Lithium-Sulfur Batteries. *Electrochim. Acta* **2021**, *370*, 137759.
(35) Boota, M.; Anasori, B.; Voigt, C.; Zhao, M.-Q.; Barsoum, M. W.; Gogotsi, Y. Pseudocapacitive Electrodes Produced by Oxidant-Free Polymerization of Pyrrole between the Layers of 2D Titanium Carbide (MXene). *Adv. Mater.* **2016**, *28* (7), 1517−1522.
(36) Sharifuzzaman, Md.; Chhetry, A.; Zahed, M. A.; Yoon, S. H.; Park, C. I.; Zhang, S.; Chandra Barman, S.; Sharma, S.; Yoon, H.; Park, J. Y. Smart Bandage with Integrated Multifunctional Sensors Based on MXene-Functionalized Porous Graphene Scaffold for Chronic Wound Care Management. *Biosens. Bioelectron.* **2020**, *169*, 112637.
(37) Riazi, H.; Taghizadeh, G.; Soroush, M. MXene-Based Nanocomposite Sensors. *ACS Omega* **2021**, *6* (17), 11103−11112.
(38) Zhu, J.; Ha, E.; Zhao, G.; Zhou, Y.; Huang, D.; Yue, G.; Hu, L.; Sun, N.; Wang, Y.; Lee, L. Y. S.; Xu, C.; Wong, K.-Y.; Astruc, D.; Zhao, P. Recent Advance in MXenes: A Promising 2D Material for Catalysis, Sensor and Chemical Adsorption. *Coord. Chem. Rev.* **2017**, *352*, 306−327.
(39) Sun, Y.; Li, Y. Potential Environmental Applications of MXenes: A Critical Review. *Chemosphere* **2021**, *271*, 129578.
(40) Kumar, J. A.; Prakash, P.; Krithiga, T.; Amarnath, D. J.; Premkumar, J.; Rajamohan, N.; Vasseghian, Y.; Saravanan, P.; Rajasimman, M. Methods of Synthesis, Characteristics, and Environmental Applications of MXene: A Comprehensive Review. *Chemosphere* **2022**, *286*, 131607.
(41) Cheng, Y.; Lyu, W.; Wang, Z.; Ouyang, H.; Zhang, A.; Sun, J.; Yang, T.; Fu, B.; He, B. MXenes: Synthesis, Incorporation, and Applications in Ultrafast Lasers. *Nanotechnology* **2021**, *32* (39), 392003.

(42) Iqbal, A.; Sambyal, P.; Koo, C. M. 2D MXenes for Electromagnetic Shielding: A Review. *Adv. Funct. Mater.* **2020**, *30* (47), 2000883.
(43) Gao, L.; Li, C.; Huang, W.; Mei, S.; Lin, H.; Ou, Q.; Zhang, Y.; Guo, J.; Zhang, F.; Xu, S.; Zhang, H. MXene/Polymer Membranes: Synthesis, Properties, and Emerging Applications. *Chem. Mater.* **2020**, *32* (5), 1703−1747.
(44) Nasrin, K.; Sudharshan, V.; Subramani, K.; Sathish, M. Insights into 2D/2D MXene Heterostructures for Improved Synergy in Structure toward Next-Generation Supercapacitors: A Review. *Adv. Funct. Mater.* **2022**, *32* (18), 2110267.
(45) Lipatov, A.; Alhabeb, M.; Lukatskaya, M. R.; Boson, A.; Gogotsi, Y.; Sinitskii, A. Effect of Synthesis on Quality, Electronic Properties and Environmental Stability of Individual Monolayer Ti3C2MXene Flakes. *Adv. Electronic Mater.* **2016**, *2* (12), 1600255.
(46) Urbankowski, P.; Anasori, B.; Makaryan, T.; Er, D.; Kota, S.; Walsh, P. L.; Zhao, M.; Shenoy, V. B.; Barsoum, M. W.; Gogotsi, Y. Synthesis of Two-Dimensional Titanium Nitride Ti4N3 (MXene). *Nanoscale* **2016**, *8* (22), 11385−11391.
(47) Warner, J. A.; Patil, S. K. R.; Khare, S. V.; Masiulaniec, K. C. Ab Initio Calculations for Properties of MAX Phases Ti 2 TlC, Zr 2 TlC, and Hf 2TlC. *Appl. Phys. Lett.* **2006**, *88* (10), 101911.
(48) Naguib, M.; Mashtalir, O.; Carle, J.; Presser, V.; Lu, J.; Hultman, L.; Gogotsi, Y.; Barsoum, M. W. Two-Dimensional Transition Metal Carbides. *ACS Nano* **2012**, *6* (2), 1322−1331.
(49) Naguib, M.; Kurtoglu, M.; Presser, V.; Lu, J.; Niu, J.; Heon, M.; Hultman, L.; Gogotsi, Y.; Barsoum, M. W. Two-Dimensional Nanocrystals Produced by Exfoliation of Ti 3AlC 2. *Adv. Mater.* **2011**, *23* (37), 4248−4253.
(50) Soleymaniha, M.; Shahbazi, M. A.; Rafieerad, A. R.; Maleki, A.; Amiri, A. Promoting Role of MXene Nanosheets in Biomedical Sciences: Therapeutic and Biosensing Innovations. *Adv. Healthcare Mater.* **2019**, *8* (1), 1801137.
(51) Xiong, D.; Li, X.; Bai, Z.; Lu, S. Recent Advances in Layered Ti3C2Tx MXene for Electrochemical Energy Storage. *Small* **2018**, *14* (17), 1703419.
(52) Shuck, C. E.; Sarycheva, A.; Anayee, M.; Levitt, A.; Zhu, Y.; Uzun, S.; Balitskiy, V.; Zahorodna, V.; Gogotsi, O.; Gogotsi, Y. Scalable Synthesis of Ti3C2Tx MXene. *Adv. Eng. Mater.* **2020**, *22* (3), 1901241.
(53) Mashtalir, O.; Naguib, M.; Dyatkin, B.; Gogotsi, Y.; Barsoum, M. W. Kinetics of Aluminum Extraction from Ti3AlC2 in Hydrofluoric Acid. *Mater. Chem. Phys.* **2013**, *139* (1), 147−152.
(54) Naguib, M.; Gogotsi, Y. Synthesis of Two-Dimensional Materials by Selective Extraction. *Acc. Chem. Res.* **2015**, *48* (1), 128−135.
(55) Alhabeb, M.; Maleski, K.; Anasori, B.; Lelyukh, P.; Clark, L.; Sin, S.; Gogotsi, Y. Guidelines for Synthesis and Processing of Two-Dimensional Titanium Carbide (Ti3C2Tx MXene). *Chem. Mater.* **2017**, *29* (18), 7633−7644.
(56) Wang, H.; Wu, Y.; Yuan, X.; Zeng, G.; Zhou, J.; Wang, X.; Chew, J. W. Clay-Inspired MXene-Based Electrochemical Devices and Photo-Electrocatalyst: State-of-the-Art Progresses and Challenges. *Adv. Mater.* **2018**, *30* (12), 1704561.
(57) Soundiraraju, B.; George, B. K. Two-Dimensional Titanium Nitride (Ti2N) MXene: Synthesis, Characterization, and Potential Application as Surface-Enhanced Raman Scattering Substrate. *ACS Nano* **2017**, *11* (9), 8892−8900.
(58) Halim, J.; Lukatskaya, M. R.; Cook, K. M.; Lu, J.; Smith, C. R.; Näslund, L. Å.; May, S. J.; Hultman, L.; Gogotsi, Y.; Eklund, P.; Barsoum, M. W. Transparent Conductive Two-Dimensional Titanium Carbide Epitaxial Thin Films. *Chem. Mater.* **2014**, *26* (7), 2374−2381.
(59) Barsoum, M. W.; El-Raghy, T.; Farber, L.; Amer, M.; Christini, R.; Adams, A. The Topotactic Transformation of Ti3SiC2 into a Partially Ordered Cubic Ti (C 0.67Si0.06) Phase by the Diffusion of Si into Molten Cryolite. *J. Electrochem. Soc.* **1999**, *146* (10), 3919−3923.
(60) Xie, X.; Xue, Y.; Li, L.; Chen, S.; Nie, Y.; Ding, W.; Wei, Z. Surface Al Leached Ti3AlC2as a Substitute for Carbon for Use as a Catalyst Support in a Harsh Corrosive Electrochemical System. *Nanoscale* **2014**, *6* (19), 11035−11040.
(61) Li, T.; Yao, L.; Liu, Q.; Gu, J.; Luo, R.; Li, J.; Yan, X.; Wang, W.; Liu, P.; Chen, B.; Zhang, W.; Abbas, W.; Naz, R.; Zhang, D. Fluorine-Free Synthesis of High-Purity Ti3C2Tx (T = OH, O) via Alkali Treatment. *Angewandte Chemie - International Edition* **2018**, *57* (21), 6115−6119.
(62) Xuan, J.; Wang, Z.; Chen, Y.; Liang, D.; Cheng, L.; Yang, X.; Liu, Z.; Ma, R.; Sasaki, T.; Geng, F. Organic-Base-Driven Intercalation and Delamination for the Production of Functionalized Titanium Carbide Nanosheets with Superior Photothermal Therapeutic Performance. *Angew. Chem.* **2016**, *128* (47), 14789−14794.
(63) Wang, L.; Zhang, H.; Wang, B.; Shen, C.; Zhang, C.; Hu, Q.; Zhou, A.; Liu, B. Synthesis and Electrochemical Performance of Ti3C2Tx with Hydrothermal Process. *Electronic Materials Letters* **2016**, *12* (5), 702−710.
(64) Feng, A.; Yu, Y.; Wang, Y.; Jiang, F.; Yu, Y.; Mi, L.; Song, L. Two-Dimensional MXene Ti3C2 Produced by Exfoliation of Ti3AlC2. *Materials and Design* **2017**, *114*, 161−166.
(65) Halim, J.; Kota, S.; Lukatskaya, M. R.; Naguib, M.; Zhao, M. Q.; Moon, E. J.; Pitock, J.; Nanda, J.; May, S. J.; Gogotsi, Y.; Barsoum, M. W. Synthesis and Characterization of 2D Molybdenum Carbide (MXene). *Adv. Funct. Mater.* **2016**, *26* (18), 3118−3127.
(66) Shahzad, F.; Alhabeb, M.; Hatter, C. B.; Anasori, B.; Hong, S. M.; Koo, C. M.; Gogotsi, Y. Electromagnetic Interference Shielding with 2D Transition Metal Carbides (MXenes). *Science* **2016**, *353* (6304), 1137−1140.
(67) Anasori, B.; Xie, Y.; Beidaghi, M.; Lu, J.; Hosler, B. C.; Hultman, L.; Kent, P. R. C.; Gogotsi, Y.; Barsoum, M. W. Two-Dimensional, Ordered, Double Transition Metals Carbides (MXenes). *ACS Nano* **2015**, *9* (10), 9507−9516.
(68) Ghidiu, M.; Lukatskaya, M. R.; Zhao, M. Q.; Gogotsi, Y.; Barsoum, M. W. Conductive Two-Dimensional Titanium Carbide "clay" with High Volumetric Capacitance. *Nature* **2014**, *516* (7529), 78−81.
(69) Zhang, C.; Beidaghi, M.; Naguib, M.; Lukatskaya, M. R.; Zhao, M. Q.; Dyatkin, B.; Cook, K. M.; Kim, S. J.; Eng, B.; Xiao, X.; Long, D.; Qiao, W.; Dunn, B.; Gogotsi, Y. Synthesis and Charge Storage Properties of Hierarchical Niobium Pentoxide/Carbon/Niobium Carbide (MXene) Hybrid Materials. *Chem. Mater.* **2016**, *28* (11), 3937−3943.
(70) Kajiyama, S.; Szabova, L.; Iinuma, H.; Sugahara, A.; Gotoh, K.; Sodeyama, K.; Tateyama, Y.; Okubo, M.; Yamada, A. Enhanced Li-Ion Accessibility in MXene Titanium Carbide by Steric Chloride Termination. *Adv. Energy Mater.* **2017**, *7* (9), 1601873.
(71) Wang, X.; Garnero, C.; Rochard, G.; Magne, D.; Morisset, S.; Hurand, S.; Chartier, P.; Rousseau, J.; Cabioc'h, T.; Coutanceau, C.; Mauchamp, V.; Célérier, S. A New Etching Environment (FeF 3 /HCl) for the Synthesis of Two-Dimensional Titanium Carbide MXenes: A Route towards Selective Reactivity vs. Water. *J. Mater. Chem. A* **2017**, *5* (41), 22012−22023.
(72) Liu, F.; Zhou, A.; Chen, J.; Jia, J.; Zhou, W.; Wang, L.; Hu, Q. Preparation of Ti 3 C 2 and Ti 2 C MXenes by Fluoride Salts Etching and Methane Adsorptive Properties. *Appl. Surf. Sci.* **2017**, *416*, 781−789.
(73) Luo, J.; Tao, X.; Zhang, J.; Xia, Y.; Huang, H.; Zhang, L.; Gan, Y.; Liang, C.; Zhang, W. Sn4+ Ion Decorated Highly Conductive Ti3C2MXene: Promising Lithium-Ion Anodes with Enhanced Volumetric Capacity and Cyclic Performance. *ACS Nano* **2016**, *10* (2), 2491−2499.
(74) Mashtalir, O.; Naguib, M.; Mochalin, V. N.; Dall'Agnese, Y.; Heon, M.; Barsoum, M. W.; Gogotsi, Y. Intercalation and Delamination of Layered Carbides and Carbonitrides. *Nat. Commun.* **2013**, *4*, 1−7.
(75) Lukatskaya, M. R.; Mashtalir, O.; Ren, C. E.; Dall'Agnese, Y.; Rozier, P.; Taberna, P. L.; Naguib, M.; Simon, P.; Barsoum, M. W.; Gogotsi, Y. Cation Intercalation and High Volumetric Capacitance of Two-Dimensional Titanium Carbide. *Science* **2013**, *341* (6153), 1502−1505.
(76) Ghidiu, M.; Halim, J.; Kota, S.; Bish, D.; Gogotsi, Y.; Barsoum, M. W. Ion-Exchange and Cation Solvation Reactions in Ti3C2MXene. *Chem. Mater.* **2016**, *28* (10), 3507−3514.

https://doi.org/10.1021/acsmaterialslett.2c00175
ACS Materials Lett. 2022, 4, 1174−1206

(77) Naguib, M.; Halim, J.; Lu, J.; Cook, K. M.; Hultman, L.; Gogotsi, Y.; Barsoum, M. W. New Two-Dimensional Niobium and Vanadium Carbides as Promising Materials for Li-Ion Batteries. *J. Am. Chem. Soc.* **2013**, *135* (43), 15966−15969.
(78) Liu, F.; Zhou, J.; Wang, S.; Wang, B.; Shen, C.; Wang, L.; Hu, Q.; Huang, Q.; Zhou, A. Preparation of High-Purity V 2 C MXene and Electrochemical Properties as Li-Ion Batteries. *J. Electrochem. Soc.* **2017**, *164* (4), A709−A713.
(79) Zhou, J.; Zha, X.; Chen, F. Y.; Ye, Q.; Eklund, P.; Du, S.; Huang, Q. A Two-Dimensional Zirconium Carbide by Selective Etching of Al3C3 from Nanolaminated Zr3Al3C5. *Angewandte Chemie - International Edition* **2016**, *55* (16), 5008−5013.
(80) Anasori, B.; Xie, Y.; Beidaghi, M.; Lu, J.; Hosler, B. C.; Hultman, L.; Kent, P. R. C.; Gogotsi, Y.; Barsoum, M. W. Two-Dimensional, Ordered, Double Transition Metals Carbides (MXenes). *ACS Nano* **2015**, *9* (10), 9507−9516.
(81) Ghidiu, M.; Naguib, M.; Shi, C.; Mashtalir, O.; Pan, L. M.; Zhang, B.; Yang, J.; Gogotsi, Y.; Billinge, S. J. L.; Barsoum, M. W. Synthesis and Characterization of Two-Dimensional Nb4C3 (MXene). *Chem. Commun.* **2014**, *50* (67), 9517−9520.
(82) Yang, J.; Naguib, M.; Ghidiu, M.; Pan, L. M.; Gu, J.; Nanda, J.; Halim, J.; Gogotsi, Y.; Barsoum, M. W. Two-Dimensional Nb-Based M4C3 Solid Solutions (MXenes). *J. Am. Ceram. Soc.* **2016**, *99* (2), 660−666.
(83) Alhabeb, M.; Maleski, K.; Mathis, T. S.; Sarycheva, A.; Hatter, C. B.; Uzun, S.; Levitt, A.; Gogotsi, Y. Selective Etching of Silicon from Ti 3 SiC 2 (MAX) To Obtain 2D Titanium Carbide (MXene). *Angew. Chem.* **2018**, *130* (19), 5542−5546.
(84) Voigt, C. A.; Ghidiu, M.; Natu, V.; Barsoum, M. W. Anion Adsorption, Ti3C2T z MXene Multilayers, and Their Effect on Claylike Swelling. *J. Phys. Chem. C* **2018**, *122* (40), 23172−23179.
(85) Kong, F.; He, X.; Liu, Q.; Qi, X.; Zheng, Y.; Wang, R.; Bai, Y. *Improving the Electrochemical Properties of MXene Ti3C2Multilayer for Li-Ion Batteries by Vacuum Calcination*; Elsevier Ltd, 2018; Vol. *265*. DOI: 10.1016/j.electacta.2018.01.196.
(86) Seredych, M.; Shuck, C. E.; Pinto, D.; Alhabeb, M.; Precetti, E.; Deysher, G.; Anasori, B.; Kurra, N.; Gogotsi, Y. High-Temperature Behavior and Surface Chemistry of Carbide MXenes Studied by Thermal Analysis. *Chem. Mater.* **2019**, *31* (9), 3324−3332.
(87) Manzanares-Palenzuela, C. L.; Pourrahimi, A. M.; Gonzalez-Julian, J.; Sofer, Z.; Pykal, M.; Otyepka, M.; Pumera, M. Interaction of Single- and Double-Stranded DNA with Multilayer MXene by Fluorescence Spectroscopy and Molecular Dynamics Simulations. *Chemical Science* **2019**, *10* (43), 10010−10017.
(88) An, H.; Habib, T.; Shah, S.; Gao, H.; Patel, A.; Echols, I.; Zhao, X.; Radovic, M.; Green, M. J.; Lutkenhaus, J. L. Water Sorption in MXene/Polyelectrolyte Multilayers for Ultrafast Humidity Sensing. *ACS Applied Nano Materials* **2019**, *2* (2), 948−955.
(89) Huang, X.; Wu, P. A Facile, High-Yield, and Freeze-and-Thaw-Assisted Approach to Fabricate MXene with Plentiful Wrinkles and Its Application in On-Chip Micro-Supercapacitors. *Adv. Funct. Mater.* **2020**, *30* (12), 1910048.
(90) Wu, X.; Wang, Z.; Yu, M.; Xiu, L.; Qiu, J. Stabilizing the MXenes by Carbon Nanoplating for Developing Hierarchical Nanohybrids with Efficient Lithium Storage and Hydrogen Evolution Capability. *Adv. Mater.* **2017**, *29* (24), 1−8.
(91) Cao, M.; Wang, F.; Wang, L.; Wu, W.; Lv, W.; Zhu, J. Room Temperature Oxidation of Ti 3 C 2 MXene for Supercapacitor Electrodes. *J. Electrochem. Soc.* **2017**, *164* (14), A3933−A3942.
(92) Rakhi, R. B.; Ahmed, B.; Hedhili, M. N.; Anjum, D. H.; Alshareef, H. N. Effect of Postetch Annealing Gas Composition on the Structural and Electrochemical Properties of Ti2CTx MXene Electrodes for Supercapacitor Applications. *Chem. Mater.* **2015**, *27* (15), 5314−5323.
(93) Xia, Q. X.; Fu, J.; Yun, J. M.; Mane, R. S.; Kim, K. H. High Volumetric Energy Density Annealed-MXene-Nickel Oxide/MXene Asymmetric Supercapacitor. *RSC Adv.* **2017**, *7* (18), 11000−11011.
(94) Xiao, P.; Wan, C.; Gu, J.; Liu, Z.; Men, Y.; Huang, Y.; Zhang, J.; Zhu, L.; Chen, T. 2D Janus Hybrid Materials of Polymer-Grafted Carbon Nanotube/Graphene Oxide Thin Film as Flexible, Miniature Electric Carpet. *Adv. Funct. Mater.* **2015**, *25* (16), 2428−2435.
(95) Fahmi, A.; Pietsch, T.; Mendoza, C.; Cheval, N. Functional Hybrid Materials. *Mater. Today* **2009**, *12* (5), 44−50.
(96) Mayerberger, E. A.; Urbanek, O.; McDaniel, R. M.; Street, R. M.; Barsoum, M. W.; Schauer, C. L. Preparation and Characterization of Polymer-Ti3C2Tx (MXene) Composite Nanofibers Produced via Electrospinning. *J. Appl. Polym. Sci.* **2017**, *134* (37), 45295.
(97) Boota, M.; Pasini, M.; Galeotti, F.; Porzio, W.; Zhao, M. Q.; Halim, J.; Gogotsi, Y. Interaction of Polar and Nonpolar Polyfluorenes with Layers of Two-Dimensional Titanium Carbide (MXene): Intercalation and Pseudocapacitance. *Chem. Mater.* **2017**, *29* (7), 2731−2738.
(98) An, H.; Habib, T.; Shah, S.; Gao, H.; Radovic, M.; Green, M. J.; Lutkenhaus, J. L. Surface-Agnostic Highly Stretchable and Bendable Conductive MXene Multilayers. *Science Advances* **2018**, *4* (3), 1−9.
(99) Hu, L.; Ren, Y.; Yang, H.; Xu, Q. Fabrication of 3D Hierarchical MoS2/Polyaniline and MoS 2/C Architectures for Lithium-Ion Battery Applications. *ACS Appl. Mater. Interfaces* **2014**, *6* (16), 14644−14652.
(100) Boota, M.; Anasori, B.; Voigt, C.; Zhao, M. Q.; Barsoum, M. W.; Gogotsi, Y. Pseudocapacitive Electrodes Produced by Oxidant-Free Polymerization of Pyrrole between the Layers of 2D Titanium Carbide (MXene). *Adv. Mater.* **2016**, *28* (7), 1517−1522.
(101) Sadki, S.; Schottland, P.; Brodie, N.; Sabouraud, G. The Mechanisms of Pyrrole Electropolymerization. *Chem. Soc. Rev.* **2000**, *29* (5), 283−293.
(102) Wang, H.; Zhang, J.; Wu, Y.; Huang, H.; Li, G.; Zhang, X.; Wang, Z. Surface Modified MXene Ti 3 C 2 Multilayers by Aryl Diazonium Salts Leading to Large-Scale Delamination. *Appl. Surf. Sci.* **2016**, *384*, 287−293.
(103) Chen, C.; Boota, M.; Urbankowski, P.; Anasori, B.; Miao, L.; Jiang, J.; Gogotsi, Y. Effect of Glycine Functionalization of 2D Titanium Carbide (MXene) on Charge Storage. *Journal of Materials Chemistry A* **2018**, *6* (11), 4617−4622.
(104) Wang, H.; Zhang, J.; Wu, Y.; Huang, H.; Jiang, Q. Chemically Functionalized Two-Dimensional Titanium Carbide MXene by in Situ Grafting-Intercalating with Diazonium Ions to Enhance Supercapacitive Performance. *J. Phys. Chem. Solids* **2018**, *115*, 172−179.
(105) Kotov, N. A.; Magonov, S.; Tropsha, E. Layer-by-Layer Self-Assembly of Alumosilicate-Polyelectrolyte Composites: Mechanism of Deposition, Crack Resistance, and Perspectives for Novel Membrane Materials. *Chem. Mater.* **1998**, *10* (3), 886−895.
(106) Hoheisel, T. N.; Hur, K.; Wiesner, U. B. Block Copolymer-Nanoparticle Hybrid Self-Assembly. *Prog. Polym. Sci.* **2015**, *40* (1), 3−32.
(107) Vahidmohammadi, A.; Moncada, J.; Chen, H.; Kayali, E.; Orangi, J.; Carrero, C. A.; Beidaghi, M. Thick and Freestanding MXene/PANI Pseudocapacitive Electrodes with Ultrahigh Specific Capacitance. *Journal of Materials Chemistry A* **2018**, *6* (44), 22123−22133.
(108) Yang, L.; Zheng, W.; Zhang, P.; Chen, J.; Tian, W. B.; Zhang, Y. M.; Sun, Z. M. MXene/CNTs Films Prepared by Electrophoretic Deposition for Supercapacitor Electrodes. *J. Electroanal. Chem.* **2018**, *830−831*, 1−6.
(109) Wang, Y.; Li, Y.; Qiu, Z.; Wu, X.; Zhou, P.; Zhou, T.; Zhao, J.; Miao, Z.; Zhou, J.; Zhuo, S. Fe3O4@Ti3C2MXene Hybrids with Ultrahigh Volumetric Capacity as an Anode Material for Lithium-Ion Batteries. *Journal of Materials Chemistry A* **2018**, *6* (24), 11189−11197.
(110) Du, C. F.; Dinh, K. N.; Liang, Q.; Zheng, Y.; Luo, Y.; Zhang, J.; Yan, Q. Self-Assemble and In Situ Formation of Ni1−xFexPS3 Nanomosaic-Decorated MXene Hybrids for Overall Water Splitting. *Adv. Energy Mater.* **2018**, *8* (26), 1801127.
(111) Tian, Y.; An, Y.; Feng, J. Flexible and Freestanding Silicon/MXene Composite Papers for High-Performance Lithium-Ion Batteries. *ACS Appl. Mater. Interfaces* **2019**, *11* (10), 10004−10011.
(112) Li, Y.; Zhang, D.; Feng, X.; Liao, Y.; Wen, Q.; Xiang, Q. Truncated Octahedral Bipyramidal TiO2/MXene Ti3C2 Hybrids with Enhanced Photocatalytic H2 Production Activity. *Nanoscale Advances* **2019**, *1* (5), 1812−1818.

(113) Lin, H.; Gao, S.; Dai, C.; Chen, Y.; Shi, J. A Two-Dimensional Biodegradable Niobium Carbide (MXene) for Photothermal Tumor Eradication in NIR-I and NIR-II Biowindows. *J. Am. Chem. Soc.* **2017**, *139* (45), 16235−16247.
(114) Li, Z.; Wang, L.; Sun, D.; Zhang, Y.; Liu, B.; Hu, Q.; Zhou, A. Synthesis and Thermal Stability of Two-Dimensional Carbide MXene Ti3C2. *Materials Science and Engineering B: Solid-State Materials for Advanced Technology* **2015**, *191* (C), 33−40.
(115) Gao, Y.; Wang, L.; Zhou, A.; Li, Z.; Chen, J.; Bala, H.; Hu, Q.; Cao, X. Hydrothermal Synthesis of TiO2/Ti3C2 Nanocomposites with Enhanced Photocatalytic Activity. *Mater. Lett.* **2015**, *150*, 62−64.
(116) Kashefi-Kheyrabadi, L.; Koyappayil, A.; Kim, T.; Cheon, Y. P.; Lee, M. H. A MoS2@Ti3C2Tx MXene Hybrid-Based Electrochemical Aptasensor (MEA) for Sensitive and Rapid Detection of Thyroxine. *Bioelectrochemistry* **2021**, *137*, 107674.
(117) Yang, Q.; Xu, Z.; Fang, B.; Huang, T.; Cai, S.; Chen, H.; Liu, Y.; Gopalsamy, K.; Gao, W.; Gao, C. MXene/Graphene Hybrid Fibers for High Performance Flexible Supercapacitors. *Journal of Materials Chemistry A* **2017**, *5* (42), 22113−22119.
(118) Bao, W.; Xie, X.; Xu, J.; Guo, X.; Song, J.; Wu, W.; Su, D.; Wang, G. Confined Sulfur in 3 D MXene/Reduced Graphene Oxide Hybrid Nanosheets for Lithium−Sulfur Battery. *Chem.—Eur. J.* **2017**, *23* (51), 12613−12619.
(119) Yan, J.; Ren, C. E.; Maleski, K.; Hatter, C. B.; Anasori, B.; Urbankowski, P.; Sarycheva, A.; Gogotsi, Y. Flexible MXene/Graphene Films for Ultrafast Supercapacitors with Outstanding Volumetric Capacitance. *Adv. Funct. Mater.* **2017**, *27* (30), 1701264.
(120) Chen, C.; Boota, M.; Xie, X.; Zhao, M.; Anasori, B.; Ren, C. E.; Miao, L.; Jiang, J.; Gogotsi, Y. Charge Transfer Induced Polymerization of EDOT Confined between 2D Titanium Carbide Layers. *Journal of Materials Chemistry A* **2017**, *5* (11), 5260−5265.
(121) Liu, G.; Zou, J.; Tang, Q.; Yang, X.; Zhang, Y.; Zhang, Q.; Huang, W.; Chen, P.; Shao, J.; Dong, X. Surface Modified Ti3C2MXene Nanosheets for Tumor Targeting Photothermal/Photodynamic/Chemo Synergistic Therapy. *ACS Appl. Mater. Interfaces* **2017**, *9* (46), 40077−40086.
(122) Qin, L.; Tao, Q.; El Ghazaly, A.; Fernandez-Rodriguez, J.; Persson, P. O. Å.; Rosen, J.; Zhang, F. High-Performance Ultrathin Flexible Solid-State Supercapacitors Based on Solution Processable Mo1.33C MXene and PEDOT:PSS. *Adv. Funct. Mater.* **2018**, *28* (2), 1703808.
(123) Zhu, M.; Huang, Y.; Deng, Q.; Zhou, J.; Pei, Z.; Xue, Q.; Huang, Y.; Wang, Z.; Li, H.; Huang, Q.; Zhi, C. Highly Flexible, Freestanding Supercapacitor Electrode with Enhanced Performance Obtained by Hybridizing Polypyrrole Chains with MXene. *Adv. Energy Mater.* **2016**, *6* (21), 1600969.
(124) Zhang, J.; Liu, Y.; Lv, Z.; Zhao, T.; Li, P.; Sun, Y.; Wang, J. Sulfonated Ti3C2Tx to Construct Proton Transfer Pathways in Polymer Electrolyte Membrane for Enhanced Conduction. *Solid State Ionics* **2017**, *310* (July), 100−111.
(125) Cao, X.; Wu, M.; Zhou, A.; Wang, Y.; He, X.; Wang, L. Non-Isothermal Crystallization and Thermal Degradation Kinetics of MXene/Linear Low-Density Polyethylene Nanocomposites. *e-Polym.* **2017**, *17* (5), 373−381.
(126) Liu, R.; Li, W. High-Thermal-Stability and High-Thermal-Conductivity Ti3C2T x MXene/Poly(Vinyl Alcohol) (PVA) Composites. *ACS Omega* **2018**, *3* (3), 2609−2617.
(127) Zhang, H.; Wang, L.; Chen, Q.; Li, P.; Zhou, A.; Cao, X.; Hu, Q. Preparation, Mechanical and Anti-Friction Performance of MXene/Polymer Composites. *Materials and Design* **2016**, *92*, 682−689.
(128) Tong, Y.; He, M.; Zhou, Y.; Zhong, X.; Fan, L.; Huang, T.; Liao, Q.; Wang, Y. Hybridizing Polypyrrole Chains with Laminated and Two-Dimensional Ti 3 C 2 T x toward High-Performance Electromagnetic Wave Absorption. *Appl. Surf. Sci.* **2018**, *434*, 283−293.
(129) Ren, Y.; Zhu, J.; Wang, L.; Liu, H.; Liu, Y.; Wu, W.; Wang, F. Synthesis of Polyaniline Nanoparticles Deposited on Two-Dimensional Titanium Carbide for High-Performance Supercapacitors. *Mater. Lett.* **2018**, *214*, 84−87.
(130) Lu, X.; Zhu, J.; Wu, W.; Zhang, B. Hierarchical Architecture of PANI@TiO2/Ti3C2Tx Ternary Composite Electrode for Enhanced Electrochemical Performance. *Electrochim. Acta* **2017**, *228*, 282−289.
(131) Zhou, B.; Zhang, Z.; Li, Y.; Han, G.; Feng, Y.; Wang, B.; Zhang, D.; Ma, J.; Liu, C. Flexible, Robust, and Multifunctional Electromagnetic Interference Shielding Film with Alternating Cellulose Nanofiber and MXene Layers. *ACS Appl. Mater. Interfaces* **2020**, *12* (4), 4895−4905.
(132) Zhao, W.; Peng, J.; Wang, W.; Jin, B.; Chen, T.; Liu, S.; Zhao, Q.; Huang, W. Interlayer Hydrogen-Bonded Metal Porphyrin Frameworks/MXene Hybrid Film with High Capacitance for Flexible All-Solid-State Supercapacitors. *Small* **2019**, *15* (18), 1901351.
(133) Weng, C.; Wang, G.; Dai, Z.; Pei, Y.; Liu, L.; Zhang, Z. Buckled AgNW/MXene Hybrid Hierarchical Sponges for High-Performance Electromagnetic Interference Shielding. *Nanoscale* **2019**, *11* (47), 22804−22812.
(134) Wang, L.; Qiu, H.; Song, P.; Zhang, Y.; Lu, Y.; Liang, C.; Kong, J.; Chen, L.; Gu, J. 3D Ti3C2Tx MXene/C Hybrid Foam/Epoxy Nanocomposites with Superior Electromagnetic Interference Shielding Performances and Robust Mechanical Properties. *Composites Part A: Applied Science and Manufacturing* **2019**, *123* (April), 293−300.
(135) Tran, M. H.; Brilmayer, R.; Liu, L.; Zhuang, H.; Hess, C.; Andrieu-Brunsen, A.; Birkel, C. S. Synthesis of a Smart Hybrid MXene with Switchable Conductivity for Temperature Sensing. *ACS Applied Nano Materials* **2020**, *3* (5), 4069−4076.
(136) Pan, Q.; Duan, C.; Liu, H.; Li, M.; Zhao, Z.; Zhao, D.; Duan, Y.; Chen, Y.; Wang, Y. Hierarchical Vertically Aligned Titanium Carbide (MXene) Array for Flexible All-Solid-State Supercapacitor with High Volumetric Capacitance. *ACS Applied Energy Materials* **2019**, *2* (9), 6834−6840.
(137) Liu, C.; Wu, W.; Shi, Y.; Yang, F.; Liu, M.; Chen, Z.; Yu, B.; Feng, Y. Creating MXene/Reduced Graphene Oxide Hybrid towards Highly Fire Safe Thermoplastic Polyurethane Nanocomposites. *Composites Part B: Engineering* **2020**, *203* (September), 108486.
(138) Liang, L.; Han, G.; Li, Y.; Zhao, B.; Zhou, B.; Feng, Y.; Ma, J.; Wang, Y.; Zhang, R.; Liu, C. Promising Ti3C2T x MXene/Ni Chain Hybrid with Excellent Electromagnetic Wave Absorption and Shielding Capacity. *ACS Appl. Mater. Interfaces* **2019**, *11* (28), 25399−25409.
(139) Li, J.; Han, L.; Li, Y.; Li, J.; Zhu, G.; Zhang, X.; Lu, T.; Pan, L. MXene-Decorated SnS2/Sn3S4 Hybrid as Anode Material for High-Rate Lithium-Ion Batteries. *Chemical Engineering Journal* **2020**, *380* (August 2019), 122590.
(140) Lipatov, A.; Alhabeb, M.; Lukatskaya, M. R.; Boson, A.; Gogotsi, Y.; Sinitskii, A. Effect of Synthesis on Quality, Electronic Properties and Environmental Stability of Individual Monolayer Ti_3C_2 MXene Flakes. *Adv. Electronic Mater.* **2016**, *2* (12), 1600255 DOI: 10.1002/aelm.201670068.
(141) Yazdanparast, S.; Soltanmohammad, S.; Fash-White, A.; Tucker, G. J.; Brennecka, G. L. Synthesis and Surface Chemistry of 2D TiVC Solid-Solution MXenes. *ACS Appl. Mater. Interfaces* **2020**, *12* (17), 20129−20137.
(142) Cheng, L.; Li, X.; Zhang, H.; Xiang, Q. Two-Dimensional Transition Metal MXene-Based Photocatalysts for Solar Fuel Generation. *J. Phys. Chem. Lett.* **2019**, *10*, 3488−3494.
(143) Thakur, R.; Hoffman, M.; VahidMohammadi, A.; Smith, J.; Chi, M.; Tatarchuk, B.; Beidaghi, M.; Carrero, C. A. Multilayered Two-Dimensional V2CTx MXene for Methane Dehydroaromatization. *ChemCatChem.* **2020**, *12* (14), 3639−3643.
(144) Osti, N. C.; Naguib, M.; Ostadhossein, A.; Xie, Y.; Kent, P. R. C.; Dyatkin, B.; Rother, G.; Heller, W. T.; Van Duin, A. C. T.; Gogotsi, Y.; Mamontov, E. Effect of Metal Ion Intercalation on the Structure of MXene and Water Dynamics on Its Internal Surfaces. *ACS Appl. Mater. Interfaces* **2016**, *8* (14), 8859−8863.
(145) Shen, J.; Liu, G.; Ji, Y.; Liu, Q.; Cheng, L.; Guan, K.; Zhang, M.; Liu, G.; Xiong, J.; Yang, J.; Jin, W. 2D MXene Nanofilms with Tunable Gas Transport Channels. *Adv. Funct. Mater.* **2018**, *28* (31), 1801511.
(146) Xu, S.; Dall'Agnese, Y.; Wei, G.; Zhang, C.; Gogotsi, Y.; Han, W. Screen-Printable Microscale Hybrid Device Based on MXene and

Layered Double Hydroxide Electrodes for Powering Force Sensors. *Nano Energy* **2018**, *50*, 479−488.
(147) Sarycheva, A.; Gogotsi, Y. Raman Spectroscopy Analysis of the Structure and Surface Chemistry of $Ti_3C_2T_x$ MXene. *Chem. Mater.* **2020**, *32*, 3480−3488.
(148) Nan, J.; Guo, X.; Xiao, J.; Li, X.; Chen, W.; Wu, W.; Liu, H.; Wang, Y.; Wu, M.; Wang, G. Nanoengineering of 2D MXene-Based Materials for Energy Storage Applications. *Small* **2021**, *17*, 1902085.
(149) Xiong, D.; Li, X.; Bai, Z.; Lu, S. Recent Advances in Layered Ti 3 C 2 T x MXene for Electrochemical Energy Storage. *Small* **2018**, *14*, 1703419.
(150) Coleman, J. N.; Lotya, M.; O'Neill, A.; Bergin, S. D.; King, P. J.; Khan, U.; Young, K.; Gaucher, A.; De, S.; Smith, R. J.; Shvets, I. V.; Arora, S. K.; Stanton, G.; Kim, H.-Y.; Lee, K.; Kim, G. T.; Duesberg, G. S.; Hallam, T.; Boland, J. J.; Wang, J. J.; Donegan, J. F.; Grunlan, J. C.; Moriarty, G.; Shmeliov, A.; Nicholls, R. J.; Perkins, J. M.; Grieveson, E. M.; Theuwissen, K.; McComb, D. W.; Nellist, P. D.; Nicolosi, V. Two-Dimensional Nanosheets Produced by Liquid Exfoliation of Layered Materials. *Science* **2011**, *331*, 568.
(151) VahidMohammadi, A.; Kayali, E.; Orangi, J.; Beidaghi, M. Techniques for MXene Delamination into Single-Layer Flakes. In *2D Metal Carbides and Nitrides (MXenes): Structure, Properties and Applications*; Anasori, B., Gogotsi, Y., Eds.; Springer International Publishing: Cham, 2019; pp 177−195. DOI: 10.1007/978-3-030-19026-2_11.
(152) Fan, Z.; Wang, Y.; Xie, Z.; Xu, X.; Yuan, Y.; Cheng, Z.; Liu, Y. A Nanoporous MXene Film Enables Flexible Supercapacitors with High Energy Storage. *Nanoscale* **2018**, *10* (20), 9642−9652.
(153) Wei, C.; Wu, C. Nonlinear Fracture of Two-Dimensional Transition Metal Carbides (MXenes). *Engineering Fracture Mechanics* **2020**, *230* (December 2019), 106978.
(154) Tang, X.; Guo, X.; Wu, W.; Wang, G. 2D Metal Carbides and Nitrides (MXenes) as High-Performance Electrode Materials for Lithium-Based Batteries. *Adv. Energy Mater.* **2018**, *8* (33), 1801897.
(155) Aslam, M. K.; Niu, Y.; Xu, M. MXenes for Non-Lithium-Ion (Na, K, Ca, Mg, and Al) Batteries and Supercapacitors. *Adv. Energy Mater.* **2021**, *11*, 2000681.
(156) Sang, X.; Naguib, M.; Alhabeb, M.; Unocic, R. R. Effect of Synthesis Methods on the Structure and Defects of Two-Dimensional MXenes. *2D Metal Carbides and Nitrides (MXenes): Structure, Properties and Applications* **2019**, 111−123.
(157) Li, J.; Yuan, X.; Lin, C.; Yang, Y.; Xu, L.; Du, X.; Xie, J.; Lin, J.; Sun, J. Achieving High Pseudocapacitance of 2D Titanium Carbide (MXene) by Cation Intercalation and Surface Modification. *Adv. Energy Mater.* **2017**, *7* (15), 1602725.
(158) Zhao, X.; Wang, Z.; Dong, J.; Huang, T.; Zhang, Q.; Zhang, L. Annealing Modification of MXene Films with Mechanically Strong Structures and High Electrochemical Performance for Supercapacitor Applications. *J. Power Sources* **2020**, *470* (June), 228356.
(159) Enyashin, A. N.; Ivanovskii, A. L. Atomic Structure, Comparative Stability and Electronic Properties of Hydroxylated Ti 2C and Ti 3C 2 Nanotubes. *Computational and Theoretical Chemistry* **2012**, *989*, 27−32.
(160) Enyashin, A. N.; Ivanovskii, A. L. Structural and Electronic Properties and Stability of MX Enes Ti 2C and Ti3C2 Functionalized by Methoxy Groups. *J. Phys. Chem. C* **2013**, *117* (26), 13637−13643.
(161) Chen, W. Y.; Jiang, X.; Lai, S. N.; Peroulis, D.; Stanciu, L. Nanohybrids of a MXene and Transition Metal Dichalcogenide for Selective Detection of Volatile Organic Compounds. *Nat. Commun.* **2020**, *11* (1), 1−10.
(162) Liu, H.; Zhang, X.; Zhu, Y.; Cao, B.; Zhu, Q.; Zhang, P.; Xu, B.; Wu, F.; Chen, R. Electrostatic Self-Assembly of 0D−2D SnO2 Quantum Dots/Ti3C2Tx MXene Hybrids as Anode for Lithium-Ion Batteries. *Nano-Micro Letters* **2019**, *11* (1), 65.
(163) Liu, X.; Chen, C. Mxene Enhanced the Photocatalytic Activity of ZnO Nanorods under Visible Light. *Mater. Lett.* **2020**, *261* (October), 127127.
(164) Hantanasirisakul, K.; Gogotsi, Y. Electronic and Optical Properties of 2D Transition Metal Carbides and Nitrides (MXenes). *Adv. Mater.* **2018**, *30* (52), 1804779.
(165) Byeon, A.; Zhao, M. Q.; Ren, C. E.; Halim, J.; Kota, S.; Urbankowski, P.; Anasori, B.; Barsoum, M. W.; Gogotsi, Y. Two-Dimensional Titanium Carbide MXene As a Cathode Material for Hybrid Magnesium/Lithium-Ion Batteries. *ACS Appl. Mater. Interfaces* **2017**, *9* (5), 4296−4300.
(166) Zhao, S.; Meng, X.; Zhu, K.; Du, F.; Chen, G.; Wei, Y.; Gogotsi, Y.; Gao, Y. Li-Ion Uptake and Increase in Interlayer Spacing of Nb4C3MXene. *Energy Storage Materials* **2017**, *8*, 42−48.
(167) Jiang, X.; Kuklin, A. V.; Baev, A.; Ge, Y.; Ågren, H.; Zhang, H.; Prasad, P. N. Two-Dimensional MXenes: From Morphological to Optical, Electric, and Magnetic Properties and Applications. *Phys. Rep.* **2020**, *848*, 1−58.
(168) Anasori, B.; Shi, C.; Moon, E. J.; Xie, Y.; Voigt, C. A.; Kent, P. R. C.; May, S. J.; Billinge, S. J. L.; Barsoum, M. W.; Gogotsi, Y. Control of Electronic Properties of 2D Carbides (MXenes) by Manipulating Their Transition Metal Layers. *Nanoscale Horizons* **2016**, *1* (3), 227−234.
(169) Pinto, D.; Anasori, B.; Avireddy, H.; Shuck, C. E.; Hantanasirisakul, K.; Deysher, G.; Morante, J. R.; Porzio, W.; Alshareef, H. N.; Gogotsi, Y. Synthesis and Electrochemical Properties of 2D Molybdenum Vanadium Carbides-Solid Solution MXenes. *Journal of Materials Chemistry A* **2020**, *8* (18), 8957−8968.
(170) Sun, S.; Xie, Z.; Yan, Y.; Wu, S. Hybrid Energy Storage Mechanisms for Sulfur-Decorated Ti3C2MXene Anode Material for High-Rate and Long-Life Sodium-Ion Batteries. *Chemical Engineering Journal* **2019**, *366* (January), 460−467.
(171) Berdiyorov, G. R. Optical Properties of Functionalized Ti3C2T2 (T = F, O, OH) MXene: First-Principles Calculations. *AIP Adv.* **2016**, *6* (5), 055105.
(172) Hu, J.; Li, S.; Zhang, J.; Chang, Q.; Yu, W.; Zhou, Y. Mechanical Properties and Frictional Resistance of Al Composites Reinforced with Ti3C2Tx MXene. *Chin. Chem. Lett.* **2020**, *31* (4), 996−999.
(173) Sliozberg, Y.; Andzelm, J.; Hatter, C. B.; Anasori, B.; Gogotsi, Y.; Hall, A. Interface Binding and Mechanical Properties of MXene-Epoxy Nanocomposites. *Compos. Sci. Technol.* **2020**, *192* (January), 108124.
(174) Fei, M.; Lin, R.; Lu, Y.; Zhang, X.; Bian, R.; Cheng, J.; Luo, P.; Xu, C.; Cai, D. MXene-Reinforced Alumina Ceramic Composites. *Ceram. Int.* **2017**, *43* (18), 17206−17210.
(175) Mazhar, S.; Qarni, A. A.; Ul Haq, Y.; Ul Haq, Z.; Murtaza, I. Promising PVC/MXene Based Flexible Thin Film Nanocomposites with Excellent Dielectric, Thermal and Mechanical Properties. *Ceram. Int.* **2020**, *46* (8, Part B), 12593−12605.
(176) Gao, Q.; Feng, M.; Li, E.; Liu, C.; Shen, C.; Liu, X. Mechanical, Thermal, and Rheological Properties of Ti3C2Tx MXene/ Thermoplastic Polyurethane Nanocomposites. *Macromol. Mater. Eng.* **2020**, *305* (10), 2000343.
(177) Cao, W.-T.; Chen, F.-F.; Zhu, Y.-J.; Zhang, Y.-G.; Jiang, Y.-Y.; Ma, M.-G.; Chen, F. Binary Strengthening and Toughening of MXene/ Cellulose Nanofiber Composite Paper with Nacre-Inspired Structure and Superior Electromagnetic Interference Shielding Properties. *ACS Nano* **2018**, *12* (5), 4583−4593.
(178) Lee, S.; Kim, J. Incorporating MXene into Boron Nitride/ Poly(Vinyl Alcohol) Composite Films to Enhance Thermal and Mechanical Properties. *Polymers* **2021**, *13* (3), 379.
(179) Tan, K. H.; Samylingam, L.; Aslfattahi, N.; Saidur, R.; Kadirgama, K. Optical and Conductivity Studies of Polyvinyl Alcohol-MXene (PVA-MXene) Nanocomposite Thin Films for Electronic Applications. *Optics and Laser Technology* **2021**, *136* (March), 106772.
(180) Chaudhuri, K.; Wang, Z.; Alhabeb, M.; Maleski, K.; Gogotsi, Y.; Shalaev, V.; Boltasseva, A. *Optical Properties of MXenes Optical Properties of 2D Materials* **2019**, 327−346.
(181) Djire, A.; Zhang, H.; Liu, J.; Miller, E. M.; Neale, N. R. Electrocatalytic and Optoelectronic Characteristics of the Two-Dimensional Titanium Nitride Ti4N3Tx MXene. *ACS Appl. Mater. Interfaces* **2019**, *11* (12), 11812−11823.

(182) Khazaei, M.; Ranjbar, A.; Arai, M.; Sasaki, T.; Yunoki, S. Electronic Properties and Applications of MXenes: A Theoretical Review. *Journal of Materials Chemistry C* **2017**, *5* (10), 2488−2503.
(183) Yang, J.; Zhou, X.; Luo, X.; Zhang, S.; Chen, L. Tunable Electronic and Magnetic Properties of Cr2M′C2T2 (M′ = Ti or V; T = O, OH or F). *Appl. Phys. Lett.* **2016**, *109* (20), 203109.
(184) *2D Metal Carbides and Nitrides (MXenes): Structure, Properties and Applications*; Anasori, B., Gogotsi, Y., Eds.; Springer International Publishing, 2019. DOI: 10.1007/978-3-030-19026-2.
(185) Zhan, X.; Si, C.; Zhou, J.; Sun, Z. MXene and MXene-Based Composites: Synthesis, Properties and Environment-Related Applications. *Nanoscale Horizons* **2020**, *5* (2), 235−258.
(186) Scheibe, B.; Tadyszak, K.; Jarek, M.; Michalak, N.; Kempiński, M.; Lewandowski, M.; Peplińska, B.; Chybczyńska, K. Study on the Magnetic Properties of Differently Functionalized Multilayered Ti3C2Tx MXenes and Ti-Al-C Carbides. *Appl. Surf. Sci.* **2019**, *479*, 216−224.
(187) Sternik, M.; Wdowik, U. D. Probing the Impact of Magnetic Interactions on the Lattice Dynamics of Two-Dimensional Ti2X (X = C, N) MXenes. *Phys. Chem. Chem. Phys.* **2018**, *20* (11), 7754−7763.
(188) Pan, J.; Lany, S.; Qi, Y. Computationally Driven Two-Dimensional Materials Design: What Is Next? *ACS Nano* **2017**, *11* (8), 7560−7564.
(189) Zhao, S.; Kang, W.; Xue, J. Manipulation of Electronic and Magnetic Properties of M2C (M = Hf, Nb, Sc, Ta, Ti, V, Zr) Monolayer by Applying Mechanical Strains. *Appl. Phys. Lett.* **2014**, *104* (13), 133106.
(190) Yue, Y. Fe2C Monolayer: An Intrinsic Ferromagnetic MXene. *J. Magn. Magn. Mater.* **2017**, *434* (March), 164−168.
(191) Sun, W.; Xie, Y.; Kent, P. R. C. Double Transition Metal MXenes with Wide Band Gaps and Novel Magnetic Properties. *Nanoscale* **2018**, *10* (25), 11962−11968.
(192) Dietzel, D.; Brndiar, J.; Štich, I.; Schirmeisen, A. Limitations of Structural Superlubricity: Chemical Bonds versus Contact Size. *ACS Nano* **2017**, *11* (8), 7642−7647.
(193) Lv, P.; Li, Y. L.; Wang, J. F. Monolayer Ti2C MXene: Manipulating Magnetic Properties and Electronic Structures by an Electric Field. *Phys. Chem. Chem. Phys.* **2020**, *22* (20), 11266−11272.
(194) Sun, Q.; Fu, Z.; Yang, Z. Tunable Magnetic and Electronic Properties of the Cr-Based MXene (Cr2C) with Functional Groups and Doping. *J. Magn. Magn. Mater.* **2020**, *514*, 167141.
(195) Bae, S.; Kang, Y. G.; Khazaei, M.; Ohno, K.; Kim, Y. H.; Han, M. J.; Chang, K. J.; Raebiger, H. Electronic and Magnetic Properties of Carbide MXenes—the Role of Electron Correlations. *Materials Today Advances* **2021**, *9* (xxxx), 100118.
(196) Yue, Y.; Wang, B.; Miao, N.; Jiang, C.; Lu, H.; Zhang, B.; Wu, Y.; Ren, J.; Wang, M. Tuning the Magnetic Properties of Zr2N MXene by Biaxial Strain. *Ceram. Int.* **2021**, *47* (2), 2367−2373.
(197) Garg, R.; Agarwal, A.; Agarwal, M. Synthesis and Optimisation of MXene for Supercapacitor Application. *Journal of Materials Science: Materials in Electronics* **2020**, *31* (21), 18614−18626.
(198) Roy, B. K.; Tahmid, I.; Rashid, T. U. Chitosan-Based Materials for Supercapacitor Applications: A Review. *J. Mater. Chem. A* **2021**, *9*, 17592.
(199) Zhang, X.; Zhang, Z.; Zhou, Z. MXene-Based Materials for Electrochemical Energy Storage. *Journal of Energy Chemistry* **2018**, *27* (1), 73−85.
(200) Bayram, V.; Ghidiu, M.; Byun, J. J.; Rawson, S. D.; Yang, P.; McDonald, S. A.; Lindley, M.; Fairclough, S.; Haigh, S. J.; Withers, P. J.; Barsoum, M. W.; Kinloch, I. A.; Barg, S. MXene Tunable Lamellae Architectures for Supercapacitor Electrodes. *ACS Applied Energy Materials* **2020**, *3* (1), 411−422.
(201) Wu, Z.; Li, L.; Yan, J. M.; Zhang, X. B. Materials Design and System Construction for Conventional and New-Concept Supercapacitors. *Adv. Sci.* **2017**, *4* (6), 1600382.
(202) Qi, D.; Liu, Y.; Liu, Z.; Zhang, L.; Chen, X. Design of Architectures and Materials in In-Plane Micro-Supercapacitors: Current Status and Future Challenges. *Adv. Mater.* **2017**, *29* (5), 1602802.
(203) Lukatskaya, M. R.; Kota, S.; Lin, Z.; Zhao, M. Q.; Shpigel, N.; Levi, M. D.; Halim, J.; Taberna, P. L.; Barsoum, M. W.; Simon, P.; Gogotsi, Y. Ultra-High-Rate Pseudocapacitive Energy Storage in Two-Dimensional Transition Metal Carbides. *Nature Energy* **2017**, *2* (8), 1−6.
(204) He, H.; Xia, Q.; Wang, B.; Wang, L.; Hu, Q.; Zhou, A. Two-Dimensional Vanadium Carbide (V2CTx) MXene as Supercapacitor Electrode in Seawater Electrolyte. *Chin. Chem. Lett.* **2020**, *31* (4), 984−987.
(205) Guan, Y.; Jiang, S.; Cong, Y.; Wang, J.; Dong, Z.; Zhang, Q.; Yuan, G.; Li, Y.; Li, X. A Hydrofluoric Acid-Free Synthesis of 2D Vanadium Carbide (V2C) MXene for Supercapacitor Electrodes. *2D Materials* **2020**, *7* (2), 025010.
(206) Wang, Y.; Dou, H.; Wang, J.; Ding, B.; Xu, Y.; Chang, Z.; Hao, X. Three-Dimensional Porous MXene/Layered Double Hydroxide Composite for High Performance Supercapacitors. *J. Power Sources* **2016**, *327*, 221−228.
(207) Yue, Y.; Liu, N.; Ma, Y.; Wang, S.; Liu, W.; Luo, C.; Zhang, H.; Cheng, F.; Rao, J.; Hu, X.; Su, J.; Gao, Y. Highly Self-Healable 3D Microsupercapacitor with MXene-Graphene Composite Aerogel. *ACS Nano* **2018**, *12* (5), 4224−4232.
(208) Zhu, Y.; Rajouâ, K.; Le Vot, S.; Fontaine, O.; Simon, P.; Favier, F. Modifications of MXene Layers for Supercapacitors. *Nano Energy* **2020**, *73* (March), 104734.
(209) Liu, R.; Zhang, A.; Tang, J.; Tian, J.; Huang, W.; Cai, J.; Barrow, C.; Yang, W.; Liu, J. Fabrication of Cobaltosic Oxide Nanoparticle-Doped 3 D MXene/Graphene Hybrid Porous Aerogels for All-Solid-State Supercapacitors. *Chem.—Eur. J.* **2019**, *25* (21), 5547−5554.
(210) Xu, S.; Wei, G.; Li, J.; Ji, Y.; Klyui, N.; Izotov, V.; Han, W. Binder-free $Ti_3C_2T_x$ MXene electrode film for supercapacitor produced by electrophoretic deposition method. *Chem. Eng. J.* **2017**, *317*, 1026.
(211) Xiao, J.; Wen, J.; Zhao, J.; Ma, X.; Gao, H.; Zhang, X. A Safe Etching Route to Synthesize Highly Crystalline Nb2CTx MXene for High Performance Asymmetric Supercapacitor Applications. *Electrochim. Acta* **2020**, *337*, 135803.
(212) Wang, Y.; Wang, X.; Li, X.; Bai, Y.; Xiao, H.; Liu, Y.; Liu, R.; Yuan, G. Engineering 3D Ion Transport Channels for Flexible MXene Films with Superior Capacitive Performance. *Adv. Funct. Mater.* **2019**, *29* (14), 1900326.
(213) Syamsai, R.; Grace, A. N. Ta4C3MXene as Supercapacitor Electrodes. *J. Alloys Compd.* **2019**, *792*, 1230−1238.
(214) Yoon, Y.; Lee, M.; Kim, S. K.; Bae, G.; Song, W.; Myung, S.; Lim, J.; Lee, S. S.; Zyung, T.; An, K. S. A Strategy for Synthesis of Carbon Nitride Induced Chemically Doped 2D MXene for High-Performance Supercapacitor Electrodes. *Adv. Energy Mater.* **2018**, *8* (15), 1703173.
(215) Xia, Q. X.; Shinde, N. M.; Yun, J. M.; Zhang, T.; Mane, R. S.; Mathur, S.; Kim, K. H. Bismuth Oxychloride/MXene Symmetric Supercapacitor with High Volumetric Energy Density. *Electrochim. Acta* **2018**, *271*, 351−360.
(216) Pan, H. Ultra-High Electrochemical Catalytic Activity of MXenes. *Sci. Rep.* **2016**, *6* (April), 1−10.
(217) Tang, Q.; Zhou, Z.; Shen, P. Are MXenes Promising Anode Materials for Li Ion Batteries? Computational Studies on Electronic Properties and Li Storage Capability of Ti 3C 2 and Ti 3C 2X 2 (X = F, OH) Monolayer. *J. Am. Chem. Soc.* **2012**, *134* (40), 16909−16916.
(218) Ashton, M.; Hennig, R. G.; Sinnott, S. B. Computational Characterization of Lightweight Multilayer MXene Li-Ion Battery Anodes. *Appl. Phys. Lett.* **2016**, *108* (2), 023901.
(219) Okubo, M.; Sugahara, A.; Kajiyama, S.; Yamada, A. MXene as a Charge Storage Host. *Acc. Chem. Res.* **2018**, *51* (3), 591−599.
(220) Sun, D.; Wang, M.; Li, Z.; Fan, G.; Fan, L. Z.; Zhou, A. Two-Dimensional Ti3C2 as Anode Material for Li-Ion Batteries. *Electrochem. Commun.* **2014**, *47*, 80−83.
(221) Kim, S. J.; Naguib, M.; Zhao, M.; Zhang, C.; Jung, H. T.; Barsoum, M. W.; Gogotsi, Y. High Mass Loading, Binder-Free MXene Anodes for High Areal Capacity Li-Ion Batteries. *Electrochim. Acta* **2015**, *163*, 246−251.

(222) Lv, X.; Wei, W.; Sun, Q.; Yu, L.; Huang, B.; Dai, Y. Sc2C as a Promising Anode Material with High Mobility and Capacity: A First-Principles Study. *ChemPhysChem* **2017**, *18* (12), 1627−1634.
(223) Wang, Y.; Zhou, M.; Xu, L. C.; Zhao, W.; Li, R.; Yang, Z.; Liu, R.; Li, X. Achieving Superior High-Capacity Batteries with the Lightest Ti2C MXene Anode by First-Principles Calculations: Overarching Role of S-Functionate (Ti 2CS2) and Multivalent Cations Carrier. *J. Power Sources* **2020**, *451* (February), 227791.
(224) Xu, Z.; Lv, X.; Chen, J.; Jiang, L.; Lai, Y.; Li, J. DFT Investigation of Capacious, Ultrafast and Highly Conductive Hexagonal Cr2C and V2C Monolayers as Anode Materials for High-Performance Lithium-Ion Batteries. *Phys. Chem. Chem. Phys.* **2017**, *19* (11), 7807−7819.
(225) Zhao, J.; Wen, J.; Bai, L.; Xiao, J.; Zheng, R.; Shan, X.; Li, L.; Gao, H.; Zhang, X. One-Step Synthesis of Few-Layer Niobium Carbide MXene as a Promising Anode Material for High-Rate Lithium Ion Batteries. *Dalton Transactions* **2019**, *48* (38), 14433−14439.
(226) Xie, Y.; Naguib, M.; Mochalin, V. N.; Barsoum, M. W.; Gogotsi, Y.; Yu, X.; Nam, K. W.; Yang, X. Q.; Kolesnikov, A. I.; Kent, P. R. C. Role of Surface Structure on Li-Ion Energy Storage Capacity of Two-Dimensional Transition-Metal Carbides. *J. Am. Chem. Soc.* **2014**, *136* (17), 6385−6394.
(227) Ahmed, B.; Anjum, D. H.; Gogotsi, Y.; Alshareef, H. N. Atomic Layer Deposition of SnO2 on MXene for Li-Ion Battery Anodes. *Nano Energy* **2017**, *34* (February), 249−256.
(228) Huang, H.; Cui, J.; Liu, G.; Bi, R.; Zhang, L. Carbon-Coated MoSe 2 /MXene Hybrid Nanosheets for Superior Potassium Storage. *ACS Nano* **2019**, *13* (3), 3448−3456.
(229) Wang, F.; Wang, Z.; Zhu, J.; Yang, H.; Chen, X.; Wang, L.; Yang, C. Facile Synthesis SnO2 Nanoparticle-Modified Ti3C2MXene Nanocomposites for Enhanced Lithium Storage Application. *J. Mater. Sci.* **2017**, *52* (7), 3556−3565.
(230) Zhang, S.; Li, X. Y.; Yang, W.; Tian, H.; Han, Z.; Ying, H.; Wang, G.; Han, W. Q. Novel Synthesis of Red Phosphorus Nanodot/Ti3C2Tx MXenes from Low-Cost Ti3SiC2MAX Phases for Superior Lithium- And Sodium-Ion Batteries. *ACS Appl. Mater. Interfaces* **2019**, *11* (45), 42086−42093.
(231) Ghassemi, H.; Harlow, W.; Mashtalir, O.; Beidaghi, M.; Lukatskaya, M. R.; Gogotsi, Y.; Taheri, M. L. In Situ Environmental Transmission Electron Microscopy Study of Oxidation of Two-Dimensional Ti3C2 and Formation of Carbon-Supported TiO2. *Journal of Materials Chemistry A* **2014**, *2* (35), 14339−14343.
(232) Chen, J. S.; Lou, X. W. SnO2-Based Nanomaterials: Synthesis and Application in Lithium-Ion Batteries. *Small* **2013**, *9* (11), 1877−1893.
(233) Liu, Z.; Yu, Q.; Zhao, Y.; He, R.; Xu, M.; Feng, S.; Li, S.; Zhou, L.; Mai, L. Silicon Oxides: A Promising Family of Anode Materials for Lithium-Ion Batteries. *Chem. Soc. Rev.* **2019**, *48* (1), 285−309.
(234) Mu, G.; Mu, D.; Wu, B.; Ma, C.; Bi, J.; Zhang, L.; Yang, H.; Wu, F. Microsphere-Like SiO2/MXene Hybrid Material Enabling High Performance Anode for Lithium Ion Batteries. *Small* **2020**, *16* (3), 1905430.
(235) Wen, C.; Zhu, T.; Li, X.; Li, H.; Huang, X.; Sun, G. Nanostructured Ni/Ti3C2Tx MXene Hybrid as Cathode for Lithium-Oxygen Battery. *Chin. Chem. Lett.* **2020**, *31* (4), 1000−1003.
(236) Lei, Y.-J.; Yan, Z.-C.; Lai, W.-H.; Chou, S.-L.; Wang, Y.-X.; Liu, H.-K.; Dou, S.-X. Tailoring MXene-Based Materials for Sodium-Ion Storage: Synthesis, Mechanisms, and Applications. *Electrochemical Energy Reviews* **2020**, *3* (4), 766−792.
(237) Zhang, Y.; Guo, B.; Hu, L.; Xu, Q.; Li, Y.; Liu, D.; Xu, M. Synthesis of SnS Nanoparticle-Modified MXene (Ti3C2Tx) Composites for Enhanced Sodium Storage. *J. Alloys Compd.* **2018**, *732*, 448−453.
(238) Tao, M.; Zhang, Y.; Zhan, R.; Guo, B.; Xu, Q.; Xu, M. A Chemically Bonded CoNiO2 Nanoparticles/MXene Composite as Anode for Sodium-Ion Batteries. *Mater. Lett.* **2018**, *230*, 173−176.
(239) Sharma, B. K.; Stoesser, A.; Mondal, S. K.; Garlapati, S. K.; Fawey, M. H.; Chakravadhanula, V. S. K.; Kruk, R.; Hahn, H.; Dasgupta, S. High-Performance All-Printed Amorphous Oxide FETs and Logics with Electronically Compatible Electrode/Channel Interface. *ACS Appl. Mater. Interfaces* **2018**, *10*, 22408−22418.
(240) Kajiyama, S.; Szabova, L.; Sodeyama, K.; Iinuma, H.; Morita, R.; Gotoh, K.; Tateyama, Y.; Okubo, M.; Yamada, A. Sodium-Ion Intercalation Mechanism in MXene Nanosheets. *ACS Nano* **2016**, *10* (3), 3334−3341.
(241) Gentile, A.; Ferrara, C.; Tosoni, S.; Balordi, M.; Marchionna, S.; Cernuschi, F.; Kim, M. H.; Lee, H. W.; Ruffo, R. Enhanced Functional Properties of Ti3C2Tx MXenes as Negative Electrodes in Sodium-Ion Batteries by Chemical Tuning. *Small Methods* **2020**, *4* (9), 2000314.
(242) Liu, F.; Liu, Y.; Zhao, X.; Liu, X.; Fan, L. Z. Pursuit of a High-Capacity and Long-Life Mg-Storage Cathode by Tailoring Sandwich-Structured MXene@carbon Nanosphere Composites. *Journal of Materials Chemistry A* **2019**, *7* (28), 16712−16719.
(243) Vahidmohammadi, A.; Hadjikhani, A.; Shahbazmohamadi, S.; Beidaghi, M. Two-Dimensional Vanadium Carbide (MXene) as a High-Capacity Cathode Material for Rechargeable Aluminum Batteries. *ACS Nano* **2017**, *11* (11), 11135−11144.
(244) Venkatkarthick, R.; Rodthongkum, N.; Zhang, X.; Wang, S.; Pattananuwat, P.; Zhao, Y.; Liu, R.; Qin, J. Vanadium-Based Oxide on Two-Dimensional Vanadium Carbide MXene (V2Ox@V2CTx) as Cathode for Rechargeable Aqueous Zinc-Ion Batteries. *ACS Applied Energy Materials* **2020**, *3* (5), 4677−4689.
(245) Li, J.; Rui, B.; Wei, W.; Nie, P.; Chang, L.; Le, Z.; Liu, M.; Wang, H.; Wang, L.; Zhang, X. Nanosheets Assembled Layered MoS2/MXene as High Performance Anode Materials for Potassium Ion Batteries. *J. Power Sources* **2020**, *449* (October), 227481.
(246) Ahmed, B.; Anjum, D. H.; Hedhili, M. N.; Gogotsi, Y.; Alshareef, H. N. H2O2 Assisted Room Temperature Oxidation of Ti2C MXene for Li-Ion Battery Anodes. *Nanoscale* **2016**, *8* (14), 7580−7587.
(247) Mashtalir, O.; Lukatskaya, M. R.; Zhao, M. Q.; Barsoum, M. W.; Gogotsi, Y. Amine-Assisted Delamination of Nb2C MXene for Li-Ion Energy Storage Devices. *Adv. Mater.* **2015**, *27* (23), 3501−3506.
(248) Wang, X.; Kajiyama, S.; Iinuma, H.; Hosono, E.; Oro, S.; Moriguchi, I.; Okubo, M.; Yamada, A. Pseudocapacitance of MXene Nanosheets for High-Power Sodium-Ion Hybrid Capacitors. *Nat. Commun.* **2015**, *6*, 1−6.
(249) Zhao, R.; Qian, Z.; Liu, Z.; Zhao, D.; Hui, X.; Jiang, G.; Wang, C.; Yin, L. Molecular-Level Heterostructures Assembled from Layered Black Phosphorene and Ti3C2MXene as Superior Anodes for High-Performance Sodium Ion Batteries. *Nano Energy* **2019**, *65* (August), 104037.
(250) Zhou, J.; Gao, S.; Guo, Z.; Sun, Z. Ti-Enhanced Exfoliation of V2AlC into V2C MXene for Lithium-Ion Battery Anodes. *Ceram. Int.* **2017**, *43* (14), 11450−11454.
(251) Lim, K. R. G.; Handoko, A. D.; Nemani, S. K.; Wyatt, B.; Jiang, H. Y.; Tang, J.; Anasori, B.; Seh, Z. W. Rational Design of Two-Dimensional Transition Metal Carbide/Nitride (MXene) Hybrids and Nanocomposites for Catalytic Energy Storage and Conversion. *ACS Nano* **2020**, *14* (9), 10834−10864.
(252) Wang, D.; Wang, L.; Lou, Z.; Zheng, Y.; Wang, K.; Zhao, L.; Han, W.; Jiang, K.; Shen, G. Biomimetic, Biocompatible and Robust Silk Fibroin-MXene Film with Stable 3D Cross-Link Structure for Flexible Pressure Sensors. *Nano Energy* **2020**, *78* (June), 105252.
(253) Huang, Y.; Fan, X.; Chen, S. C.; Zhao, N. Emerging Technologies of Flexible Pressure Sensors: Materials, Modeling, Devices, and Manufacturing. *Adv. Funct. Mater.* **2019**, *29* (12), 1808509.
(254) Ma, Y.; Liu, N.; Li, L.; Hu, X.; Zou, Z.; Wang, J.; Luo, S.; Gao, Y. A Highly Flexible and Sensitive Piezoresistive Sensor Based on MXene with Greatly Changed Interlayer Distances. *Nat. Commun.* **2017**, *8* (1), 1−7.
(255) Akkuş, Ü. Ö.; Balcı, E.; Berber, S. $Mo_2TiC_2O_2$ MXene-Based Nanoscale Pressure Sensor. *Physica E: Low-Dimensional Systems and Nanostructures* **2020**, *116* (October 2019), 113762.
(256) Gao, Y.; Yan, C.; Huang, H.; Yang, T.; Tian, G.; Xiong, D.; Chen, N.; Chu, X.; Zhong, S.; Deng, W.; Fang, Y.; Yang, W. Microchannel-Confined MXene Based Flexible Piezoresistive Multi-

functional Micro-Force Sensor. *Adv. Funct. Mater.* **2020**, *30* (11), 1909603.
(257) Li, L.; Fu, X.; Chen, S.; Uzun, S.; Levitt, A. S.; Shuck, C. E.; Han, W.; Gogotsi, Y. Hydrophobic and Stable MXene-Polymer Pressure Sensors for Wearable Electronics. *ACS Appl. Mater. Interfaces* **2020**, *12* (13), 15362−15369.
(258) Wang, F.; Hu, S.; Jia, Q.; Zhang, L. Advances in Electrospinning of Natural Biomaterials for Wound Dressing. *J. Nanomater.* **2020**, *2020*, 1.
(259) Yang, J.; Wang, K.; Yu, D. G.; Yang, Y.; Bligh, S. W. A.; Williams, G. R. Electrospun Janus Nanofibers Loaded with a Drug and Inorganic Nanoparticles as an Effective Antibacterial Wound Dressing. *Materials Science and Engineering C* **2020**, *111* (November 2019), 110805.
(260) Mayerberger, E. A.; Street, R. M.; McDaniel, R. M.; Barsoum, M. W.; Schauer, C. L. Antibacterial Properties of Electrospun Ti3C2Tz (MXene)/Chitosan Nanofibers. *RSC Adv.* **2018**, *8* (62), 35386−35394.
(261) Miranda, D. G.; Malmonge, S. M.; Campos, D. M.; Attik, N. G.; Grosgogeat, B.; Gritsch, K. A Chitosan-Hyaluronic Acid Hydrogel Scaffold for Periodontal Tissue Engineering. *Journal of Biomedical Materials Research - Part B Applied Biomaterials* **2016**, *104* (8), 1691−1702.
(262) Rozmysłowska-Wojciechowska, A.; Karwowska, E.; Gloc, M.; Woźniak, J.; Petrus, M.; Przybyszewski, B.; Wojciechowski, T.; Jastrzębska, A. M. Controlling the Porosity and Biocidal Properties of the Chitosan-Hyaluronate Matrix Hydrogel Nanocomposites by the Addition of 2D Ti3 C2 Tx Mxene. *Materials* **2020**, *13* (20), 4587.
(263) Bhang, S. H.; Jang, W. S.; Han, J.; Yoon, J. K.; La, W. G.; Lee, E.; Kim, Y. S.; Shin, J. Y.; Lee, T. J.; Baik, H. K.; Kim, B. S. Zinc Oxide Nanorod-Based Piezoelectric Dermal Patch for Wound Healing. *Adv. Funct. Mater.* **2017**, *27* (1), 1603497.
(264) Zhao, X.; Wu, H.; Guo, B.; Dong, R.; Qiu, Y.; Ma, P. X. Antibacterial Anti-Oxidant Electroactive Injectable Hydrogel as Self-Healing Wound Dressing with Hemostasis and Adhesiveness for Cutaneous Wound Healing. *Biomaterials* **2017**, *122*, 34−47.
(265) Mao, L.; Hu, S.; Gao, Y.; Wang, L.; Zhao, W.; Fu, L.; Cheng, H.; Xia, L.; Xie, S.; Ye, W.; Shi, Z.; Yang, G. Biodegradable and Electroactive Regenerated Bacterial Cellulose/MXene (Ti3C2Tx) Composite Hydrogel as Wound Dressing for Accelerating Skin Wound Healing under Electrical Stimulation. *Adv. Healthcare Mater.* **2020**, *9* (19), 2000872.
(266) Zhao, X.; Wang, L. Y.; Tang, C. Y.; Zha, X. J.; Liu, Y.; Su, B. H.; Ke, K.; Bao, R. Y.; Yang, M. B.; Yang, W. Smart Ti3C2TxMXene Fabric with Fast Humidity Response and Joule Heating for Healthcare and Medical Therapy Applications. *ACS Nano* **2020**, *14* (7), 8793−8805.
(267) Basara, G.; Saeidi-Javash, M.; Ren, X.; Bahcecioglu, G.; Wyatt, B. C.; Anasori, B.; Zhang, Y.; Zorlutuna, P. Electrically Conductive 3D Printed Ti3C2Tx MXene-PEG Composite Constructs for Cardiac Tissue Engineering. *Acta Biomaterialia* **2022**, *139*, 179.
(268) Farokhi, M.; Mottaghitalab, F.; Samani, S.; Shokrgozar, M. A.; Kundu, S. C.; Reis, R. L.; Fatahi, Y.; Kaplan, D. L. Silk Fibroin/Hydroxyapatite Composites for Bone Tissue Engineering. *Biotechnology Advances* **2018**, *36* (1), 68−91.
(269) Kargozar, S.; Mozafari, M. Nanotechnology and Nanomedicine: Start Small, Think Big. *Materials Today: Proceedings* **2018**, *5* (7), 15492−15500.
(270) Bhardwaj, N.; Devi, D.; Mandal, B. B. Tissue-Engineered Cartilage: The Crossroads of Biomaterials, Cells and Stimulating Factors. *Macromol. Biosci.* **2015**, *15* (2), 153−182.
(271) Chen, C.; Bai, X.; Ding, Y.; Lee, I. S. Electrical Stimulation as a Novel Tool for Regulating Cell Behavior in Tissue Engineering. *Biomaterials Research* **2019**, *23* (1), 1−12.
(272) Saberi, A.; Jabbari, F.; Zarrintaj, P.; Saeb, M. R.; Mozafari, M. Electrically Conductive Materials: Opportunities and Challenges in Tissue Engineering. *Biomolecules* **2019**, *9*, 448.
(273) Rafieerad, A.; Sequiera, G. L.; Yan, W.; Kaur, P.; Amiri, A.; Dhingra, S. Sweet-MXene Hydrogel with Mixed-Dimensional Components for Biomedical Applications. *J. Mech. Behavior Biomed. Mater.* **2020**, *101*, 103440.
(274) Huang, R.; Chen, X.; Dong, Y.; Zhang, X.; Wei, Y.; Yang, Z.; Li, W.; Guo, Y.; Liu, J.; Yang, Z.; Wang, H.; Jin, L. MXene Composite Nanofibers for Cell Culture and Tissue Engineering. *ACS Applied Bio Materials* **2020**, *3* (4), 2125−2131.
(275) Xing, C.; Chen, S.; Liang, X.; Liu, Q.; Qu, M.; Zou, Q.; Li, J.; Tan, H.; Liu, L.; Fan, D.; Zhang, H. Two-Dimensional MXene (Ti3C2)-Integrated Cellulose Hydrogels: Toward Smart Three-Dimensional Network Nanoplatforms Exhibiting Light-Induced Swelling and Bimodal Photothermal/Chemotherapy Anticancer Activity. *ACS Appl. Mater. Interfaces* **2018**, *10* (33), 27631−27643.
(276) Hussein, E. A.; Zagho, M. M.; Rizeq, B. R.; Younes, N. N.; Pintus, G.; Mahmoud, K. A.; Nasrallah, G. K.; Elzatahry, A. A. Plasmonic MXene-Based Nanocomposites Exhibiting Photothermal Therapeutic Effects with Lower Acute Toxicity than Pure MXene. *Int. J. Nanomed.* **2019**, *14*, 4529−4539.
(277) Dai, C.; Lin, H.; Xu, G.; Liu, Z.; Wu, R.; Chen, Y. Biocompatible 2D Titanium Carbide (MXenes) Composite Nanosheets for PH-Responsive MRI-Guided Tumor Hyperthermia. *Chem. Mater.* **2017**, *29* (20), 8637−8652.
(278) Hroncekova, S.; Bertok, T.; Hires, M.; Jane, E.; Lorencova, L.; Vikartovska, A.; Tanvir, A.; Kasak, P.; Tkac, J. Ultrasensitive Ti3C2TX MXene/Chitosan Nanocomposite-Based Amperometric Biosensor for Detection of Potential Prostate Cancer Marker in Urine Samples. *Processes* **2020**, *8* (5), 580.
(279) Chen, G.; Wang, H.; Wei, X.; Wu, Y.; Gu, W.; Hu, L.; Xu, D.; Zhu, C. Efficient Z-Scheme Heterostructure Based on TiO2/Ti3C2Tx/Cu2O to Boost Photoelectrochemical Response for Ultrasensitive Biosensing. *Sensors Actuators, B: Chem.* **2020**, *312* (December 2019), 127951.
(280) Li, Y.; Kang, Z.; Kong, L.; Shi, H.; Zhang, Y.; Cui, M.; Yang, D. P. MXene-Ti3C2/CuS Nanocomposites: Enhanced Peroxidase-like Activity and Sensitive Colorimetric Cholesterol Detection. *Materials Science and Engineering C* **2019**, *104* (January), 110000.
(281) Lei, Y.; Zhao, W.; Zhang, Y.; Jiang, Q.; He, J. H.; Baeumner, A. J.; Wolfbeis, O. S.; Wang, Z. L.; Salama, K. N.; Alshareef, H. N. A MXene-Based Wearable Biosensor System for High-Performance In Vitro Perspiration Analysis. *Small* **2019**, *15* (19), 1901190.
(282) Gu, H.; Xing, Y.; Xiong, P.; Tang, H.; Li, C.; Chen, S.; Zeng, R.; Han, K.; Shi, G. Three-Dimensional Porous Ti3C2Tx MXene-Graphene Hybrid Films for Glucose Biosensing. *ACS Applied Nano Materials* **2019**, *2* (10), 6537−6545.
(283) Özcan, N.; Medetalibeyoglu, H.; Akyıldırım, O.; Atar, N.; Yola, M. L. Electrochemical Detection of Amyloid-β Protein by Delaminated Titanium Carbide MXene/Multi-Walled Carbon Nanotubes Composite with Molecularly Imprinted Polymer. *Materials Today Communications* **2020**, *23* (March), 101097.
(284) Li, M.; Fang, L.; Zhou, H.; Wu, F.; Lu, Y.; Luo, H.; Zhang, Y.; Hu, B. Three-Dimensional Porous MXene/NiCo-LDH Composite for High Performance Non-Enzymatic Glucose Sensor. *Appl. Surf. Sci.* **2019**, *495* (June), 143554.
(285) Wanasinghe, D.; Aslani, F.; Ma, G.; Habibi, D. Review of Polymer Composites with Diverse Nanofillers for Electromagnetic Interference Shielding. *Nanomaterials* **2020**, *10* (3), 541.
(286) Kumar, P.; Narayan Maiti, U.; Sikdar, A.; Kumar Das, T.; Kumar, A.; Sudarsan, V. Recent Advances in Polymer and Polymer Composites for Electromagnetic Interference Shielding: Review and Future Prospects. *Polym. Rev.* **2019**, *59* (4), 687−738.
(287) Hasan, Md. M.; Hossain, Md. M.; Chowdhury, H. K. Two-Dimensional MXene-Based Flexible Nanostructures for Functional Nanodevices: A Review. *Journal of Materials Chemistry A* **2021**, *9*, 3231.
(288) Du, Z.; Chen, K.; Zhang, Y.; Wang, Y.; He, P.; Mi, H. Y.; Wang, Y.; Liu, C.; Shen, C. Engineering Multilayered MXene/Electrospun Poly(Lactic Acid) Membrane with Increscent Electromagnetic Interference (EMI) Shielding for Integrated Joule Heating and Energy Generating. *Composites Communications* **2021**, *26* (April), 100770.
(289) Gao, Q.; Pan, Y.; Zheng, G.; Liu, C.; Shen, C.; Liu, X. Flexible Multilayered MXene/Thermoplastic Polyurethane Films with Excellent Electromagnetic Interference Shielding, Thermal Conductivity,

https://doi.org/10.1021/acsmaterialslett.2c00175
ACS Materials Lett. 2022, 4, 1174−1206

and Management Performances. *Advanced Composites and Hybrid Materials* **2021**, *4* (2), 274−285.
(290) Ji, B.; Fan, S.; Kou, S.; Xia, X.; Deng, J.; Cheng, L.; Zhang, L. Microwave Absorption Properties of Multilayer Impedance Gradient Absorber Consisting of Ti3C2TX MXene/Polymer Films. *Carbon* **2021**, *181*, 130−142.
(291) Gao, X.; Wang, B.; Wang, K.; Xu, S.; Liu, S.; Liu, X.; Jia, Z.; Wu, G. Design of Ti3C2Tx/TiO2/PANI Multi-Layer Composites for Excellent Electromagnetic Wave Absorption Performance. *J. Colloid Interface Sci.* **2021**, *583*, 510−521.
(292) Hou, T.; Jia, Z.; Wang, B.; Li, H.; Liu, X.; Bi, L.; Wu, G. MXene-Based Accordion 2D Hybrid Structure with Co9S8/C/Ti3C2Tx as Efficient Electromagnetic Wave Absorber. *Chemical Engineering Journal* **2021**, *414*, 128875.
(293) Wang, S. J.; Li, D. S.; Jiang, L. Synergistic Effects between MXenes and Ni Chains in Flexible and Ultrathin Electromagnetic Interference Shielding Films. *Advanced Materials Interfaces* **2019**, *6* (19), 1900961.
(294) Yuan, W.; Yang, J.; Yin, F.; Li, Y.; Yuan, Y. Flexible and Stretchable MXene/Polyurethane Fabrics with Delicate Wrinkle Structure Design for Effective Electromagnetic Interference Shielding at a Dynamic Stretching Process. *Composites Communications* **2020**, *19* (March), 90−98.
(295) Xu, H.; Yin, X.; Li, X.; Li, M.; Liang, S.; Zhang, L.; Cheng, L. Lightweight Ti 2 CT x MXene/Poly(Vinyl Alcohol) Composite Foams for Electromagnetic Wave Shielding with Absorption-Dominated Feature. *ACS Appl. Mater. Interfaces* **2019**, *11* (10), 10198−10207.
(296) Tong, Y.; He, M.; Zhou, Y.; Nie, S.; Zhong, X.; Fan, L.; Huang, T.; Liao, Q.; Wang, Y. Three-Dimensional Hierarchical Architecture of the TiO2/Ti3C2Tx/RGO Ternary Composite Aerogel for Enhanced Electromagnetic Wave Absorption. *ACS Sustainable Chem. Eng.* **2018**, *6* (7), 8212−8222.
(297) Wang, L.; Liu, H.; Lv, X.; Cui, G.; Gu, G. Facile Synthesis 3D Porous MXene Ti3C2Tx@RGO Composite Aerogel with Excellent Dielectric Loss and Electromagnetic Wave Absorption. *J. Alloys Compd.* **2020**, *828*, 154251.
(298) Liang, L.; Yang, R.; Han, G.; Feng, Y.; Zhao, B.; Zhang, R.; Wang, Y.; Liu, C. Enhanced Electromagnetic Wave-Absorbing Performance of Magnetic Nanoparticles-Anchored 2D Ti3C2T x MXene. *ACS Appl. Mater. Interfaces* **2020**, *12* (2), 2644−2654.
(299) Cui, C.; Guo, R.; Ren, E.; Xiao, H.; Zhou, M.; Lai, X.; Qin, Q.; Jiang, S.; Qin, W. MXene-Based RGO/Nb2CTx/Fe3O4 Composite for High Absorption of Electromagnetic Wave. *Chemical Engineering Journal* **2021**, *405* (July 2020), 126626.
(300) Wang, Y.; Gao, X.; Zhang, L.; Wu, X.; Wang, Q.; Luo, C.; Wu, G. Synthesis of Ti 3 C 2 /Fe 3 O 4 /PANI Hierarchical Architecture Composite as an Efficient Wide-Band Electromagnetic Absorber. *Appl. Surf. Sci.* **2019**, *480* (March), 830−838.
(301) Cui, Y.; Yang, K.; Wang, J.; Shah, T.; Zhang, Q.; Zhang, B. Preparation of Pleated RGO/MXene/Fe3O4Microsphere and Its Absorption Properties for Electromagnetic Wave. *Carbon* **2021**, *172*, 1−14.
(302) Yang, M.; Yuan, Y.; Li, Y.; Sun, X.; Wang, S.; Liang, L.; Ning, Y.; Li, J.; Yin, W.; Li, Y. Anisotropic Electromagnetic Absorption of Aligned Ti3C2T XMXene/Gelatin Nanocomposite Aerogels. *ACS Appl. Mater. Interfaces* **2020**, *12* (29), 33128−33138.
(303) He, J.; Liu, S.; Deng, L.; Shan, D.; Cao, C.; Luo, H.; Yan, S. Tunable Electromagnetic and Enhanced Microwave Absorption Properties in CoFe2O4 Decorated Ti3C2MXene Composites. *Appl. Surf. Sci.* **2020**, *504*, 144210.
(304) He, J.; Shan, D.; Yan, S.; Luo, H.; Cao, C.; Peng, Y. Magnetic FeCo Nanoparticles-Decorated Ti3C2MXene with Enhanced Microwave Absorption Performance. *J. Magn. Magn. Mater.* **2019**, *492* (June), 165639.
(305) Gao, X.; Wang, B.; Wang, K.; Xu, S.; Liu, S.; Liu, X.; Jia, Z.; Wu, G. Design of Ti3C2Tx/TiO2/PANI Multi-Layer Composites for Excellent Electromagnetic Wave Absorption Performance. *J. Colloid Interface Sci.* **2021**, *583*, 510−521.
(306) Rajavel, K.; Luo, S.; Wan, Y.; Yu, X.; Hu, Y.; Zhu, P.; Sun, R.; Wong, C. 2D Ti3C2Tx MXene/Polyvinylidene Fluoride (PVDF) Nanocomposites for Attenuation of Electromagnetic Radiation with Excellent Heat Dissipation. *Composites Part A: Applied Science and Manufacturing* **2020**, *129*, 105693.
(307) Wang, L.; Chen, L.; Song, P.; Liang, C.; Lu, Y.; Qiu, H.; Zhang, Y.; Kong, J.; Gu, J. Fabrication on the Annealed Ti3C2Tx MXene/Epoxy Nanocomposites for Electromagnetic Interference Shielding Application. *Composites Part B: Engineering* **2019**, *171* (March), 111−118.
(308) Liu, R.; Miao, M.; Li, Y.; Zhang, J.; Cao, S.; Feng, X. Ultrathin Biomimetic Polymeric Ti 3 C 2 T x MXene Composite Films for Electromagnetic Interference Shielding. *ACS Appl. Mater. Interfaces* **2018**, *10* (51), 44787−44795.
(309) Weng, C.; Xing, T.; Jin, H.; Wang, G.; Dai, Z.; Pei, Y.; Liu, L.; Zhang, Z. Mechanically Robust ANF/MXene Composite Films with Tunable Electromagnetic Interference Shielding Performance. *Composites Part A: Applied Science and Manufacturing* **2020**, *135* (May), 105927.
(310) Cui, C.; Xiang, C.; Geng, L.; Lai, X.; Guo, R.; Zhang, Y.; Xiao, H.; Lan, J.; Lin, S.; Jiang, S. Flexible and Ultrathin Electrospun Regenerate Cellulose Nanofibers and D-Ti3C2Tx (MXene) Composite Film for Electromagnetic Interference Shielding. *J. Alloys Compd.* **2019**, *788*, 1246−1255.
(311) Xin, W.; Xi, G. Q.; Cao, W. T.; Ma, C.; Liu, T.; Ma, M. G.; Bian, J. Lightweight and Flexible MXene/CNF/Silver Composite Membranes with a Brick-like Structure and High-Performance Electromagnetic-Interference Shielding. *RSC Adv.* **2019**, *9* (51), 29636−29644.
(312) Wang, Z.; Han, X.; Han, X.; Chen, Z.; Wang, S.; Pu, J. MXene/Wood-Derived Hierarchical Cellulose Scaffold Composite with Superior Electromagnetic Shielding. *Carbohydr. Polym.* **2021**, *254* (May), 117033.
(313) Hu, D.; Huang, X.; Li, S.; Jiang, P. Flexible and Durable Cellulose/MXene Nanocomposite Paper for Efficient Electromagnetic Interference Shielding. *Compos. Sci. Technol.* **2020**, *188* (December 2019), 107995.
(314) Jin, X.; Wang, J.; Dai, L.; Liu, X.; Li, L.; Yang, Y.; Cao, Y.; Wang, W.; Wu, H.; Guo, S. Flame-Retardant Poly(Vinyl Alcohol)/MXene Multilayered Films with Outstanding Electromagnetic Interference Shielding and Thermal Conductive Performances. *Chem. Eng. J.* **2020**, *380* (August 2019), 122475.
(315) Wang, Z.; Cheng, Z.; Xie, L.; Hou, X.; Fang, C. Flexible and Lightweight Ti3C2Tx MXene/Fe3O4@PANI Composite Films for High-Performance Electromagnetic Interference Shielding. *Ceram. Int.* **2021**, *47* (4), 5747−5757.
(316) Wei, H.; Wang, M.; Zheng, W.; Jiang, Z.; Huang, Y. 2D Ti3C2Tx MXene/Aramid Nanofibers Composite Films Prepared via a Simple Filtration Method with Excellent Mechanical and Electromagnetic Interference Shielding Properties. *Ceram. Int.* **2020**, *46* (5), 6199−6204.
(317) Liu, F.; Li, Y.; Hao, S.; Cheng, Y.; Zhan, Y.; Zhang, C.; Meng, Y.; Xie, Q.; Xia, H. Well-Aligned MXene/Chitosan Films with Humidity Response for High-Performance Electromagnetic Interference Shielding. *Carbohydr. Polym.* **2020**, *243* (May), 116467.
(318) Choi, S.-J.; Kim, I.-D. Recent Developments in 2D Nanomaterials for Chemiresistive-Type Gas Sensors. *Electron. Mater. Lett.* **2018**, *14*, 221−260.
(319) Xiao, B.; Li, Y.; Yu, X.; Cheng, J. MXenes: Reusable Materials for NH3 Sensor or Capturer by Controlling the Charge Injection. *Sens. Actuators, B* **2016**, *235*, 103−109.
(320) Yu, X. F.; Li, Y. C.; Cheng, J. B.; Liu, Z. B.; Li, Q. Z.; Li, W. Z.; Yang, X.; Xiao, B. Monolayer Ti2CO2: A Promising Candidate for NH3 Sensor or Capturer with High Sensitivity and Selectivity. *ACS Appl. Mater. Interfaces* **2015**, *7* (24), 13707−13713.
(321) Wu, M.; He, M.; Hu, Q.; Wu, Q.; Sun, G.; Xie, L.; Zhang, Z.; Zhu, Z.; Zhou, A. Ti3C2MXene-Based Sensors with High Selectivity for NH3 Detection at Room Temperature. *ACS Sensors* **2019**, *4* (10), 2763−2770.

https://doi.org/10.1021/acsmaterialslett.2c00175
ACS Materials Lett. 2022, 4, 1174−1206

(322) Gao, L.; Li, C.; Huang, W.; Mei, S.; Lin, H.; Ou, Q.; Zhang, Y.; Guo, J.; Zhang, F.; Xu, S.; Zhang, H. MXene/Polymer Membranes: Synthesis, Properties, and Emerging Applications. *Chem. Mater.* **2020**, *32* (5), 1703−1747.
(323) Srimuk, P.; Kaasik, F.; Krüner, B.; Tolosa, A.; Fleischmann, S.; Jäckel, N.; Tekeli, M. C.; Aslan, M.; Suss, M. E.; Presser, V. MXene as a Novel Intercalation-Type Pseudocapacitive Cathode and Anode for Capacitive Deionization. *Journal of Materials Chemistry A* **2016**, *4* (47), 18265−18271.
(324) Rasool, K.; Helal, M.; Ali, A.; Ren, C. E.; Gogotsi, Y.; Mahmoud, K. A. Antibacterial Activity of Ti3C2Tx MXene. *ACS Nano* **2016**, *10* (3), 3674−3684.
(325) Shahzad, A.; Rasool, K.; Nawaz, M.; Miran, W.; Jang, J.; Moztahida, M.; Mahmoud, K. A.; Lee, D. S. Heterostructural TiO2/Ti3C2Tx (MXene) for Photocatalytic Degradation of Antiepileptic Drug Carbamazepine. *Chemical Engineering Journal* **2018**, *349*, 748−755.
(326) Zhang, P.; Wang, L.; Du, K.; Wang, S.; Huang, Z.; Yuan, L.; Li, Z.; Wang, H.; Zheng, L.; Chai, Z.; Shi, W. Effective Removal of U(VI) and Eu(III) by Carboxyl Functionalized MXene Nanosheets. *J. Hazard. Mater.* **2020**, *396* (February), 122731.
(327) Wang, L.; Yuan, L.; Chen, K.; Zhang, Y.; Deng, Q.; Du, S.; Huang, Q.; Zheng, L.; Zhang, J.; Chai, Z.; Barsoum, M. W.; Wang, X.; Shi, W. Loading Actinides in Multilayered Structures for Nuclear Waste Treatment: The First Case Study of Uranium Capture with Vanadium Carbide MXene. *ACS Appl. Mater. Interfaces* **2016**, *8* (25), 16396−16403.
(328) Ying, Y.; Liu, Y.; Wang, X.; Mao, Y.; Cao, W.; Hu, P.; Peng, X. Two-Dimensional Titanium Carbide for E Ffi Ciently Reductive Removal of Highly Toxic Chromium (VI) from Water. *ACS Appl. Mater. Interfaces* **2015**, *7* (3), 1795.
(329) Shahzad, A.; Rasool, K.; Miran, W.; Nawaz, M.; Jang, J.; Mahmoud, K. A.; Lee, D. S. Two-Dimensional Ti3C2Tx MXene Nanosheets for Efficient Copper Removal from Water. *ACS Sustainable Chem. Eng.* **2017**, *5* (12), 11481−11488.
(330) Zhang, Z.; Li, H.; Zou, G.; Fernandez, C.; Liu, B.; Zhang, Q.; Hu, J.; Peng, Q. Self-Reduction Synthesis of New MXene/Ag Composites with Unexpected Electrocatalytic Activity. *ACS Sustainable Chem. Eng.* **2016**, *4* (12), 6763−6771.
(331) Anasori, B.; Gogotsi, Y. *2D Metal Carbides and Nitrides (MXenes)* **2019**, 3.
(332) Wang, H.; Cui, H.; Song, X.; Xu, R.; Wei, N.; Tian, J.; Niu, H. Facile Synthesis of Heterojunction of MXenes/TiO2 Nanoparticles towards Enhanced Hexavalent Chromium Removal. *J. Colloid Interface Sci.* **2020**, *561*, 46−57.
(333) Al-Hamadani, Y. A. J.; Jun, B. M.; Yoon, M.; Taheri-Qazvini, N.; Snyder, S. A.; Jang, M.; Heo, J.; Yoon, Y. Applications of MXene-Based Membranes in Water Purification: A Review. *Chemosphere* **2020**, *254*, 126821.
(334) Ihsanullah, I. MXenes (Two-Dimensional Metal Carbides) as Emerging Nanomaterials for Water Purification: Progress, Challenges and Prospects. *Chem. Eng. J.* **2020**, *388* (February), 124340.
(335) Huang, X.; Wang, R.; Jiao, T.; Zou, G.; Zhan, F.; Yin, J.; Zhang, L.; Zhou, J.; Peng, Q. Facile Preparation of Hierarchical AgNP-Loaded MXene/Fe3O4 Polymer Nanocomposites by Electrospinning with Enhanced Catalytic Performance for Wastewater Treatment. *ACS Omega* **2019**, *4* (1), 1897−1906.
(336) Tang, Y.; Yang, C.; Que, W. A Novel Two-Dimensional Accordion-like Titanium Carbide (MXene) for Adsorption of Cr(VI) from Aqueous Solution. *J. Adv. Dielectrics* **2018**, *8* (5), 1850035.
(337) Zou, G.; Guo, J.; Peng, Q.; Zhou, A.; Zhang, Q.; Liu, B. Synthesis of Urchin-like Rutile Titania Carbon Nanocomposites by Iron-Facilitated Phase Transformation of MXene for Environmental Remediation. *Journal of Materials Chemistry A* **2016**, *4* (2), 489−499.
(338) He, L.; Huang, D.; He, Z.; Yang, X.; Yue, G.; Zhu, J.; Astruc, D.; Zhao, P. Nanoscale Zero-Valent Iron Intercalated 2D Titanium Carbides for Removal of Cr(VI) in Aqueous Solution and the Mechanistic Aspect. *Journal of Hazardous Materials* **2020**, *388* (Vi), 121761.
(339) Shahzad, A.; Rasool, K.; Miran, W.; Nawaz, M.; Jang, J.; Mahmoud, K. A.; Lee, D. S. Two-Dimensional Ti3C2Tx MXene Nanosheets for Efficient Copper Removal from Water. *ACS Sustainable Chem. Eng.* **2017**, *5* (12), 11481.
(340) Gan, D.; Huang, Q.; Dou, J.; Huang, H.; Chen, J.; Liu, M.; Wen, Y.; Yang, Z.; Zhang, X.; Wei, Y. Bioinspired Functionalization of MXenes (Ti3C2TX) with Amino Acids for Efficient Removal of Heavy Metal Ions. *Appl. Surf. Sci.* **2020**, *504* (October), 144603.
(341) Jin, L.; Chai, L.; Yang, W.; Wang, H.; Zhang, L. Two-Dimensional Titanium Carbides (Ti3C2Tx) Two-Dimensional Titanium Carbides (Ti3C2Tx) Functionalized by Poly(m-phenylenediamine) for Efficient Adsorption and Reduction of Hexavalent Chromium. *Int. J. Environ. Res. Public Health* **2020**, *17* (1), 167.
(342) Shahzad, A.; Jang, J.; Lim, S. R.; Lee, D. S. Unique Selectivity and Rapid Uptake of Molybdenum-Disulfide-Functionalized MXene Nanocomposite for Mercury Adsorption. *Environmental Research* **2020**, *182*, 109005.
(343) Fard, A. K.; Mckay, G.; Chamoun, R.; Rhadfi, T.; Preud'Homme, H.; Atieh, M. A. Barium Removal from Synthetic Natural and Produced Water Using MXene as Two Dimensional (2-D) Nanosheet Adsorbent. *Chemical Engineering Journal* **2017**, *317*, 331−342.
(344) Dong, Y.; Sang, D.; He, C.; Sheng, X.; Lei, L. Mxene/Alginate Composites for Lead and Copper Ion Removal from Aqueous Solutions. *RSC Adv.* **2019**, *9* (50), 29015−29022.
(345) Du, Y.; Yu, B.; Wei, L.; Wang, Y.; Zhang, X.; Ye, S. Efficient Removal of Pb(II) by Ti3C2Tx Powder Modified with a Silane Coupling Agent. *J. Mater. Sci.* **2019**, *54* (20), 13283−13297.
(346) Shahzad, A.; Rasool, K.; Miran, W.; Nawaz, M.; Jang, J.; Mahmoud, K. A.; Lee, D. S. Mercuric Ion Capturing by Recoverable Titanium Carbide Magnetic Nanocomposite. *Journal of Hazardous Materials* **2018**, *344*, 811−818.
(347) Zhang, Q.; Teng, J.; Zou, G.; Peng, Q.; Du, Q.; Jiao, T.; Xiang, J. Efficient Phosphate Sequestration for Water Purification by Unique Sandwich-like MXene/Magnetic Iron Oxide Nanocomposites. *Nanoscale* **2016**, *8* (13), 7085−7093.
(348) Shahzad, A.; Nawaz, M.; Moztahida, M.; Jang, J.; Tahir, K.; Kim, J.; Lim, Y.; Vassiliadis, V. S.; Woo, S. H.; Lee, D. S. Ti3C2Tx MXene Core-Shell Spheres for Ultrahigh Removal of Mercuric Ions. *Chem. Eng. J.* **2019**, *368* (December 2018), 400−408.
(349) Wang, S.; Liu, Y.; Lü, Q. F.; Zhuang, H. Facile Preparation of Biosurfactant-Functionalized Ti2CTX MXene Nanosheets with an Enhanced Adsorption Performance for Pb(II) Ions. *J. Mol. Liq.* **2020**, *297* (Ii), 111810.
(350) Jun, B. M.; Her, N.; Park, C. M.; Yoon, Y. Effective Removal of Pb(Ii) from Synthetic Wastewater Using Ti3C2T: X MXene. *Environmental Science: Water Research and Technology* **2020**, *6* (1), 173−180.
(351) Cui, C.; Guo, R.; Xiao, H.; Ren, E.; Song, Q.; Xiang, C.; Lai, X.; Lan, J.; Jiang, S. Bi2WO6/Nb2CTx MXene Hybrid Nanosheets with Enhanced Visible-Light-Driven Photocatalytic Activity for Organic Pollutants Degradation. *Appl. Surf. Sci.* **2020**, *505* (October), 144595.
(352) Su, T.; Peng, R.; Hood, Z. D.; Naguib, M.; Ivanov, I. N.; Keum, J. K.; Qin, Z.; Guo, Z.; Wu, Z. One-Step Synthesis of Nb2O5/C/Nb2C (MXene) Composites and Their Use as Photocatalysts for Hydrogen Evolution. *ChemSusChem* **2018**, *11* (4), 688−699.
(353) Shao, M.; Yang, M.; Shao, Y.; Chai, J.; Qu, Y.; Yang, M.; Wang, Z.; Ip, W. F.; Kwok, C. T.; Shi, X.; Lu, Z.; Wang, S.; Wang, X.; Pan, H. Synergistic Effect of 2D Ti2C and G-C3N4 for Efficient Photocatalytic Hydrogen Production. *Journal of Materials Chemistry A* **2017**, *5* (32), 16748−16756.
(354) Wang, H.; Peng, R.; Hood, Z. D.; Naguib, M.; Adhikari, S. P.; Wu, Z. Titania Composites with 2 D Transition Metal Carbides as Photocatalysts for Hydrogen Production under Visible-Light Irradiation. *ChemSusChem* **2016**, *9* (12), 1490−1497.
(355) Feng, X.; Yu, Z.; Long, R.; Sun, Y.; Wang, M.; Li, X.; Zeng, G. Polydopamine Intimate Contacted Two-Dimensional/Two-Dimensional Ultrathin Nylon Basement Membrane Supported RGO/PDA/

https://doi.org/10.1021/acsmaterialslett.2c00175
ACS Materials Lett. 2022, 4, 1174−1206

MXene Composite Material for Oil-Water Separation and Dye Removal. *Sep. Purif. Technol.* **2020**, *247* (April), 116945.
(356) Hu, L.; Gao, S.; Ding, X.; Wang, D.; Jiang, J.; Jin, J.; Jiang, L. Photothermal-Responsive Single-Walled Carbon Nanotube-Based Ultrathin Membranes for on/off Switchable Separation of Oil-in-Water Nanoemulsions. *ACS Nano* **2015**, *9* (5), 4835−4842.
(357) Cui, M.; Mu, P.; Shen, Y.; Zhu, G.; Luo, L.; Li, J. Three-Dimensional Attapulgite with Sandwich-like Architecture Used for Multifunctional Water Remediation. *Sep. Purif. Technol.* **2020**, *235* (August 2019), 116210.
(358) Lorencova, L.; Bertok, T.; Dosekova, E.; Holazova, A.; Paprckova, D.; Vikartovska, A.; Sasinkova, V.; Filip, J.; Kasak, P.; Jerigova, M.; Velic, D.; Mahmoud, K. A.; Tkac, J. Electrochemical Performance of Ti3C2Tx MXene in Aqueous Media: Towards Ultrasensitive H2O2 Sensing. *Electrochim. Acta* **2017**, *235*, 471−479.
(359) Kim, S. J.; Koh, H. J.; Ren, C. E.; Kwon, O.; Maleski, K.; Cho, S. Y.; Anasori, B.; Kim, C. K.; Choi, Y. K.; Kim, J.; Gogotsi, Y.; Jung, H. T. Metallic Ti3C2Tx MXene Gas Sensors with Ultrahigh Signal-to-Noise Ratio. *ACS Nano* **2018**, *12* (2), 986−993.
(360) Zhao, L.; Wang, K.; Wei, W.; Wang, L.; Han, W. High-performance Flexible Sensing Devices Based on Polyaniline/MXene Nanocomposites. *InfoMat* **2019**, *1* (3), 407−416.
(361) Chen, W. Y.; Lai, S. N.; Yen, C. C.; Jiang, X.; Peroulis, D.; Stanciu, L. A. Surface Functionalization of Ti3C2TxMXene with Highly Reliable Superhydrophobic Protection for Volatile Organic Compounds Sensing. *ACS Nano* **2020**, *14* (9), 11490−11501.
(362) Mehdi Aghaei, S.; Aasi, A.; Panchapakesan, B. Experimental and Theoretical Advances in MXene-Based Gas Sensors. *ACS Omega* **2021**, *6* (4), 2450−2461.

https://doi.org/10.1021/acsmaterialslett.2c00175
ACS Materials Lett. 2022, 4, 1174−1206